LAMINAR FLOW OVER TRANSVERSE RECTANGULAR CAVITIES

Thesis by

Thomas Charles Reihman

In Partial Fulfillment of the Requirements

For the Degree of

Doctor of Philosophy

California Institute of Technology

Pasadena, California

1967

(Submitted May 19, 1967)

ACKNOWLEDGMENTS

The author wishes to express his sincere thanks and gratitude for the advice and encouragement of Professor R. H. Sabersky, under whose guidance this work was carried on.

Support for this research was provided by a National Science Foundation Grant. Financial assistance was afforded the author by an Alfred P. Sloan Foundation Fellowship, a U. S. Steel Foundation Fellowship, and several Ford Foundation Fellowships. The author is grateful for this assistance.

Special thanks are due to Mr. E. F. Daly, Mr. R. L. Greenway and Mr. C. Eastvedt of the California Institute of Technology staff for their cooperation. For assistance in the preparation of the manuscript the author expresses his thanks to Mrs. Phyllis Henderson, Miss Cecilia Lin and Mrs. Madeline Fagergren.

Finally, the author wishes to express his deepest gratitude for the understanding and encouragement given him by his wife during the period of this study. He also wishes to thank her for the assistance she rendered and the many sacrifices she gladly made during the preparation of this dissertation.

ABSTRACT

An experimental investigation was conducted on the laminar flow of water over transverse rectangular cavities. Most of the cavities were square ranging in size from 1/8 in. to 1 in. The flow over the cavities was observed for an ϵ^* range of from 16 to 400. The quantity ϵ^* may be regarded as a Reynolds number for the cavity. It is defined as $\epsilon^* = \epsilon u_\tau / \nu$ where ϵ is the cavity depth, u_τ is the shear velocity, and ν is the kinematic viscosity of the fluid. The desired flow approaching the cavities was obtained one foot from the leading edge of a flat plate suspended in an open surface water tunnel at free stream velocities from 0.125 to 0.75 ft/sec. Visual studies, instantaneous velocity measurements, and velocity profile determinations confirmed that the flow was laminar. The velocity measurements were obtained by means of a hot-film anemometer.

The primary goal of the investigation was to determine whether the strong random mass-exchange activity observed in identical cavities in turbulent flow in the same ϵ^* range was due to an inherent instability of the cavity flow or due to the excitation from turbulent fluctuations at the cavity opening. As the present experiments showed no such strong mass exchange, it was concluded that the latter mechanism was indeed the essential factor. In conjunction with these studies the flow patterns in the cavities were

examined by visualization techniques and cavity velocity measurements were made. The cavity vortex velocities were found to be less than 8 percent of the free stream velocity in the range of ϵ^* examined. In addition a laminar oscillation was observed in the shear layer at the cavity opening and its frequencies are reported.

Photographic material on pp. 93-133 are essential and will not clearly reproduce on Xerox copies. Photographic copies should be ordered.

TABLE OF CONTENTS

LIST OF TABLES

LIST OF FIGURES

I. INTRODUCTION

For the past several decades there has been considerable interest in the nature of the flow field about the roughness elements that comprise a rough surface. The interest comes primarily from the desire to obtain a better understanding of the fluid flow and heat transfer phenomena that are encountered with rough walls, so that more effective heat-exchange surfaces may be designed.

Whereas most previous studies on flow over rough surfaces have concerned themselves with turbulent flow, the present work is concerned with laminar flow over the roughness elements. The principal goal of the study is to determine whether the previously observed unsteady flow between two-dimensional roughnesses was caused by the external turbulent flow or whether it was the consequence of an inherent instability of the flow in between the roughness elements.

The original incentive for this study dates back to the work of Dipprey (11, 12)[1], who conducted heat transfer experiments with artificially roughened tubes for turbulent flow. In particular, he observed that for high Prandtl numbers the upper portion of the

---

[1]Numbers in parentheses refer to references.

transition region, in the "hydraulically smooth" to "fully developed rough" flow transition, exhibited certain favorable heat transfer characteristics, in that the ratio $2C_h/C_f$ was greater for rough tubes than for the corresponding smooth tubes. This was in contrast to some earlier observations for flow over rough surfaces where it was found that the shear represented by C_f increased proportionally more than the heat transfer represented by C_h, the heat transfer effectiveness $2C_h/C_f$ thus falling below the values that exist for corresponding smooth surfaces. Interest was then expressed in the flow pattern which might cause this observed behavior and the examination of the flow in this regime became the subject of Townes' work (44, 45).

Townes' experimental study in the roughness transition region on square two-dimensional cavities (cavity length = cavity height << cavity span) showed that random mass-exchange bursts occurred in this flow regime. These bursts expelled fluid from the cavity with a violent action, thus scouring the heat-exchange surfaces and promoting the overall heat transfer. Since Townes' cavities had been subjected to an approaching turbulent flow, the question arose as to whether these mass-exchange bursts were caused by the turbulent fluctuations in the boundary layer above the cavities or whether they were caused by an instability in the cavity flow. The latter possibility had to be considered especially as Maull and East (26) had shown that the flow in a cavity could be unstable and lead to a three-dimensional cellular flow.

The principal goal of the present work was, therefore, to study whether the observed mass-exchange bursts were caused by the turbulent fluctuations in the outer flow. For this purpose it was planned to subject geometrically similar cavities to flow conditions as nearly similar to those of Townes, but without the turbulent fluctuations.

In addition it was intended to survey the velocity field within and adjacent to the cavity and to determine the magnitude of the shear stress across the cavity opening, as well as upstream and downstream of the cavity. These observations were to be made by both visual studies and by hot-film anemometry. For the visual studies, dye was to be injected from either small orifices or from slots depending on whether cross-sectional or three-dimensional characteristics were to be studied.

The range of square cavity sizes and water flow velocities in the present work are comparable to those of Townes. By selecting a location near the leading edge of a flat plate, it was possible to produce values of surface shear in the range studied by Townes allowing the intended comparative study to be carried out.

The data presented are in the form of velocity profiles, visual and photographic observations, and derived quantities such as shear velocities. It is believed to be sufficient to determine the characteristic features and differences of the flow in cavities exposed respectively to an outer laminar or turbulent flow.

As a "by-product" of the principal investigation some observations were also made on an instability in the shear layer above the cavity. These laminar oscillations were periodic and seemed to depend on the local velocities and cavity dimensions. These oscillations differ from those observed by Townes in the sense that they are periodic rather than random and do not materially affect the flow in the cavities.

In summary, the present work was performed to help in the formulation of a suitable model for cavity flows and to ascertain the causes of various phenomena observed in the turbulent regime as well as to determine the properties of laminar cavity flows.

II. REVIEW OF LITERATURE

Many investigations have been made to study the friction drop and heat transfer behavior for rough surfaces of various kinds. Much of this effort has been directed toward obtaining engineering data to permit efficient design of heat transfer surfaces. Some of the investigations have been concerned with the study of the flow near relatively large scale roughness elements. These latter investigations, many of which may be classified as cavity flow studies, are of primary interest here.

Most previous cavity flow investigations were experimental studies in turbulent flow. Since the flow over most heat exchange surfaces is usually turbulent, this type of flow is of primary engineering interest. The present experimental work is one of the few which was performed in laminar flow. The results of the turbulent flow investigations will be outlined here and will later be compared to those from the present laminar flow experiments. The basic differences between the two will then be discussed.

Historically the first comprehensive investigation of a rough surface was the study on pipe-friction by Nikuradse (29), published in 1933. Nikuradse constructed a rough surface by attaching sand grains to the inner wall of a pipe. The sand grains were nearly uniform in size and gave a close-packed, three-dimensional rough

surface. Turbulent flow of water was examined for most of the investigation. From the data, Nikuradse developed relationships for the frictional behavior in pipes as a function of Re and ϵ^*. Of special interest to the present investigation is the parameter ϵ^*, which is defined as

$$\epsilon^* = \frac{\epsilon u_\tau}{\nu} \qquad (2\text{-}1)$$

where ϵ is the sand grain size, $u_\tau = \sqrt{\tau_o/\rho}$ is the shear velocity and ν is the kinematic viscosity. The dimensionless quantity ϵ^*, which was found to govern the behavior of the friction coefficient, is a "wall parameter", formed entirely from quantities associated with the wall region. The present investigation is also concerned with flow conditions in the vicinity of the wall and therefore one should expect ϵ^* to be one of the principal parameters.

Nikuradse observed three characteristic regions for the friction coefficient and found it possible to specify these regions in terms of ϵ^*. For ϵ^* values ≤ 3.5 the friction coefficient of the rough surface was seen to be the same as that of a smooth surface. This region is called "hydraulically smooth". For values of ϵ^* between about 3.5 and 67 the friction coefficient deviates from that of a smooth surface, passes through a minimum and then increases toward a constant value. The region of $3.5 \leq \epsilon^* \leq 67$ is termed the "roughness transition" region. For values of $\epsilon^* \geq 67$ the friction coefficient remains fairly constant, independent of the Reynolds

number; the corresponding flow condition is called "fully rough".

In Nikuradse's work the parameter ϵ^* was based on the sand grain diameter ϵ. For different roughness types, for which ϵ is an arbitrarily selected characteristic size, the exact numerical value of ϵ^* at the boundaries of the flow regions described above may well be different. For transverse rectangular cavities, with which the present work is concerned, the cavity depth is taken as ϵ. Frequent use of the parameter ϵ^* will be made in the following sections when describing the behavior of the flow near the cavities. The range of ϵ^* for the present investigation is approximately 15 to 400.

A later investigation pertinent to the present work is the one by Folsom (13). Folsom used an experimental arrangement consisting of an annulus with series of disks of various diameters and spacings. The effect of these disks was to create an annular flow passage with thin fins on the inner cylinder. In effect, the geometry between the fins was that of a cavity similar to those examined in the present work. In addition to pressure drop measurements, Folsom also made some visual observations of the flow in the space between the annular fins. The flow in the annulus was turbulent. In "square" cavities between the fins Folsom found a single, fairly steady vortex. Of further interest was the observation by Folsom of a "pulsating flow" within the cavities, causing a fluctuation in the pressure drop across the test section. This occurred when the spacing of the disks formed an ϵ/L (cavity depth/cavity length) value of approximately 0.3.

Wieghardt (46) also has reported some visual observations of flow in single rectangular cavities on a flat plate with turbulent flow perpendicular to the axis of the cavity. Despite the differences in geometry, Folsom and Wieghardt observed quite similar flow conditions within the cavity; in both cases a single, fairly steady vortex formed in the "square" cavity. Wieghardt also reported some observations for ϵ/L values other than 1. In narrow cavities (for example $\epsilon/L = 2$) the space was occupied by two counter-rotating vortices, the lower or deeper vortex being very weak. The values of ϵ^* for this work ranged from approximately 1,000 to 10,000.

Roshko (34) studied the wall pressure distribution and measured local cavity velocities in a single rectangular cavity of fixed width and variable depth in a wind tunnel at 75 to 210 ft/sec. There was no large difference in the shape of the pressure distribution on the cavity walls for the two speeds, indicating little if any influence of the approaching turbulent boundary layer thickness. The maximum velocities of the vortex in the cavity were found to be in the range of 30 to 40 percent of the free stream velocity. Roshko also noted a fluctuation in pressure readings on the cavity walls in the ranges of ϵ/L from approximately 0.45 to 0.85 and from ϵ/L of 2 to 2.5.

The work of Maull and East (26) is of importance as it refers to certain pulsations and three-dimensional aspects of cavity flow. Using an experimental arrangement similar to that of Roshko, Maull and East conducted their flow studies by noting the pattern formed by

an oil film on the cavity bottom. From these observations Maull and East concluded that under certain conditions a three-dimensional cellular type flow occurs in the cavities. As evidence of this cellular structure they cite the curved shape of the oil film on the cavity bottom formed by the flow. Maull and East postulate that the unsteady pressures observed by Roshko and others were caused by the inability of the cavity spans to accommodate an integral number of the preferred three-dimensional cell spans, the cavity flow thus fluctuating between two flow configurations. Maull and East noted an absence of the cellular flow for $0 \leq \epsilon/L \leq \asymp 0.45$, $0.85 \leq \epsilon/L \leq 1.25$, $\epsilon/L > \asymp 2.2$. The findings by Roshko and Maull and East in regard to the stable regions are, therefore, in fair agreement.

Tani et al (43) investigated the distribution of surface pressure, mean velocities and fluctuating velocities in the flow over a backward-facing step and over rectangular cavities in turbulent air flow by means of piezometric orifices in the wall, small pitot probes and hot-wire apparatus. The free stream velocity was varied between 33 and 92 feet per second. The cavity studied had a depth, ϵ, of 1.58 inches and a variable length, L, of from 0.79 to 3.94 inches. Of primary interest to the present work are the measurements of Reynolds stresses near the cavity opening. These together with the measured velocity profile in this region permit estimates of the total shear stress acting across the cavity opening. Tani et al broadly divided the cavities studied into "deep" and "shallow", the demarcating value of ϵ/L being about 0.7. In deep grooves, the maximum

pressure on the downstream wall was found at the shoulder, indicating a smooth flow past the shoulder. In shallow grooves, the maximum pressure, corresponding to a stagnation point, occurred slightly below the shoulder of the downstream wall. The resulting flow around the angular shoulder led to higher values of drag coefficient C_d for the cavity.

Further studies of the flow in transverse rectangular notches were performed by Fox (15) in the range of ϵ/L from 0.57 to 4.0 by means of turbulence intensity measurements, mean-speed surveys, dust pattern observations and surface-pressure measurements. The free stream speed in the wind tunnel ranged from 160 to 600 feet per second. Typical notch dimensions were 1 to 2 inches and the span was 6 inches. For a velocity of 160 ft/sec the flow in the approaching boundary layer was laminar, a fact which was ascertained by turbulence intensity measurements. Fox also paid special attention to the free shear layer over the top of the notch. He observed a marked increase in u'/U_∞ above the free stream value quite close to the front edge of the notch (less than 0.08 inches) indicating transition to turbulence in the small region adjacent to the front edge. The fact that transition did occur was substantiated by the observed straight-line spreading of the free shear layer which is characteristic of turbulent free shear layers. The mean-speed traverses of the cavity also showed the presence of cavity vortex velocities of the order of 35 percent of the free stream velocity.

A series of heat transfer and friction studies for finned annular tubes was conducted by Knudsen and Katz (22) who also visually examined the flow between the annular fins. The observations for turbulent flow were similar to those of Folsom; however, Knudsen and Katz actually extended their work into the laminar flow region. These laminar studies which are particularly pertinent to the present work show that the dye, used for visualization, does not enter the space between the fins even though it is introduced very close to the fin tips. This indicates very poor exchange of fluid between the cavity and the outside flow which may be contrasted with the very good exchange of fluid across the cavity opening noted by other investigators for turbulent flows.

Velocities inside square cavities were also measured by Mills (27, 28). The outside stream was turbulent and the average velocity at the cavity interface was shown to be about 55 percent of the free stream value. Additional rather ingenious experiments are reported where the cavity flow motion was generated by the action of a flat belt passing over the open side of the cavity.

Mills also offered an analytical solution for the cavity flow on the basis of a model comprising an inviscid core surrounded by a spatially periodic boundary layer. An analysis was also performed by Burggraf (2) who calculated the cavity flow field and pressure field using Batchelor's (1) model of an inviscid rotational core separated from the external flow by a recirculating viscous shear layer. This model is said to apply for relatively large cavity dimensions and

moderate ϵ/L. Burggraf furthermore calculated the pressure and flow fields for deep cavities, where the recirculation becomes negligible, using Chapman's model (3) of a free shear layer, and its extension by Denison and Baum (10) to include the boundary layer upstream of separation.

Special mention is to be made of the work of Dipprey (11, 12) which, in a way, served as an incentive for the present study. Dipprey measured heat and momentum transfer in smooth and rough tubes in a turbulent water flow. The rough tubes contained a close-packed, granular type of roughness with roughness-height-to-diameter ratios ranging from 0.0024 to 0.049. The Prandtl number range of 1.20 - 5.94 was investigated and the Reynolds number range was from 6×10^4 to 5×10^5. Increases in heat-transfer coefficients C_h due to roughness of as high as 270 percent were obtained. These increases were, in general, accompanied by even larger increases in friction coefficient C_f. However, an exception to this general behavior occurred at high Prandtl number in the region of transition between the "smooth" and "fully rough" flows where values of $2C_h/C_f$ greater than those for corresponding smooth tubes were observed.

Dipprey's results stimulated interest in the flow around roughness elements. As a consequence Townes (44, 45) initiated studies of the flow around roughness elements under conditions similar to those occurring near the wall of a pipe. The transverse square cavities of Townes were to represent simplified roughness

elements. The roughness sizes ranged from 1/8 to 1 inch and the free stream velocities in the open surface water channel varied from 0.1 to 0.75 ft/sec. Velocity profiles taken with a hot-film anemometer showed the flow approaching the cavities to be turbulent. The range of ϵ^* covered was from 11 to 260. Ratios of slot depth to laminar sub-layer thickness as low as 2 or 3 were obtained with the physical dimensions sufficiently large to allow convenient visualization. The visualization study of the cavity flows led to the classification of five characteristic flow modes. When the slot size exceeded the thickness of the laminar sub-layer by a factor of about 20 ($\epsilon^* > 200$) a more or less steady vortex pattern would form in the slots. This is the pattern that had been observed by most investigators mentioned previously. However, for ϵ^* values below 100 the flow in the cavity was subject to random disturbances; a fairly steady vortex pattern would form only to be destroyed almost completely by the disturbances. The instantaneous appearance of the cavity flow pattern could be described in terms of four fairly well distinguishable patterns which were denoted as "inflow", "divide", "weak exchange" and "strong exchange". As mentioned earlier, it is to these findings that the results of the present work in laminar flow are to be compared.

III. EXPERIMENTAL APPROACH

A. Apparatus Criteria

As has already been mentioned in the introduction, the major purpose of the present laminar flow work was to serve as a comparison study to Townes' cavity flow investigation in a turbulent flow. Thus it was desired that the flow conditions outside the cavities correspond to those of Townes' study in all respects except that the turbulent fluctuations be absent. This of course is not entirely possible since, for a given wall shear, laminar flow requires a different boundary layer thickness than turbulent flow even though the free stream velocities may be the same. Similarly the length for the development of the boundary layers will differ. Hence the question arises as to which parameters should be maintained constant for a comparison study and which should be allowed to change.

Since wall parameters were considered to be of greatest influence in cavity flows the wall shear or equivalently the shear velocity was selected as the primary parameter to be maintained constant in the comparative studies. Also since flow visualization and local velocity determinations were to be made, an adequate cavity size was required. A nominal size range of from 1/8 to one inch, which corresponds to that of Townes, was specified. Furthermore, due to the desire for maintaining laminar flow the free stream

velocity range was bounded. Preliminary calculations, shown in the Appendix, determined the required boundary layer development length, the free stream velocity range and the corresponding boundary layer thicknesses. On the basis of these requirements the test apparatus described below was selected.

B. Water Tunnel

With the above requirements in mind, the low-speed, low-turbulence water tunnel in the Keck Laboratory of Hydraulics and Water Resources was found to be most suitable for the intended experiments. A photograph of this water tunnel is shown in Figure 1, and a diagram of the flow circuit is shown in Figure 2.

The working section, which is 105-3/8 in. long, is 12 in. x 12 in. in cross section at the upstream end and 12 in. wide x 14 in. high at the downstream end. The side windows, which are of 1-1/4 in. thick plate glass, are parallel to each other and 12 in. apart. The top and bottom windows are of Lucite and are removable to permit access to the working section. In fact, for all of the present work the top windows were removed and the water tunnel was operated as a free surface channel.

The nozzle upstream of the working section is square in cross section, being 46 in. x 46 in. at the inlet end and 5 ft. long. Upstream of the nozzle there is a prismatic section 46 in. x 46 in. in cross section and about 4 ft. long which contains three turbulence damping

screens woven of 0.018 in. diameter wire with 18 meshes to the inch. A sheet metal honeycomb baffle with equilateral triangular passages about 1 in. in altitude and 7 in. long is located at the upstream end of the prismatic section. The first two vaned elbows upstream of the nozzle are also 46 in. x 46 in. in cross section, and differ only in the size and number of turning vanes at the corners. The vanes in the first elbow upstream have a spacing of about 1 in. and a chord length of 2-7/8 in. Those in the second elbow are spaced at 3-7/8 in. and have a chord length of 11 in. The flare angles of the diffusers (downstream of the working section and in the return pipe) are small (about 5 degrees, or less) so that there is little likelihood of separation of the flow.

The water is circulated by a 30-in. pump of the mixed flow type. The pump is driven by a 30 h.p. direct current motor through a vee-belt transmission. The water velocity in the working section is controlled by the motor speed, which is in turn controlled by varying the field current.

In order to take satisfactory photographs and to make hot-film anemometer measurements it was necessary to keep the water clean. The principal device for accomplishing this was a filter with diatomaceous earth on cylindrical porous stones as the filtering elements. This filter, which had a capacity of about 30 gallons per minute, was on a by-pass circuit in parallel with the lower portion of the tunnel circuit and was operated almost continuously when the program was in progress. Also an algaecide was added to the water to retard

the growth of micro-organisms.

In order to reduce the air content of the water without constructing a de-aeration facility the tunnel was filled with hot tap water through the filter system. After circulating the water in the tunnel for about three days the water temperature dropped to room temperature (approximately 68°F) at which time the series of experiments was started. It was found that in this way the air content of the water would remain sufficiently below saturation to permit hot-film anemometer measurements for two to three weeks before it was necessary to change the water.

With the motor-pump coupling used for the experiments, stable water tunnel operation was obtained for a free stream velocity range of from 0.125 to 2.0 ft/sec. Below these speeds the motor speed was not steady. Above these speeds the free surface became rippled. The average free stream velocity was determined by timing the displacement of dye droplets over known distances. The dye droplets were introduced approximately one foot ahead of the initial measurement station to eliminate free surface effects. The displacement intervals were selected such that the time intervals were at least five seconds. Individual timings over these intervals were reproducible to within ± 0.1 sec. in most cases. The free stream turbulence level was found to be less than 0.6 percent in all cases.

C. Initial Tests on Channel Bottom

As the calculations in the Appendix show, one would expect the boundary layer to be laminar for a distance of at least 2.0 feet at a free stream velocity of 1.2 ft/sec. In a first attempt the possibility of using the bottom of the test section itself as the test surface was investigated. At a station 1 foot from the entrance to this section velocity profiles and turbulence intensities were measured to determine the nature of the boundary layer at this station. A linearized hot film output signal that was proportional to the velocity was recorded on a Sanborn recorder. These traces showed a turbulence intensity of as high as 5 percent in the boundary layer for 0.9 ft/sec. From these observations it was concluded that the boundary layer was in the transition range and that it started to grow at some rather large distance upstream of the test section entrance, probably at the screen section that was approximately 9 feet upstream. Thus the floor of the test section was abandoned as a possible test surface.

D. Flat Plate at Channel Centerline

As the channel bottom was not considered suitable, a flat plate mounted near the centerline of the channel was taken as the test surface instead. A photograph of the working section with this plate in place is shown in Figure 3.

The plate was supported between the two vertical walls of the test section by 2 x 2 x 1/4 in. aluminum angles. The leading edge

of the flat plate was 1 foot downstream of the entrance to the water tunnel working section. This distance was selected since it keeps the influence of the side-wall boundary layer at a minimum and still permits easy access to the plate. The leading edge portion of the flat plate was cantilevered for 3 inches ahead of the support angles, the plate being mounted on top of these angles. Thus the flow field above the plate, the region of interest, was not influenced by the support angles.

The flat plate itself consists of three sections of 3/8 in. thick plexiglass each 12 in. wide, thus spanning the entire channel and dividing the channel flow into two regions. The leading edge section was 9-1/2 in. long and was fitted with a 2:1 elliptical nose. The central section was 12 inches long and contained a 7 in. wide x 7 in. long x 2 in. deep chamber in which several different inserts could be mounted. One of the inserts was a solid block resulting in a smooth and unbroken surface for the entire plate. The other inserts were provided with different transverse slots or cavities. The aft section was 12 in. long and terminated in a semi-circular trailing edge. To insure the smoothness of the entire plate the three sections were mounted and then sanded smooth while in place.

The 2:1 elliptical leading edge was selected after considerable experimentation. Initial attempts to use a sharp or a semi-circular leading edge led to boundary layer separation at approximately 1 in. behind the stagnation point. With the elliptical nose the separated region became intermittent showing that the problem was almost

solved. To insure complete suppression of separation it was found necessary to slightly tilt the nose of the plate downward. A slope of 0.009 was found to have the desired characteristic of complete suppression of separation at all velocities. This slope was maintained throughout the work discussed in this thesis. The slope plus the boundary layer growth of course produced an acceleration of the fluid as it flows over the plate. The magnitudes and effects of this acceleration are discussed in Chapter IV.

E. Description of Cavity Geometry

As mentioned earlier the interchangeable cavity plate inserts fit into the 7 in. wide x 7 in. long x 2 in. deep chamber in the central section of the flat plate. Figure 4 shows the cross section of one of these cavity plates. The insert plates were set on blocks within the chamber and held in place by 5 screws which thread into the chamber bottom. The mounting blocks were shimmed until the rib of the first cavity was within 0.001 inch of the flat plate surface. The upstream wall of the chamber formed the upstream wall for the first cavity of the series for all cavity sizes. Beeswax was used to fill the small gaps between the chamber and the cavity plates.

The cavity sizes in the plexiglass inserts were 1/8 x 1/8 in., 1/4 x 1/4 in., 1/2 x 1/2 in. and 1 x 1 in., respectively. The ratio of cavity depth, ϵ, to cavity length, L, was 1.0 for most cavity plates. The ratio of cavity depth to rib length was 1/2. The span, s, of the cavity plates was 7 inches; hence the ratio s/ϵ varied between

7 and 56 for the different cavities. Thus the cavity span was sufficiently large to have an essentially two-dimensional flow near the middle of the span.

For several exploratory tests ribs were either removed or added to form 1/2 in. deep x 1-1/4 in. long cavities with a 1/4 in. rib length and 1 in. deep x 1/2 in. long cavities with a 1/4 in. rib length.

F. Description of Dye Injection Systems

In order to make flow visualization studies dye was injected into the flow at various locations around the cavities. The dye solution was stored in a 5 gallon polyethylene bottle, which was suspended approximately 4 feet above the flat plate. From there the dye flowed through polyethylene tubing to a six-port distribution manifold. The valves in the manifold were adjustable to control the injection velocity of the dye. From the manifold the dye flowed through 0.055 in. I.D. polyethylene tubing to the injection orifices.

The injection orifices consisted of 0.025 in. diameter holes drilled through the plexiglass cavity plates. All orifices were located on the spanwise centerline of the cavity plates. Orifice No. 1 was common to all cavities and was located 1/8 in. upstream of the leading edge of the chamber. Orifice No. 2 was located in the center of the first cavity bottom. Orifice No. 3 was located in the center of the downstream wall of the first cavity. Orifice No. 4 was located in the center of the first rib. Two other orifices were located on two

ribs further downstream to observe the effect of successive cavities.

A black aniline dye was used. The dye solution was checked for neutral buoyancy by placing drops in a beaker of water. If care was taken in placing the dye drops in the water the water dye solutions were found to remain at almost the same level for several minutes, the effect of currents in the water being as great as the effect of gravity. However for some of the denser dye solutions used at higher velocities the drops would steadily sink at rates of up to .002 ft/sec. This small sinking rate is less than 0.5 percent of U_∞ at the velocities at which the denser dye solutions were used.

The injection velocity of the dye through the orifices was carefully controlled to insure that the dye stream would not affect the existing flow. The valves in the distribution manifold were regulated so that the dye just seeped out of the orifices to be carried away by the main flow. The method of arriving at the proper dye injection velocity was one of trial and error.

In order to study the three-dimensionality of the flow a special cavity insert, similar to the previous 1/2 in. x 1/2 in. insert, was prepared. Figure 5 shows the cross section of this insert plate which has a span of 7 inches, and is provided with two injection slots along the full span of the cavity. A uniform steady flow through the slots was observed for a gap spacing of 0.007 in. for the entire velocity range examined (0.125 to 1.0 ft/sec). Again the flow of dye was regulated by valves in the distribution manifold. To make the observations, the dye in one of the slots was turned on for several

seconds and then shut off. The flow pattern of the dye sheet could then be observed.

In addition to injecting dye as described above, the flat plate was seeded with finely ground potassium permanganate crystals as an alternate method of making the flow visible. A solution of the potassium permanganate crystals and water was injected to the desired locations on the flat plate with the aid of a hypodermic syringe having a 1/16 in. I.D. tube. This seeding method was particularly suitable for observing the flow upstream of the cavity section and for studying the side-wall boundary layer effects.

G. Photographic System

As an aid in analyzing the flow patterns and flow phenomena that occur in and near the cavities both still photographs and motion pictures were taken. Several of these photographs and motion picture strips are shown and analyzed in Chapter V and VII.

All photographs were taken through one of the test section walls. The lens axis was set at an angle of approximately 20° from the horizontal. The lens system was sharply focused on the spanwise center of the first cavity, the plane of the dye injection. Points outside this plane thus gradually became out of focus.

The lens system consisted of a 165mm focal length achromatic lens mounted on the front of a 2-foot long bellows and a still or motion picture camera placed at the rear of the bellows. Both front and rear bellows plates were movable. With this arrangement it was possible

to adjust the field of view for both cameras from between 1/4 x 3/8 inch to 1-1/2 x 2-1/4 inch. This was more than sufficient to insure optimum photographic conditions. The depth of field was of the order of 1/2 inch for most photographs. The lighting for photography was provided by a single 1500 watt floodlamp placed 2 feet above the flat plate.

The still pictures of the flow field in the cavities were taken with a 35mm camera through the lens system described above. All photographs included the first cavity within the field of view and were focused on the dividing streamline made visible by the dye emanating from dye orifice No. 1. To obtain the pictures the dye injection from orifices No. 1 and/or No. 2 was started once the desired free stream velocity had been obtained. As soon as there was a sufficient and steady dye flow, a series of photographs was taken, showing more and more dye in the cavity in successive pictures. The photograph best showing the cavity flow pattern was selected from these for each set of test conditions.

The motion pictures were necessary to record and to permit the analysis of the laminar oscillation that was found to occur in the shear layer at the top of the cavity for certain velocities and cavity sizes. Since the magnitude of the oscillation was best suited for timing in the second cavity the motion pictures were taken of this cavity. Since the oscillation frequencies were in the range of 1 to 12 cycles per second a standard 16mm motion picture camera with a framing rate of from 10 to 64 frames per second was found to be suitable.

To obtain these pictures the dye injection from orifice No. 1 was started and as soon as sufficient dye was present to make the oscillations visible the motion picture camera was started.

To obtain the oscillation frequencies from the motion pictures the film was analyzed frame by frame and the total number of frames per 50 cycles was recorded. The framing rate was determined by recording the time required to expose 400 frames. From these the frequency was determined. It should be pointed out that for the lower frequencies the use of motion pictures was unnecessary, as it was possible to time a given number of cycles by direct observation.

H. Measurement of Local Velocities

The measurement of low local velocities in water presents serious difficulties, but these were precisely the velocities that were to be measured in the present experiments. The three fundamental methods of velocity measurement, involving either the pitot tube, tracer particles, or hot-film anemometers (or hot-wire anemometers), all have serious drawbacks when used to measure water velocities in the range that exists in the present experiments. In this range ($u < 1.00$ ft/sec and frequently $u < 0.10$ ft/sec) accurate pitot tube readings are most difficult to obtain because of the low velocity heads involved. Since for the present study the total boundary layer thickness is less than 0.5 inches, even for the lowest free stream velocity, tracer particles are difficult to locate and follow with the required accuracy. This leaves the hot-film method which also is by no means trouble-free

if water is the working fluid. Nevertheless, this method had the most promise and consequently was selected.

The hot-film system offered the great advantage in that the position of any given velocity measurement could be accurately determined since the size of the velocity sensing element was quite small compared to the extent of the boundary layer. In all of the present work the sensor diameter was 0.001 in. which corresponds to a minimum of 200 sensor diameters per boundary layer thickness and 125 sensor diameters for even the smallest cavity. Furthermore, the active sensor length was only 0.10 in.

Among the disadvantages of the hot-film system in water is that the surface of the hot-film must be kept below the water temperature at which air comes out of solution. Air bubbles on the sensor surface inhibit the heat transfer mechanism on which the velocity determination as well as the calibration of the instrument depend. This seriously limits the allowable overheat (i.e., temperature difference between the hot-film and the surrounding water) on which the accuracy of the measurement depends. This low overheat limitation therefore imposes stringent requirements on the stability of the sensor. At low overheats a very slight shift in the resistance of the sensor caused by a deterioration of the film produces relatively large changes in the velocity calibration and as a consequence it was necessary to perform continual calibration checks during operation.

The hot film probes were commerically available.[2] Figure 6 shows the sensing element and a portion of the supporting needles of one of these probes. Figure 7 shows the cross section of the active portion of the sensor. The sensing element consists of a 0.001 inch diameter Vycor glass tube, a 1000 angstrom thick layer of platinum deposited on the tube (the active resistive element), and a 12,000 angstrom thick sputtered quartz coating. The quartz coating is required for operation in water in order to electrically insulate the current-carrying platinum film from the conductive water and to protect the sensor from chemical attack. The advantage of a hot-film sensor over that of a quartz coated wire is that a sufficiently high operating resistance is obtained while the size of the element is large enough to give it mechanical strength. The element was sufficiently strong to allow even cleaning and bubble-removal with a soft brush.

The hot-wire anemometer set used for the experiments was a modified Shapiro and Edwards model 60B. The circuit diagram is shown in Figure 8. The hot-wire set output signal is proportional to the current required to maintain a given sensor temperature. To a good approximation this current is related to the flow velocity past the sensor by the well-known King's Law (7, 21):

$$Nu = A + B\,Re^{\frac{1}{2}} \qquad (3\text{-}1)$$

---

[2] From Thermo-Systems, Inc., 2500 Cleveland Avenue N., St. Paul, Minnesota.

where Nu is the Nussult number, Re is the Reynolds number of the wire, and A and B are constants involving hot-film and fluid properties. This equation can be written in a more useful form for the present work as:

$$u = \left[(C_1 e_i)^2 - C_2\right]^2$$

where e_i is a voltage proportional to the current to the hot film, u is the fluid velocity past the sensor, and C_1 and C_2 are again constants involving hot-film and fluid properties.

For calibration purposes and for ease in data reduction, it was advantageous to record a signal that was directly proportional to the fluid velocity. To accomplish this the signal from the hot film was processed through a linearizing circuit. The operations are described below.

(a) The hot-film output was amplified to a convenient level.

(b) This signal was then squared by means of a quadratron circuit.

(c) From the output of (b) the constant C_2 was subtracted by means of a bias voltage. This constant corresponded to the natural convection component at the given temperature difference. To determine the required bias voltage the sensor was immersed in a 4 in. high, 1 in. I.D. tube filled with water from the water tunnel. Then the bias voltage was adjusted until the output of the sum of the squared hot-film signal plus the bias voltage was zero.

(d) The probe was then replaced in the flowing fluid. The signal $(C_1 e_i)^2 - C_2$ was then squared by another quadratron circuit. The result was proportional to the velocity u according to Equation (3-2).

(e) Part or all of this output signal could be biased by an accurately known voltage to obtain greater reading accuracy in the measurement of the output voltage. This bias voltage was obtained from a calibrated -300 V to +300 V power supply built into the linearizing system.

The linearizing circuit which performed the above functions is shown in Figure 9. The voltages at various stages of the linearizing circuit were read from a Hewlett Packard Model 425A DC Micro Volt-Ammeter by means of a 1000:1 divider probe. This voltmeter was calibrated against accurately known standard voltages. The possible reading error of the voltmeter scales was less than ± 1 percent in all cases.

For the velocity profile measurements the hot-film probe was positioned by the traversing mechanism shown on Figure 10. This piece of apparatus was equipped with a micrometer feed which was accurate to within ± 0.0005 inches. The initial determination of the distance y_1 from the center of the sensor to the flat plate ($y = 0$) was accomplished with the aid of a brass pointer, shown on Figure 11, which was made to touch the flat plate (or the cavity bottom for cavity profiles). The distance y_1 between the pointer tip and the center of the sensor was previously measured by an optical comparator to

within 0.0001 in. After the initial determination of the probe zero point the pointer was of course removed. To obtain a further check on the accuracy of positioning the pointer was reset and the pointer-sensor distance remeasured after the velocity profile had been taken. In all cases the error was less than ±0.0005 in. Thus the maximum possible cumulative error in position was estimated to be less than ± 0.001 in.

To determine the velocity at a given point in the boundary layer or in the cavity the procedure presented below was followed. First the specified free stream velocity was attained by adjusting the speed of the circulating pump of the water tunnel. In this way the desired velocity could be obtained to within ± 1 percent. The average free stream velocity was then measured by timing dye droplets for a known distance as described earlier. Five readings were taken. Only when the five readings were within ± 0.1 sec. of the mean was the tunnel considered at steady state conditions and ready for tests. At this time the hot-film cold resistance of the sensor was measured, the 4 percent overheat (defined in terms of the increase in electrical resistance) was set, and the hot-wire instrument was balanced (at the free stream velocity). The pre-amplifier gain was adjusted to the proper output level for the successive amplifiers. The sensor was immersed in the tube and the bias voltage was adjusted to read zero output. The sensor was replaced in the free stream and the second stage amplifier gain was adjusted to a convenient output level. The output of the third stage

was now proportional to any velocity in the range from zero to free stream.

To check the proportionality of the third stage output to velocity, a series of calibration tests was performed. These tests were conducted in a tow tank, the probe being towed on a carriage being driven by a variable speed D. C. motor regulated by a speed control. The true towing velocity of the probe was determined by timing the probe travel over known distances. Four calibration tests were performed, each having a maximum velocity that corresponds to one of the four free stream velocities of the main test series (U_∞ = 0.125, 0.250, 0.50 and 0.75 ft/sec). The maximum velocity and zero velocity were taken to balance and adjust the system parameters by a method analogous to that used in the velocity profile runs. The water in the tow tank was siphoned from the water tunnel to insure comparable operating conditions. The overheat in all calibration tests was about 4 percent. Typical results for these calibration tests are shown in Figures 12 and 13, each corresponding to one of the desired maximum velocities.

These figures are plotted with $(u/U_\infty)_i$ as the abscissa and $(u/U_\infty)_t$ as the ordinate. The subscript i refers to the so-called indicated velocity which is computed from the electrical signal of the hot-film system assuming King's law to hold and perfect operation of the entire hot-film system. The velocity u_t is based on the speed of the carriage in the tow tank. This was the most convenient form for applying the calibrations to the data. The quantity $\left[(C_1 e_i)^2 - C_2\right]^2/$

$\left[(C_1 e_{i\infty})^2 - C_2\right]^2$ is ideally equal to the ratio (u/U_∞), i.e., if the above-mentioned assumptions are strictly obeyed for the entire range of velocity. In that event the $(u/U_\infty)_t$ vs. $(u/U_\infty)_i$ curve should be the 45° line shown on the calibration curves. The deviation of the experimental calibration curve from the 45° line indicates the extent to which these requirements are not satisfied.

The calibration curves show good reproducibility for the data taken before and after the velocity profile measurements. This insures that the particular probe and the adjustments of the electrical apparatus used for the measurements did not change or deteriorate during the course of the measurements. It also lends credibility to the fact that the exact overheat is not a critical variable in the reproducibility of data since the overheat could only be set to within ± 2 percent of the desired value, i.e., (4.00 ± 0.08) percent overheat. This is further substantiated by some of the data on Figure 12 which was taken by James (20) in distilled water using a different probe (of the same size) and at 5 percent overheat.

Although it has no direct bearing on the accuracy of the velocity measurements, some thought was given to the possible causes for the deviation of the calibration curve from the 45° line. It was concluded that the electronic system of the hot-film was most likely responsible. This conclusion was supported by the results of a separate series of tests on the heat transfer from the sensor by James (20). In these tests there were definite indications that in the low velocity range the control system allowed the wire temperature to deviate in a systematic

way from the selected value. Consideration was also given to the possibility that King's law may not be sufficiently accurate at the low heat transfer rates, to possible wall effects for readings taken close to the surface, and to the limitations of the electronic squaring circuit. None of these effects is believed to be responsible for the observed deviations. This opinion is based in part on experimental tests conducted as part of the present work and on information given in the literature on the convection from wires. The references in the literature include studies on the effect of the proximity of the wall and in addition a full series of calibration tests was performed in this laboratory with the velocity sensor located from 3 to 20 diameters from the wall.

The principal non-systematic errors stem, of course, from the low overheat allowable with water and the stringent requirements which, therefore, have to be placed on the stability of the amplifiers and the electrical properties of the sensor. One particular hot-film sensor was found to be superior in this respect and almost all of the velocity measurements reported herein were taken with this unit. Considering all the uncertainties the error in the velocities is estimated to be less than ±3 percent of the free stream value.

I. Recording of Instantaneous Velocities

As one check to determine if the boundary layer was indeed laminar a series of experiments was performed in which the output of the linearizing circuit (proportional to the velocity) was recorded

by a Sanborn recorder. In these tests most of the linearizing circuit output was cancelled out by a bias voltage. The remaining signal was then applied successively to a Sanborn model 150-1000 AC-DC pre-amplifier, a Sanborn model 150-200B driver amplifier, and a Sanborn model 152-100B recorder. The low biased input signal allowed the use of sensitive scales of the instruments to aid in the detection of turbulent bursts. The entire boundary layer was traversed for all four free stream velocities at which experiments were conducted. Stations 1/4 inch ahead of the cavity, in the center of the cavity, and on the center of the rib behind the cavity were examined. The frequency response of the above combination of instruments is flat between 0.4 to 50 cycles/second with a rise time of 10 milliseconds. The sensitivity is variable between 1 mv. to 2 volts per millimeter. The system did prove suitable for the intended measurements and the results are discussed in Chapter IV.

IV. FLOW CONDITIONS

A. Instantaneous Velocity Measurements

Prior to taking the hot-film velocity measurements and studying the flow structure in the cavities it was necessary to firmly establish the flow conditions ahead of the cavities. Most importantly it was necessary to establish that a laminar boundary layer indeed existed ahead of the cavity. To obtain this information several series of preliminary experiments were performed.

Based on the results published in the literature one would expect the boundary layer on the flat plate immediately ahead of the cavity to be well within the laminar flow regime as for the present experiments the Reynolds number based on the free stream velocity, U_∞, and the distance from the leading edge, x, is below 75,000. This number is well below the figure of 300,000 which is characteristic for the laminar-turbulent transition of the boundary layer.

In order to examine the type of flow more directly instantaneous velocity studies using the Sanborn recorder were performed to indicate any possible presence of turbulence. Measurements taken ahead of the cavities for the two lowest free stream velocities ($U_\infty = 0.125$ and $U_\infty = 0.250$ ft/sec) showed no signs of any velocity disturbances. The run at $U_\infty = 0.500$ ft/sec showed only 6 velocity disturbances in about one-half hour that might be classed as turbulent

bursts. These disturbances occurred in the boundary layer between y = 0.05 in. and y = 0.20 in. Their average duration was 5 seconds (approximately 3 maxima in this time) and the average rms intensity observed, defined as $\frac{\sqrt{\overline{u'^2}}}{u}$, was about 2 percent. A tracing of the strip chart showing two such disturbances is shown in Figure 14. The U_∞ = 0.75 ft/sec run also showed only occasional turbulence-like patches in the boundary layer between y = 0.05 in. and y = 0.175 in. The average rms intensity observed was about 1.75 percent and the peak-to-peak period averaged 1.7 seconds with the number of patches approximately twice as frequent as for the U_∞ = 0.50 ft/sec case.

Similar series of instantaneous velocity records were also taken in the center section of the cavities and on the center of the rib behind the cavity. The results of these measurements were similar to those just upstream of the cavity. In general no increase in the intensity nor in the frequency of occurrence of the random disturbances was noted.

It was concluded that the flow in the boundary layer at the cavity station and for velocities below 0.75 ft/sec was laminar and free of significant disturbances. The occasional fluctuations are believed to be "patches" of turbulence which occur as a forerunner of transition, or possibly amplified disturbances originating in the main stream and carried by the circulation system.

B. Flat Plate Transition Studies Using Potassium Permanganate Seeding

As an independent test to study the existence of laminar-turbulent transition on the flat plate, the cavity section was covered with the smooth insert and potassium permanganate crystals were seeded at various locations. The potassium permanganate crystals were crushed with a mortar and pestle until their size was less than 0.004 in. in diameter so that the crystals themselves would not disturb the flow appreciably. These small crystal fragments were then deposited at the desired location on the flat plate by injecting them, mixed with water, through a hypodermic needle with a 1/16 inch internal diameter. The dye trails of the crystals could then be studied. A laminar streakline spread quite slowly due to diffusion making the region from $y = 0$ to $y = \approx 0.02$ in. visible. Any turbulent burst (similar to those observed by Runstadler, et al (36) in the laminar sublayer of a turbulent boundary layer) was readily discernible as a rapid movement of the dye filament normal to its usual line of travel. For these tests dye crystals were deposited at $x = 2$ in. and $x = 20$ in. In addition the cavity dye system orifice No. 1, 1/8 inch upstream of the normal cavity location, was used to determine the flow properties along the channel centerline immediately upstream and across the normal location of the cavities.

The span of the plate may be divided into a central portion and the two outer portions which were influenced by the side walls of the channel. The undisturbed central portion was the one of importance

for the present investigations. The regions of influence of the boundary layers which were growing on the side walls of the channel were restricted to the outer portions. These boundary layers which start a considerable distance upstream of the test plate became turbulent within the velocity range of this test series. The outer portions spread as the velocity was increased thus encroaching on the central portion.

The observations showed that at velocities up to about 1.0 ft/sec the entirely laminar central portion had widths of 6 in. at x = 24 in. and 10 in. at x = 12 in. At velocities of about 1.5 ft/sec the portions influenced by the side-wall boundary layers extended to the center of the plate at x = 24 in. The point at which the two outer portions met moved upstream with increasing velocity. At the position at which most of the experimental work was performed (x = 12 in.) the central laminar portion was about 3 in. wide even at the highest flow rate (U_∞ = 1.75 ft/sec). No measurements were made, however, at velocities above 1.75 ft/sec, because of the waviness of the free surface beyond this speed.

C. Cavity Potassium Permanganate Seeding Studies

Flow visualization tests by means of potassium permanganate seeding as well as by dye injection were also performed with one of the cavity inserts in position (four 1/2 in. deep by 1-1/4 in. long cavities). This study was performed to investigate the effect of the cavities themselves on the turbulent transition. The permanganate

crystals were seeded at x = 2 in. and x = 20 in., the latter being just downstream of the cavity section.

Concentrating on the central 10-inch portion of the plate no bursts indicative of turbulent transition were observed for velocities from 0.23 to 0.38 ft/sec. All streaklines from the individual dye crystals remained coherent and showed only laminar characteristics to the end of the entire 33-1/2 in. long plate.

At about 0.4 ft/sec a weak oscillation was detected near the interface of the last cavity. As the free stream velocity was increased to about 0.5 ft/sec the oscillation became stronger and the third cavity began to show some activity. In addition the flow downstream of the cavities began to look quite turbulent with the dye being rapidly dispersed. This turbulent-like condition was first observed downstream of the cavities and then moved upstream as the velocity was increased until it occurred as far upstream as the last cavity for $U_\infty = 0.5$ ft/sec.

From $U_\infty = 0.50$ to 0.75 ft/sec all cavities exhibited the laminar oscillation, the magnitude of the oscillation increasing with increasing free stream velocity and with increasing x. In this velocity range the flow downstream of the mid-point of the cavity insert plate showed considerable turbulence as evidenced by the swirling dye motions and the rapid disintegration of dye filaments. In fact it was necessary to also seed permanganate crystals at x = 10 inches in order to obtain a sufficient dye concentration to observe the dye filaments in the cavity region. However, the flow within and immedi-

iately above the first two cavities did not show evidence of turbulence. The flow in these cavities showed a standing vortex pattern with no random motions characteristic of turbulence. In this velocity range the influence of the turbulent side-wall boundary layer penetrated to within the sides of the cavities (2-1/2 inches from the wall). In fact for the highest velocities the outside 1/2 inch of the 7-inch wide cavities showed signs of turbulence indicating a side-wall boundary layer influence on the cavity flow.

As the free stream velocity was increased from 0.80 to 1.75 ft/sec, the turbulence became more evident over the cavity section and everywhere within the cavities. The three-inch wide central portion of the first cavity did not show signs of turbulence until U_∞ approached 1.0 ft/sec.

In summary one should note that for even the highest velocities examined here (over twice the maximum primary test velocity) transition did not appear to occur ahead of the cavity section in the central three inches of the channel. Furthermore, the central three inches of the first cavity, the only one studied in subsequent tests, did not show evidence of turbulence in the range of the primary test velocities.

D. Side-Wall Boundary Layer

Although, as pointed out in the previous section, the boundary layers on the side walls do not interfere with the experiments, a brief description of these layers will be given.

The boundary layer on the side walls of the channel begins to grow somewhere in the settling chamber upstream of the nozzle. As the flow passes through the nozzle (approximately 5 feet) and through the upstream two feet of the test section the side-wall boundary layer continues to grow. By the upstream end of the cavity section this boundary layer has been growing for approximately 10 feet and it is turbulent along the side walls of the test section for most of the velocities used in the experiments. This fact was verified by seeding permanganate crystals on the side walls (small crystals clung to the vertical walls) and noting the turbulence in the dye streaks. This turbulence was noted even at the entrance of the working section for a velocity of 0.25 ft/sec. It may be pointed out that the boundary layer on the channel bottom (a similar boundary layer growth length for this case) is also turbulent as indicated by the preliminary tests described in Chapter III.

E. Free Surface

The channel test section had a height of 12 inches and was operated as a free surface channel. Since the test plate was mounted on the centerline of this channel it was located only 6 inches below the free surface and the question arose as to whether the free surface would have any effect on the results.

There are several reasons why the effect of surface tension and secondary flow phenomena at the free surface can be neglected, even though such phenomena were observed. (For instance, at

U_∞ = 0.125 ft/sec dye and dirt particles on the surface would flow upstream, not just relative to the free stream but also absolutely with respect to the channel walls.) The first reason, and probably the most important, is that the flow character being examined, namely the interaction of cavities with a laminar boundary layer, should depend strongly on only the properties of that boundary layer rather than on the free stream portion of the flow. The properties of the boundary layer that are used for the evaluation are physcially measured and would automatically include any effects of the proximity of the free surface. Secondly, velocity measurements made in the free stream show a 5 inch high region of uniform velocity between the boundary layer and the free surface, indicating that the surface effects do not seem to penetrate deeply.

The above is true, however, only as long as the free surface does not form any significant waves as some effects of these are transmitted through the free stream portion of the fluid and affect the boundary layer. It was noted for example that the fluid near the plate was set in motion when the surface was manually agitated such that waves of about 1/8 inch height were produced. The effect of these waves was found on the velocity records of the hot-film measurements and was also visually observable in the dye traces over the cavities. It was found that these waves would damp out in a period of from one to three minutes. Waves of smaller amplitude did not produce an observable effect in the boundary layer. It was found that without intentional agitation the free surface was smooth to the degree that it

produced no observable effect for velocities of less than 1.75 ft/sec which is well above the range of test velocities.

F. Velocity Profile in the Central Portion of the Channel

No complete velocity mapping at a given channel cross section was made. However, several simple experiments were conducted to obtain an estimate of the uniformity of the free stream velocity profiles across the square channel.

First of all the average free stream velocity was measured at various stations away from the channel centerline. This was accomplished by injecting drops of dye at various z (spanwise dimension; $z = 0$ at test section centerline) stations at $x = -5$ inches (5 inches ahead of the leading edge of the flat plate) and by timing these drops between $x = 0$ and $x = 24$ inches with a stopwatch. The drops were introduced at the free surface and would sink as they traversed downstream, the average y distance being approximately 3 inches. These tests were conducted at a free stream velocity of 0.250 ft/sec. Five readings were taken for each value of z. These were all found to be with $\pm$ 0.1 second ($\pm$ 1.25 percent) for the given z station. The z locations studied were ± 4, ± 2, and 0 inches. The sum of the five readings for each station was found to be within 1.5 percent of the value for $z = 0$. Thus it was concluded that the flow in the free stream itself was uniform.

A further check was made using the hot-film system. The set was balanced at $U_\infty = 0.25$ ft/sec, $y = 2$ inches, $z = 0$, $x = 12$ inches.

Then y was varied from y = 2 inches to y = 5 inches and z was varied from z = -3 inches to z = +3 inches, in increments of 1 inch in both directions. No detectable variation in hot wire output signal was noticed during this experiment.

G. Acceleration of the Free Stream

Due to the slope at which the test plate was mounted to eliminate flow separation near the leading edge and due to the growth of the boundary layers on the tunnel walls as well as on the plate itself the fluid accelerates as it passes through the test section. The magnitude of the acceleration was determined by measuring the local velocity as a function of x (x = 0 at the leading edge of the flat plate) for fixed y outside of the boundary layer. Measurements were made at several flow rates and for different distances y above the plate. Plots of $U_\infty(x)/U_{\infty_o}$, versus x (where U_{∞_o} denotes $U_\infty(x)$ at x = 12 inches) are shown for U_{∞_o} = 0.125 ft/sec and 0.75 ft/sec in Figures 15 and 16, respectively. The front edge of the cavity section corresponds to x = 12 inches. As Figures 15 and 16 show the acceleration is approximately constant over the cavity section. The magnitudes of the average flow acceleration from x = 0 to 12 inches are recorded in Table 1 as $\frac{1}{U_{\infty_o}} d U_\infty(x) / dx$.

For discussion purposes the term "free stream velocity" and the symbol U_∞ are used to indicate the average free stream velocity in all but the present part of this dissertation. It should be noted that the average free stream velocity, by its method of measurement and

definition, closely corresponds to the local free stream velocity at x = 12 inches, the section of primary interest in this work.

H. Velocity Profiles Upstream of the Cavities

Velocity profiles were measured on the flat entrance plate 1/4 inch ahead of the cavities (x = 11.75 in.) in order to determine the actual approaching flow conditions. These measurements were made both with the 1/2 x 1/2 inch cavity insert in place and with the smooth insert instead of the cavities. No differences were noted in the approaching velocity profiles for these two cases indicating no measurable upstream disturbances due to the cavities. The profile measurements were made for average free stream velocities of 0.125, 0.25, 0.50, and 0.75 ft/sec. The data are plotted as u/U_∞ versus y/δ^* in Figure 17. As can be seen from this figure, the data for all four free stream velocities fall on a single curve.

The primary objective of the detailed velocity profile measurements ahead of the cavities was to determine the actual shear velocity u_τ (or equivalently the wall shear stress) at this point. The magnitudes of the shear velocity derived from the wall slope of these profiles ahead of the cavities are tabulated in Table 2. In addition, the values of the displacement thickness δ^* are also given in this table. From the measured values of shear the parameter $\epsilon^* = \epsilon u_\tau/\nu$ was calculated. These ϵ^* values are given in Table 3 as functions of the cavity depth ϵ and the free stream velocity U_∞. Considering the data scatter, the reproducibility of measured quantities, as well

as the other uncertainties, the accuracies of u_τ and ϵ^* are estimated to be ± 4 percent. The accuracy estimate for δ^* is also about ± 4 percent.

The velocity profile obtained is one corresponding to an acceleration of the free stream and is not a classic Blasius profile. No attempts were made to eliminate this acceleration as for the present purposes the exact velocity profile was immaterial. To obtain a rough comparison, however, a laminar profile was computed taking into account the measured average acceleration of the outer stream. The resulting profile matched the actual one considerably better than the Blasius profile. Nevertheless there remained a discrepancy of about 20 percent in δ^* and about 40 percent in u_τ. No attempts to refine the computation or to modify the test installation were made as the prevailing flow was believed to be adequate as indicated above.

V. EXPERIMENTAL RESULTS

A. Photographs of Flow Pattern in Square Cavities

Photographs of the flow patterns within the cavities were taken as described in Chapter III. The flow was made visible by means of the dye injection system described in the same chapter. Several representative photographs are shown in Figures 18-24.

The size of the smallest cavity was 1/8 x 1/8 inch and the lowest free stream velocity was 0.125 ft/sec. This set of conditions led to the lowest value of ϵ^* ($\epsilon^* = 15.8$), and the corresponding flow is shown in Figure 18 in which the first three cavities are visible. The flow was from right to left. Dye was injected from the orifices 1/8 inch upstream of the leading edge of the first cavity in the center section of the plate. The photograph shows this dye sweeping over the first three cavities. The standing vortex in the first cavity was made visible by injecting dye from an orifice in the center of the cavity bottom which was shut off several seconds before the picture was taken. Due to the very low velocities in the cavity and the lack of fluid exchange at the interface the dye remained very dense and showed the steady vortex pattern for periods of several minutes.

This same steady vortex pattern is also observed in Figures 19 to 24 for all of which ϵ^* was below 192. Figure 19 shows the first three 1/8 x 1/8 inch cavities at $U_\infty = 0.75$ ft/sec. The dye

from the upstream orifice again sweeps over the cavities without exhibiting any fluid interchange. The dye emanating from the bottom orifice in the first cavity clearly traces the vortex pattern in the cavity. Figures 20 and 21 show the flow patterns in the first two 1/4 x 1/4 inch cavities. For Figure 20 the free stream velocity was 0.125 ft/sec and for Figure 21 it was 0.50 ft/sec. Both figures show the dividing dye streamline passing over the cavity without fluid exchange, the dye making the flow visible in the first cavity having been injected from the bottom orifice several seconds before. For Figure 21 the dye injection velocity was slightly too high and the basic flow was being disturbed somewhat; the dye filament was separated from the pre-cavity flat plate and the rib behind the cavity.

The flow in the first of the 1/2 x 1/2 inch cavities is shown in Figures 22 and 23, the free stream velocities being respectively 0.125 and 0.50 ft/sec. Both figures show that the cavity vortex is shifted slightly toward the downstream wall of the cavity. Figure 23, taken at a higher velocity than Figure 22, shows some of the dye that had previously settled in the boundary layer on the cavity bottom being entrained into the cavity vortex, whereas Figure 23 shows little activity in this region. Note that the dye appears to be slightly too dense so that it sinks in these two figures. Again the steady vortex is noted.

The flow pattern in the 1 x 1 inch cavity, the largest square cavity for the present experiments, is shown in Figure 24 for a free stream velocity of 0.25 ft/sec. Again the well-established steady

vortex exists in the central portion of the cavity but the fluid near the cavity bottom shows little trace of movement.

For the observations described above ($15.8 \leq \epsilon^* \leq 192$) both the approaching flow and the cavity flow were entirely steady and laminar. At an ϵ^* value of approximately 200 a new phenomenon was observed which consisted of a rather weak periodic oscillation of the shear layer over the cavity. This oscillation was confined to the immediate vicinity of the opening of the cavity and left the vortex flow essentially undisturbed. This phenomenon, which was termed "laminar oscillation" will be discussed in some more detail in Chapter VII.

As the free stream velocity was increased to a value above 2.0 ft sec the approaching boundary layer at the cavity location and the cavity flow became turbulent. This flow regime is outside the region of principal interest in the present experiments. It is the region of turbulent flow at high ϵ^* for which Townes observed a *rather steady though strongly turbulent vortex.* The same type of pattern was also observed here.

B. Study of Three-Dimensional Effects in Cavity Flows

The 1/2 x 1/2 inch cavity insert constructed with dye slots running the entire 7 inch span of the cavity (described in Chapter III) was installed in the test section to investigate any possible three-dimensional effects of the flow in the cavities. For these tests a relatively dense dye solution was prepared that would sink slightly

so as to provide dye throughout the cavity.

For the first series of tests dye was injected through the slot in the cavity bottom in a uniform sheet. After several seconds the injection was terminated and the motion of the dye sheet was noted. Most of the dye injected from the slot lay on the cavity bottom (i.e., only a small portion entrained by the cavity vortex), indicating very low velocities in this region even at the highest free stream velocity (U_∞ = 0.75 ft/sec). For U_∞ = 0.125 ft/sec the dye creeping from the slot extended both upstream and downstream, indicating an almost complete absence of velocity in the dye layer. For higher free stream velocities the fluid motion in the cavity was sufficient to sweep the dye onto the upstream half of the cavity bottom. The dye sheet on the cavity bottom became stationary approximately 10-40 seconds after the end of dye injection (depending on the free stream velocity) and showed no evidence of three-dimensional cells. Also, except for some end effects at the spanwise extremes, the cavity flow appeared to be completely two-dimensional. The above observations are the composite result of 6-10 tests made for each free stream velocity. The duration of dye injection and hence the amount of dye in the cavity was varied slightly from test to test.

The second series of tests to examine possible three-dimensionality of the flow consisted of observing the movement of the uniform dye sheet from the slot 1/8 inch ahead of the cavity. Due to the density of the dye a portion would flow over the rib behind the cavity and the remainder would sink making the cavity flow visible.

Both portions of the dye sheet were found to exhibit steady uniform characteristics for $U_\infty \leq 0.5$ ft/sec. No spanwise variation was noted for either portion of the dye sheet in the central three-fourths of the cavity span. At the next higher velocity, $U_\infty = 0.75$ ft/sec, the laminar oscillations at the cavity interface were noted, but no three-dimensionality was detected even in this case.

In summary, no three-dimensional cellular patterns were observed in any of these tests. In addition, the flow in the central five inches of the cavity was found to be entirely two-dimensional. It should be pointed out that since ϵ/L was equal to 1 for the cavities studied, this result is compatible with the findings of Maull and East (26) in turbulent flows.

C. Velocity Profiles Within and Above the Cavities

Profiles showing the velocity field within and above the first cavity are shown in Figures 25-31. These were selected as being representative of the 17 different sets of test conditions (U_∞, x_1 and ϵ variable). The conditions corresponding to each of these profiles are listed in Table 4.

Figures 25-30 correspond to velocity profiles measured above and within the center section of the cavities. The profile obtained for the lowest value of ϵ^* ($\epsilon^* = 31.6$, $\epsilon = 1/4$ in., $U_\infty = 0.125$ ft/sec) for which measurements within the cavity were made is represented in Figure 25. The profiles in Figures 29 and 30 were taken in a 1 x 1 inch cavity and for a free stream velocity of 0.50 ft/sec. These

two figures correspond to the highest value of ϵ^* ($\epsilon^* = 286.4$) for which cavity velocity profiles were measured.

For all cavity-center velocity profiles one finds that the velocity in the y = 0 plane of the cavity interface is in the range of 1/4 to 1/3 of the free stream value. The velocity then becomes undetectable as one proceeds downward through the cavity. The point where the velocity approaches this zero value varies with x_1 and U_∞, but in general lies in the y/ϵ range of $-\frac{1}{10}$ to $-\frac{1}{3}$. After the region of non-detectable velocity, which probably corresponds to the solid-body-type vortex center, the velocity again becomes measurable with the present instrumentation as long as $U_\infty \geq \frac{1}{4}$ ft/sec. This velocity in the lower portion of the vortex in all cases was found to be less than 8 percent of the free stream value. For a free stream velocity of 0.125 ft/sec no velocity could be detected in the lower half of the cavity with the given hot-film system. This is not surprising since the velocities in this portion of the cavity are expected to be of the order of a few thousandths of a foot per second for this free stream velocity.

Off-center velocity profiles were also measured for the 1 x 1 inch cavity at the upstream and downstream quarter points of the cavity. The lower portions of these profiles are shown in Figure 31 for $U_\infty = 0.50$ ft/sec. From the location and magnitude of the velocity peaks in the cavity it seems that the vortex was slightly shifted toward the downstream bottom corner of the cavity. This is verified by the photographs of the flow pattern in the square cavities presented

earlier. The magnitude of the peak vortex velocity for a given free stream velocity, as detected by the three separate profile measurements, is approximately the same.

As a check on the cavity velocities measured with the hot-film system (as reported above) an independent study by means of timing dye drops was made in the 1 x 1 inch cavity. The radius of the maximum-velocity dye filament was estimated and the time for the dye filament to trace one revolution of the cavity was noted. The velocities determined from these measurements were of course average velocities for one revolution. Since the velocity in the shear layer across the cavity is greater than the velocity in the remainder of the circuit these average velocities would be expected to be slightly higher than the velocities detected by the hot-film measurements in the lower half of the cavity. The tests at $U_\infty = 0.125$ ft/sec showed cavity velocities of approximately 0.004 ft/sec as compared to undetectable velocities for the hot-film measurements. For $U_\infty = 0.50$ ft/sec these tests showed cavity velocities of approximately 0.017 ft/sec as compared to hot-film values of 0.015 ft/sec.

The shear velocity (or shear stress) in the fluid at the cavity opening is a measure of the amount of momentum exchange between the cavity and the adjacent boundary layer. These values for all the cavity profiles are tabulated in Table 4. As expected the free stream velocity exerts a strong effect on these values. A diminishing of this shear as one proceeds downstream along the cavity is noted. The velocity profile exhibits an extended straight line portion near y = 0

and the slope of this line is based on as many as 30 velocity points. The data scatter was negligible and the shear velocities are estimated to be accurate within 2 percent. In general, the shear velocity at the cavity interface (y = 0) was found to be about one-half of the value immediately upstream of the cavity.

A value of ϵ^* based on the approximate average shear across the cavity can be calculated from these shear stress measurements. The measurements on the 1 x 1 inch cavities show that the shear velocity remains fairly constant from the upstream to the downstream quarter points of the cavity. Thus taking the shear at the cavity centerline as an average for the cavity opening a parameter ϵ_c^* defined as $\epsilon_c^* = \epsilon u_{\tau c} / \nu$ was calculated. These values are given in Table 4 and are found to be close to one-half of the ϵ^* based on the shear just ahead of the cavity. Due to the higher shear stress that must be present in the transition regions at the front and back edges of the cavity ϵ_c^* as computed here will be somewhat lower than the corresponding parameter based on the true average for the cavity interface.

D. Velocity Profiles Downstream of the Cavity

The velocity profiles shown on Figures 32-34 were measured above the center of the rib behind the cavities. Each profile corresponds to one cavity size, and hence one value of x_1 (the distance from the upstream cavity wall). The data for all free stream velocities are found to fall on a single curve for each figure when

plotted as u/U_∞ versus y/δ^*.

From these profiles the shear velocity u_τ and the displacement thickness δ^* were calculated. These values are reported in Table 2. In general one observes that these shear velocities are about 8 percent higher than the pre-cavity values. This higher wall shear is a consequence of the sudden start of a new surface, the rib.

To summarize the development of the shear velocity ($u_\tau = \sqrt{\nu \frac{du}{dy}\Big|_{y=0}}$ on the y = 0 plane as one traverses downstream across the 1 x 1 inch cavity Figure 35 was plotted. Separate curves of u_τ as function of x_1 for U_∞ = 0.125, 0.25, and 0.50 ft/sec are shown. The shear velocities reported were computed from the wall shear 1/4 inch ahead of the cavity, the y = 0 cavity interface shear for the upstream quarter point, center, and downstream quarter point of the cavity, and the wall shear on the center of the rib downstream of the cavity. Generally the shear velocity at the cavity interface is approximately 50 percent below the value ahead of the cavity; that behind the cavity about 8 percent above. The dashed lines represent estimates and are not based on measurements.

E. Photographs of the Flow Pattern in Non-Square Cavities

In order to obtain some indication of the effect of the shape of the cavity some exploratory tests were conducted with two cavities for which the length L differed from the depth ϵ. These cavities were exposed to a range of free stream velocities from 0.125 to

1.0 ft/sec and the observed flow patterns are reported below.

The series of photographs in Figures 36 - 40 show a 1/2 inch deep by 1-1/4 inch long cavity located 12 inches downstream of the leading edge of the flat plate. The free stream velocities in Figures 36-40 are consecutively 0.125, 0.25, 0.50, 0.75 and 1.0 ft/sec. In all photographs the dye was injected 1/8 inch ahead of the upstream wall of the cavity and from one of several orifices located around the perimeter of the cavity. Figure 36 shows an elongated vortex shifted toward the downstream edge of the cavity. The fluid flow near the upstream bottom corner is toward the upper right, indicating that this fluid is traveling as part of the primary vortex. On the other hand in Figure 37 some motion of the fluid near the upstream bottom corner toward the bottom left may be observed, indicating the presence of a weak second vortex in this region rotating opposite to the primary vortex. Figure 38 at a still higher velocity (U_∞ = 0.50 ft/sec) shows the presence of an increasingly stronger secondary vortex in the upstream bottom corner. In Figure 39 at U_∞ = 0.75 ft/sec the secondary vortex is quite distinct. In addition, if one examines the dye flowing over the rib following the cavity, one sees evidence of the laminar oscillation in the form of a dye finger just past the rib. The evidence of the oscillation is more distinct in Figure 40 which shows a waviness in the dividing streamline as far upstream as the cavity center as well as the dye finger escaping over the rib. In this photograph, which was taken at U_∞ = 1.0 ft/sec, a considerable amount of turbulence is also noticed.

The photograph in Figure 41 shows a 1 inch deep by 1/2 inch long cavity at a free stream velocity of 0.25 ft/sec. Evidence of two counter-rotating vortices is indicated. The sinking "finger" of dye that is observed is caused by the relatively high dye density. Similar observations for $U_\infty = 0.125$ ft/sec do not show the bottom vortex because of the very low absolute velocities.

These observations for non-square cavities have shown steady flow characteristics in the same region where steady characteristics were observed in the square cavities. Also the onset of the laminar oscillations was detected for about the same ϵ^* as for the square cavities. In their flow pattern studies in finned annuli in laminar flow Knudsen and Katz (22) also failed to observe the bottom vortex in deep cavities at the low flow velocities.

VI. DISCUSSION OF RESULTS

A. Parameters for the Comparison of Laminar and Turbulent Flow Over Cavities

The primary goal of the present work was to compare the flow in geometrically similar cavities exposed alternately to laminar and turbulent flow. In a previous investigation Townes (44, 45) had performed the turbulent flow studies and found significant fluid exchange between the cavities and the adjacent boundary layer. By subjecting the cavities to a "similar" flow without the boundary layer fluctuations and observing the cavity activity the influence of the turbulent fluctuations was determined.

To obtain this kind of "similar" flow it was decided to establish the same surface shear stress at the cavity. In dimensionless terms this similarity may be expressed by the parameter $\epsilon^* = \frac{\epsilon \sqrt{\tau_o/\rho}}{\nu}$ which was introduced earlier. The comparison will then be made between flows in a cavity for which the only difference is the boundary condition at the open interface. At this interface the shear stress is to be maintained the same, but in one case the interface is subject to turbulent fluctuations whereas in the other case such disturbances are to be absent.

It is to be understood that ϵ^* alone will not insure a complete similarity of the entire flow field. The two flows of course differ in boundary layer thickness, distance from the leading edge, etc., and these differences are the very ones which lead to a turbulent boundary layer in one case against a laminar one in the other. Complete similarity would, in fact, defeat the purpose for the present experiments.

For full similarity a second dimensionless parameter would have to be introduced. Any parameter such as x/ϵ, δ^*/ϵ or Re_x would serve this purpose. Of these, Re_x is particularly convenient as it is generally used in the literature in reporting transition from laminar to turbulent flow. For flat plate flow the transition Re_x is in the range of 3.0×10^5 to 10^6 depending on the free stream turbulence intensity. The present work for which Re_x is below 10^5 is therefore well within the laminar range. For Townes' turbulent flow work Re_x varied between 6×10^5 and 3.6×10^6.

In the foregoing it has been assumed that a single dimension, ϵ, is sufficient to specify the cavity. If rectangular cavities with various ratios of depth ϵ to length L are to be introduced an additional parameter such as ϵ/L would have to be added.

B. The Shear Term in the Parameter ϵ^*

It is necessary to comment on whether ϵ^* based on the measured wall shear stress immediately ahead of the cavity, rather than ϵ_c^* based on the true shear stress that exists at the cavity interface, is

a valid wall layer similarity parameter for the laminar-turbulent comparison. Intuitively it appears that the true shear stress in the fluid at the cavity interface is the meaningful shear stress. It is this quantity that one would expect to govern the mutual interaction between the cavity and the adjacent boundary layer. It is also this quantity, rather than the stress ahead of the cavity that one would expect to develop and propagate an instability in the interface region.

To compute the turbulent shear stress at the cavity interface measurements of the velocity profile as well as of the turbulent fluctuations are required. Townes did not measure either of these quantities and, therefore, a direct comparison with his work on the basis of ϵ_c^* is not feasible. One can, however, make some estimates of the ratio ϵ_c^*/ϵ^* from available measurements in both laminar and turbulent flow. From the present work one finds that, on the average, for the four free stream velocities for which measurements were made, the value of ϵ_c^*/ϵ^* was about 1/2. For turbulent flow, on the other hand, from the data of Tani, et al (43) one finds ϵ_c^* about equal to ϵ^*. In this case the shear stress was computed from the relation $\tau = \mu \frac{du}{dy} + \rho \overline{u'v'}$ where du/dy and $\overline{u'v'}$ were measured at y = 0 in the center of the cavity. The corresponding value ahead of the cavity was obtained using the equation $C_f = 0.0592\ (Re_x)^{-0.2}$ (39). While these measurements in turbulent flow were performed at an ϵ^* about 10 times greater than those in Townes' experiments they do indicate that the total cavity interface

shear is not expected to differ drastically from the pre-cavity value in turbulent flow. The Reynolds stress is of course included in the estimate of the total shear, and it is interesting to note that the Reynolds stress comprises over 95 percent of the total shear stress at the cavity interface for the case cited.

For the present work both ϵ^* (based on the shear ahead of the cavity) and ϵ_c^* (based on the shear at the center of the cavity interface) were computed. The experiments by Townes covered a range of ϵ^* from 12-260 and the present experiments extended from 16-400 in terms of ϵ^* and 8-200 for ϵ_c^*. Although ϵ^* and ϵ_c^* differ by a factor of about 2 for the laminar flow, both ranges well overlap the experiments by Townes. In addition the observed flow patterns in the present experiments are not sensitive to ϵ^* and the findings may well be reported in terms of either parameter. Since ϵ_c^* is entirely composed of measured quantities whereas ϵ requires certain approximations, the laminar and turbulent flows will be presented on the basis of ϵ^*. In the discussion, however, it will be kept in mind that ϵ_c^* may be the more significant parameter.

C. Comparison of Cavity Flow for Laminar and Turbulent Approaching Flows

Accepting ϵ^* (based on the shear ahead of the cavity) as a suitable parameter for the presentation of results, we may now proceed to compare the present work and that of Townes on this basis. As mentioned earlier both experiments included the ϵ^* range from

about 10-200.

For the same ϵ^* any difference in the observed flow in the cavities must stem from the nature of the flow just outside the cavity, i.e., from the presence or absence of turbulent fluctuations.

Let us recall then the principal findings concerning cavities exposed to turbulent flow. Townes had observed randomly changing flow phases inside the cavity which he classed as "inflow", "divide", "weak exchange", and "strong exchange". All four flow phases occurred for ϵ^* less than 100 with the "strong exchange" mode disappearing for ϵ^* greater than about 100. The changes in flow pattern resulted in rather large and violent velocity fluctuations throughout the cavity. In particular, the "strong exchange" pattern would often cause an almost complete exchange of cavity fluid with fluid from the adjacent turbulent boundary layer. No continuous stable vortex motion in the cavity could be observed in this range of ϵ^* with the cavity exposed to turbulent flow.

In contrast to this, for the present laminar flow study, especially below $\epsilon^* = 200$ ($\epsilon_c^* \doteq 100$), the cavity was in a perpetual "divide" phase with little or no fluid exchange with the adjacent boundary layer. As the cavity flow pattern photographs and the visual observations have shown, in laminar flow the vortex system in the cavity was completely steady and stable in this range of ϵ^*. Even above $\epsilon^* = 200$ the stable vortex continued to exist within the cavity; however, the dividing streamline between the outer and inner flow

began to be unstable and to fluctuate in a periodic sinusoidal manner. The effect of these oscillations was confined to the immediate vicinity of the dividing streamline and did not disturb the steady vortex pattern to a significant degree.

One may state, therefore, that with a laminar boundary layer flow, the steady vortex pattern persisted for a wide range of ϵ^*. This is true no matter whether ϵ^* is defined on the basis of the shear over the cavity or the shear directly upstream. This steady flow is contrasted with the randomly changing flow patterns observed by Townes.

Thus it can be concluded that the apparent cavity vortex flow instability in the turbulent flow was the result of the velocity fluctuations in the adjacent boundary layer penetrating to within the cavity and not the result of any inherent instability of the flow within the cavity. This is the information which was desired at the outset and for which the present experimental study was designed. It confirms the hypothesis proposed as a result of the observations by Townes.

D. Velocities in the Cavity Region

Although the observations of the steadiness of the flow patterns was the principal purpose of the investigation, some attempts to measure the velocity within the cavity were made. From these it was noted that the ratio of the maximum velocity in the lower half of the cavity to the velocity of the free stream was much different in the case of a turbulent free stream than in that of a laminar one. For

turbulent approaching flow the magnitude of the maximum cavity vortex velocities observed by Roshko (34), Fox (15), Tani et al (43), and others was found to be of the order of 30-40 percent of the free stream velocity. Although Townes did not measure local cavity velocities directly one may derive from his original films values of the order of 15-30 percent for this ratio. For the present laminar flow studies, on the other hand, the ratio of maximum velocity in the lower half of the cavity to free stream velocity was always below 8 percent. In fact, for all cases, the velocities at the cavity interface ($y = 0$ plane) for the laminar flows were only between 1/4 and 1/3 of the free stream. Thus even these values are below those observed in the cavity vortex in turbulent flows.

These results indicate, as one may expect, that the turbulent shear stress in the fluid acts as a more efficient mechanism of momentum transfer to the cavity than a purely viscous shear stress.

VII. LAMINAR OSCILLATIONS

A. Description of the Laminar Oscillations

In the previous sections it was mentioned that under certain conditions an instability was observed at the interface between the fluid in the cavity and the outside flow. The streamline over the opening of the cavity would begin to show a sinusoidal motion and for reference purposes the phenomenon has been called "laminar oscillations". The oscillations were made visible by dye injection just upstream of the cavity. They were also detected by velocity measurements at the cavity opening.

It should be emphasized that the study of these oscillations is not a part of the main work of this thesis. As a result, not all facets of the phenomenon have been thoroughly investigated. However, since the oscillations were observed in the flow regime of the cavity studies, the description of the phenomenon, the conditions under which it occurred, and some correlations of the observed frequencies are reported here.

When viewing the dividing streamline the sinusoidal motion could be seen clearly. At the downstream edge of the cavity the oscillation would result in an alternating overflow and inflow. The sequence of motion picture film in Figure 42 illustrates this motion. The film strip shows the top portion of the downstream half of the

second 1 x 1 inch cavity plus the rib behind the cavity. The free stream velocity was 0.50 ft/sec and the framing rate was 12.0 frames/second. The observed oscillation occurs at a frequency of 2.00 cycles/second.

The two photographs in Figures 43 and 44 also show evidence of the laminar oscillations. Both show the first 1 x 1 inch cavity. In the former the free stream velocity is 0.50 ft/sec and for the latter the free stream velocity is 0.75 ft/sec. The waviness of the dividing streamline and the finger of dye extending over the rib behind the 1/2 inch deep by 1-1/4 inch long cavity have already been pointed out in Chapter V (Figures 39 and 40).

Velocity measurements exhibiting the oscillations are shown in the form of two portions of Sanborn strips (Figures 45 and 46). The strip in Figure 45 was taken on the rib following the first 1 x 1 inch cavity at $U_\infty = 0.50$ ft/sec. The measurements were made for $y = 0.015$ in. at which point $u/U_\infty = 0.33$. The signal on the chart is proportional to the velocity. The frequency of the fluctuation is 2.04 cycles/second and the root-mean-square amplitude is found to be 2.3 percent of the local mean velocity. The strip of Figure 46 represents measurements in the center section of the 1 x 1 inch cavity for $U_\infty = 0.50$ ft/sec and $y = -0.10$ in. (i.e., 0.10 inches below the top of the cavity) at which point $u/U_\infty = 0.043$. The root-mean-square fluctuation intensity based on the local mean velocity is 10.02 percent, and the frequency is again 2.04 cycles/second.

It should be emphasized that the character of the laminar oscillations observed in the present work differed entirely from the random fluctuations observed by Townes. First the former are regular and periodic as distinct from the random occurrence of the latter. Secondly the turbulent fluctuations were quite violent affecting a major portion of the fluid in the cavity whereas the laminar oscillations left the continuous vortex pattern inside the cavity undisturbed with only the flow near the downstream top corner of the cavity being slightly modified.

In the literature similar oscillations have been theoretically predicted by Lessen (24) for the free shear layer between two parallel flows and observed by Sato (38) for a half jet. Lessen theoretically treated the stability of the boundary layer between two semi-infinite parallel flows. A solution for the mean velocity distribution was derived and one branch of the neutral stability curve was calculated. Lessen concluded that the boundary layer between parallel streams is an unstable flow configuration except at low Reynolds numbers (Re_δ less than 10). Sato's experiments on a laminar half jet were conducted in a wind tunnel in the free stream velocity range of from 9.8 to 49 ft/sec. The flow was two-dimensional without pressure gradient, and the boundary layer before separation had a Blasius-type velocity distribution. Entrance plates varying from 1.77 to 13.6 in. were used to study the effect of boundary layer thickness. Hot-wire anemometer measurements detected the existence of regular sinusoidal velocity fluctuations of up to several percent of the main

stream velocity in the transition region of the separated layer. The present cavity geometry differs from the geometry in both of these works, but for all three the laminar free shear layer exists and the occurrence of the oscillations appears to depend on the stability of this laminar free shear layer.

B. Flow Regime of the Laminar Oscillations

The lowest boundary layer Reynolds number $(\frac{U_\infty x}{\nu})$ at which the oscillations were observed was approximately 30,000 and the highest Reynolds number at which the oscillations were distinct and occurred at a well-defined frequency was 150,000. Thus the boundary layer flow conditions in the entire range where the oscillations were observed were laminar, hence the name "laminar oscillations" for the observed phenomenon. Above the highest boundary layer Reynolds number reported here, the flow in the cavity interface region became quite violent with the presence of large scale eddies being observed. It appeared that the cavity was tripping the flow to a turbulent flow state. Thus the indications are that the observed oscillations are present just prior to and during the early stages of a laminar to turbulent transition of the free shear layer at the cavity interface. This is the same flow regime where Sato (38) observed the fluctuations in the half jet.

Of the four sizes of square cavities examined (1/8 x 1/8, 1/4 x 1/4, 1/2 x 1/2 and 1 x 1 inch) only the latter two exhibited the laminar oscillations at the velocities examined (up to 1.5 ft/sec) in

these studies. The two non-square cavities (1/2 inch deep and 1-1/4 inch long; 1 inch deep and 1/2 inch long) also showed the oscillations. Each cavity size appeared to have a critical velocity below which the oscillations did not exist. As the critical velocity was approached from below the downstream cavity in the series (4 cavities in the 1 x 1 inch cavity plate, 9 cavities in the 1/2 x 1/2 inch cavity plate, etc.) was the first to show the oscillation. As the velocity was increased, successive upstream cavities exhibited the oscillation until finally all cavities were active. The upstream travel of the oscillation activity seemed to be uniform and generally occurred within a U_∞ range of 0.05 ft/sec.

The lowest free stream velocity for which the oscillations could be detected in the first cavity, for both the square and the non-square cavities, was about 0.3 ft/sec for ϵ = 1 inch and about 0.6 ft/sec for ϵ = 1/2 inch. This corresponds to a cavity Reynolds number (based on ϵ and U_∞) of 2400 for both instances.

C. Frequencies of the Laminar Oscillations

The oscillation frequencies for all active cavities in a given cavity plate were identical and thus could be measured in any of the cavities. Since the dye concentration in the dividing streamline appeared best for observing the oscillations at the rear of the second cavity, all measurements, both the visual timings and the motion picture data, were taken there.

The frequencies of the laminar oscillations are tabulated as a function of the free stream velocity in Table 5 for each of the four cavities examined that exhibited the oscillations. Also shown are the Strouhal number defined as $S_\epsilon = f\epsilon / U_\infty$ and the cavity Reynolds number defined as $Re_\epsilon = U_\infty \epsilon / \nu$. Plots of frequency versus free stream velocity and Strouhal number versus Reynolds number are shown in Figures 47 and 48, respectively, with the data keyed to indicate the particular cavity geometry for which it was taken.

The data can be summarized to some extent as follows. For ϵ = 1 inch the inception velocity is about 0.3 ft/sec with a corresponding Re_ϵ of approximately 2400. The lowest observed frequency was approximately 1.1 cycles/second at inception. For ϵ = 1/2 inch the inception velocity was about 0.6 ft/sec with the Re_ϵ again at approximately 2400. For this case the observed frequency varied from 3.70 to 12.0 cycles/second as the velocity was varied between 0.58 and 1.5 ft/sec.

The correlation velocity used in computing the Strouhal number was the free stream velocity and on this basis a relatively constant value of S_ϵ was obtained. As Figure 48 shows - except for the 1 inch deep by 1/2 inch long cavity above about Re_ϵ = 4800 - the values of S_ϵ using this velocity are bounded between 0.24 to 0.36 for the entire range of Re_ϵ examined (2400 to 7500).

It should be pointed out that the oscillation frequency appears to be influenced by the cavity depth in addition to the other characteristic lengths, such as the cavity length, L, and the displacement

thickness of the outer boundary layer, δ^*, which are also expected to be of importance. In fact, for the four cavities examined in which the oscillations were observed the cavity depth appears to be the principal dimension governing the frequency. As Figure 47 shows the 1/2 inch square and the 1/2 inch deep x 1-1/4 inch long cavities exhibited the same relationship between frequency and velocity (U_∞), and also led to a considerably higher frequency at a given velocity than the 1 inch square cavity. The 1 inch deep by 1/2 inch long cavity on the other hand showed the same frequencies as an inch deep cavity at low velocities. Beyond a velocity, U_∞, of about 0.6 ft/sec, however, it showed frequencies corresponding to a one-half inch deep cavity. It should be noted that this velocity corresponds to the inception velocities noted for the ϵ = 1/2 inch cavities.

It is expected that the laminar oscillations depend on at least three parameters, for instance δ^*, ϵ^*, and ϵ/L. A complete and thorough analysis would require a detailed program in which these parameters were systematically varied. But as pointed out earlier, the analysis of the flow stability of the shear layer over the cavity was not the primary goal of this investigation. The findings are reported here as incidental information, in the hope that the data may be of use in future investigations of this specific problem.

In order to compare the laminar oscillation frequencies observed with those of other investigators the data are plotted as $S_\theta = \frac{2\pi f \theta}{U_\infty}$ vs. $Re_\theta = U_\infty \theta/\nu$ in Figure 49 following the procedure

of Sato (38). To obtain the values of momentum thickness θ the pre-cavity displacement thicknesses were divided by a factor of 2.57. This value was obtained from Curle's (9) summary of laminar boundary layer flows with pressure gradient. The amount of deviation from Blasius flow was determined by the comparison of the measured displacement thicknesses to those for a Blasius profile. Values of displacement thickness for velocities above 0.75 ft/sec were obtained by extrapolation. While these methods of estimating the existing θ values could result in some error, the ratio δ^* to θ is a very insensitive function of the acceleration and the error in θ is estimated to be less than 10 percent. The oscillation frequencies that Sato measured for the half jet and the upper half of the theoretical neutral stability curve for the free shear layer between two semi-infinite parallel flows calculated by Lessen (24) are also shown in Figure 49. A parameter representing the effect of the cavity size, ϵ, does not appear as Lessen and Sato consider only one geometrical arrangement corresponding to $\epsilon \rightarrow \infty$. The data from the present work fall into two groups indicating an effect of the geometry. It is noted that all of the data points from the current work fall below the upper branch of the neutral stability curve and are thus probably in the unstable zone. However, since the lower branch of the neutral stability curve has not been calculated one cannot be certain that all points are above this branch of the theoretical neutral stability curve. Although a direct comparison between the data presented here and that of Sato is not possible because of the differences in geometry it is

seen that the Strouhal numbers for the two cases are of the same general magnitude. This gives further credence to the view that the same basic phenomenon is involved.

SYMBOLS AND ABBREVIATIONS

A	Constant used in King's Law, Equation (3-1)
B	Constant used in King's Law, Equation (3-1)
C_1	Constant in King's Law as written in Equation (3-2)
C_2	Constant in King's Law as written in Equation (3-2)
C_3	Constant in King's Law as written in Equation (3-2)
C_d	Cavity drag coefficient $C_d = \text{Drag} / \frac{1}{2} \rho U_\infty^2$
C_f	Friction coefficient $C_f = \tau_o / \frac{1}{2} \rho U_\infty^2$
C_h	Heat transfer coefficient $C_h = \dot{q} / \rho U_\infty C_p (T_w - T_r)$
e_i	Hot-wire set output voltage
$e_{i\infty}$	Hot-wire set output voltage at free stream velocity
f	Frequency of laminar oscillation
L	Length of cavity
Nu	Nusselt number
Re	Pipe or wire Reynolds number $Re = U_\infty d/\nu$
Re_δ	Reynolds number based on boundary layer thickness, $Re_\delta = U_\infty \delta / \nu$
Re_ϵ	Cavity Reynolds number, $Re_\epsilon = U_\infty \epsilon / \nu$
Re_θ	Reynolds number based on momentum thickness, $Re_\theta = U_\infty \theta / \nu$

Re_x Flat plate Reynolds number based on distance x from leading edge, $Re_x = U_\infty x/\nu$

s Cavity span

S_ϵ Cavity Strouhal number, $S = f\epsilon / U_\infty$

S_θ Strouhal number based on momentum thickness, $S_\theta = 2\pi f \theta / U_\infty$

t Time

u Local mean velocity in x direction, $u = u(x, y)$

u' Fluctuating component of u

u_τ Shear velocity, $u_\tau = \sqrt{\tau_o/\rho}$

u_{τ_c} Cavity shear velocity, $u_{\tau_c} = \sqrt{\nu \frac{du}{dy} (y = 0,\ x = L/2)}$

U_∞ Average free stream velocity between x = 0 and x = 24 in.

U_{∞_o} Free stream velocity at x = 12 in.

v' Fluctuating component of velocity in y direction

x Distance from leading edge of flat plate

x_1 Distance from upstream wall of cavity

y Distance above flat plate surface

y_1 Distance between sensor and locating rod

y_m Location of maximum velocity in lower half of cavity

y_δ Location where velocity approaches zero in shear layer across the top of the cavity

z Spanwise dimension, z = 0 at channel centerline

Greek Letters:

δ Thickness of boundary layer

δ^* Displacement thickness of boundary layer

$$\delta^* = \int_0^\infty (1 - u/U_\infty)\, dy$$

θ Momentum thickness of boundary layer

$$\theta = \int_0^\infty u/U_\infty\, (1 - u/U_\infty)\, dy$$

ϵ Cavity depth

ϵ^* Dimensionless roughness parameter based on pre-cavity wall shear, $\epsilon^* = e\, u_\tau/\nu$

ϵ_c^* Dimensionless roughness parameter based on cavity interface wall shear, $\epsilon^* = \epsilon\, u_{\tau_c}/\nu$

τ_o Shear stress at y = 0

ρ Fluid density

μ Absolute viscosity

ν Kinematic viscosity

REFERENCES

1. Batchelor, G., "On Steady Laminar Flow with Closed Streamlines at Large Reynolds Number," Jour. Fluid Mech., Vol. 1, Part 1, 177 (1956).

2. Burggraf, O. R., "A Model of Steady Separated Flow in Rectangular Cavities at High Reynolds Number," Proceedings of the 1965 Heat Transfer and Fluid Mechanics Institute, Stanford University Press, 190-229 (1965).

3. Chapman, D. R., "A Theoretical Analysis for Heat Transfer in Regions of Separated Flow," NACA TN 3792 (1956).

4. Chapman, D. R., Kuehn, D. M., Larsen, H. K., "Investigation of Separated Flows in Supersonic and Subsonic Streams with Emphasis on the Effect of Transition, NACA TN 3869 (1957).

5. Charwat, A. F., Dewey, F. C. Jr., Roos, J. N., Hitz, J. A., "An Investigation of Separated Flows -- Part I: The Pressure Field," Jour. of the Aerospace Sciences, Vol. 28, No. 6, 457-470 (1961).

6. Charwat, A. F., Roos, J. N., Dewey, F. C. Jr., Hitz, J. A., "An Investigation of Separated Flows -- Part II: Flow in the Cavity and Heat Transfer," Jour. of the Aerospace Sciences, Vol. 28, No. 7, 513-527 (1961).

7. Collis, D. C., Williams, M. J., "Two-Dimensional Convection From Heated Wires at Low Reynolds Numbers," Jour. Fluid Mech., Vol. 6, Part 3, 375-384 (1959).

8. Cope, W. F., "The Friction and Heat Transmission Coefficients of Rough Pipes," Proceedings of the Institute of Mechanical Engineers, Vol. 105, 99-105 (1941).

9. Curle, N., The Laminar Boundary Layer Equations, Clarendon Press, Oxford (1962).

10. Denison, M. R., Baum, E., "Compressible Free Shear Layer with Finite Initial Thickness," AIAA Journal, Vol. 1, No. 2, 342 (1963).

11. Dipprey, D. F., "An Experimental Investigation of Heat and Momentum Transfer in Smooth and Rough Tubes at Various Prandtl Numbers," Ph.D. Thesis, California Institute of Technology (1961).

12. Dipprey, D. F., Sabersky, R. H., "Heat and Momentum Transfer in Smooth and Rough Tubes at Various Prandtl Numbers," Int. J. Heat and Mass Transfer, Vol. 6, 329-353, (1963).

13. Folsom, R. G., "An Experimental Investigation of the Phenomena Produced by the Highly Turbulent Flow of Water Past a Series of Sharp Obstacles," Ph.D. Thesis, California Institute of Technology (1932).

14. Fortescue, P., Hall, W. B., "Heat Transfer Experiments on the Fuel Elements," Jour. of British Nuclear Energy Conf., Vol. 2, No. 2, 83-91 (1957).

15. Fox, J., "Surface Pressure and Turbulent Airflow in Transverse Rectangular Notches," NASA TN D-2501 (1964).

16. Greenspan, H. P., Benney, D. J., "On Shear-Layer Instability, Breakdown, and Transition," Jour. Fluid Mech., Vol. 15, Part 1, 133-153 (1963).

17. Handbook of Chemistry and Physics, 44th Edition, The Chemical Rubber Publishing Co., Cleveland, Ohio (1963).

18. van der Hegge Zijnen, B. G., "Modified Correlation Formula for Heat Transfer by Natural and Forced Convection from Horizontal Cylinders," App. Sci. Res., Vol. VI, Sec. A, 129-141 (1957).

19. van der Hegge Zijnen, B. G., "Heat Transfer from Horizontal Cylinders in a Turbulent Airflow," App. Sci. Res., Vol. VII, Sec. A, 205-223 (1958).

20. James, D. F., "Laminar Flow of Dilute Polymer Solutions Around Circular Cylinders," Ph.D. Thesis, California Institute of Technology (1967).

21. King, L. V., "On the Convection of Heat from Small Cylinders in a Stream of Fluid," Phil. Trans. Roy. Soc., Ser. A, Vol. 214, 373-432 (1914).

22. Knudsen, J. G., Katz, D. L., "Heat Transfer and Pressure Drop in Annuli." Chem. Eng. Progress, Vol. 46, 490 (1950).

23. Laurence, J. C., Sanborn, V. A., "Heat Transfer from Cylinders," Symposium on Measurements in Unsteady Flow, presented at the ASME Hyd. Div. Conf., Worchester, Mass., May 21-23, 1962.

24. Lessen, M., "On Stability of Free Laminar Boundary Layer Between Parallel Stream," NACA Report No. 979 (1950).

25. Ling, S. C., "Measurement of Flow Characteristics by the Hot Film Technique," University Microfilms, Publication No. 12, 905, Ann Arbor, Michigan, Ph.D. Thesis, State Univ. of Iowa (1955).

26. Maull, D. J., East, L. F., "Three-Dimensional Flow in Cavities," Jour. Fluid Mech., Vol. 16, 620-632 (1963).

27. Mills, R. D., "The Flow in Rectangular Cavities," University of London, Ph. D. Thesis (1961).

28. Mills, R. D., "On the Closed Motion of a Fluid in a Square Cavity," Royal Aeronautical Soc. J., Vol. 69, No. 650, 116-120 (1965).

29. Nikuradse, J., "Laws of Flow in Rough Pipes," NACA TM 1292 (1950).

30. Nunner, W., "Heat Transfer and Pressure Drop in Rough Tubes," VDI-Forschungsheft 455, Series B, 22, 5-39 (1956); also A.E.R.E. Lib/Trans. 786 (1958).

31. Owen, P. R., Thomson, W. R., "Heat Transfer Across Rough Surfaces," Jour. Fluid Mech., Vol. 15, Part 3, 321-324 (1963).

32. Piercy, N. A. V., Richardson, E. G., Winny, H. F., "On the Convection of Heat from a Wire Moving Through Air Close to a Cooling Surface," Proc. Phys. Soc., Series B., Vol. 69 (1956).

33. Piret, E. L., James, W., Stacy, M., "Heat Transmission from Fine Wire to Water," Ind. and Engin. Chem., Vol. 39, 1098-1103 (1947).

34. Roshko, A., "Some Measurements of Flow in a Rectangular Cutout," NACA TN 3488 (1955).

35. Roshko, A., Lau, J. C., "Some Observations on Transition and Reattachment of a Free Shear Layer in Incompressible Flow," Proceedings of the 1965 Heat Transfer and Fluid Mechanics Institute, Stanford University Press, 157-167 (1965).

36. Runstadler, P. W., Kline, S. J., Reynolds, W. C., "An Experimental Investigation of the Flow Structures of the Turbulent Boundary Layer," AFORS-TN-5241, Report MD-8, Thermo-Sciences Division, Dept. of Mech. Engin., Stanford University (June 1963).

37. Sams, E. L., "Experimental Investigation of Average Heat-Transfer and Friction Coefficients for Air Flowing in Circular Tubes Having Square-Thread-Type Roughness," NACA RM E52D17 (1952).

38. Sato, H., "Experimental Investigation of the Transition of Laminar Separated Layer," Jour. of the Physical Society of Japan, Vol. 11, No. 6, 702-709 (1956).

39. Schlichting, H., Boundary Layer Theory, McGraw-Hill, New York (1955).

40. Schubauer, G. B., Skramstad, H. K., "Laminar-Boundary-Layer Oscillations and Transition on a Flat Plate," NACA Report No. 909 (1948).

41. Seban, R. A., "Heat Transfer and Flow in Shallow Rectangular Cavities with Subsonic Turbulent Air Flow," Int. J. Heat and Mass Transfer, Vol. 8, No. 11, 1353-1368 (1965).

42. Tani, I., Komoda, H., Komatsu, Y., Iuchi, M., "Boundary-Layer Transition by Isolated Roughness," Aeronautical Research Institute, University of Tokyo, Report 375, 129-142 (1962).

43. Tani, I., Iuchi, M., Komoda, H., "Experimental Investigation of Flow Separation Associated with a Step or a Groove," Aeronautical Research Institute, University of Tokyo, Report 364, 119-136 (1961).

44. Townes, H. W., "Flow Over a Rough Surface," Ph.D. Thesis, California Institute of Technology (1965).

45. Townes, H. W., Sabersky, R. H., "Experiments on the Flow Over a Rough Surface," Int. J. Heat and Mass Transfer, Vol. 9, 729-738 (1966).

46. Wieghardt, K., "Erhohung des turbulenten Reibungswiderstandes durch Oberflachenstorungen (Increase of the Turbulent Frictional Resistance Caused by Surface Irregularities), " Forschungsbericht 1563, ZWB (March 1942); also Jahrb., deutchen Luftfhartforschung.

47. Wills, J. A. B., "The Correction of Hot-Wire Readings for Proximity to a Solid Boundary, " Jour. Fluid Mech., Vol. 12, Part 3, 388-396 (1962).

APPENDIX

DESIGN CALCULATIONS

Preliminary design calculations were made to determine the boundary layer development length and the free stream velocity range to span a given shear velocity range in a laminar flat plate flow. The shear velocity range desired was that of Townes' study, i.e., $0.0075 \text{ ft/sec} \leq u_\tau \leq 0.031 \text{ ft/sec}$. The working fluid was to be water at about 23.5°C. Thus the kinematic viscosity ν is $1.01 \times 10^{-5} \text{ ft}^2/\text{sec}$. For these calculations the results of the Blasius solution are used.

From the Blasius solution for laminar flat plate flow:

$$\frac{1}{U_\infty} \left.\frac{du}{d\eta}\right|_{\eta=0} = 0.33206 \tag{A-1}$$

where

$$\eta = y \sqrt{U_\infty/\nu\, x} \tag{A-2}$$

Eliminating η:

$$x = \frac{(0.33206)^2 U_\infty^{\,3}}{\nu} \left[\left.du/dy\right|_{y=0}\right]^{-2} \tag{A-3}$$

or in terms of u_τ:

$$x = \frac{(0.33206)^2 U_\infty^{\,3} \nu}{u_\tau^{\,4}} \tag{A-4}$$

The above is the primary relation between x, U_∞, and u_τ. A second relationship between these variables is obtained from the requirement of laminar flow. The Reynolds number xU_∞/ν for laminar-turbulent transition is given in the literature as between 3.0×10^5 to 10^6 (39). To be on the safe side a maximum Re_x of 300,000 is allowed. A further requirement of the boundary layer is that it be thick enough so that velocity profiles can be precisely measured. A minimum δ value of 0.10 inch was considered satisfactory.

From Equation (A-4) the following table was prepared using the maximum and minimum desired shear velocities:

x (ft)	$(U_\infty)_{u_\tau}$ max (ft/sec)	$(U_\infty)_{u_\tau}$ min (ft/sec)	$(Re_x)_{u_\tau}$ max	$(\delta)_{u_\tau}$ max (inch)
0.5	0.113	0.76	38,000	0.154
1.0	0.142	0.96	96,000	0.196
1.5	0.162	1.10	165,000	0.221
2.0	0.179	1.21	242,000	0.244
2.5	0.193	1.30	325,000	0.264
3.0	0.204	1.38	414,000	0.280
4.0	0.226	1.52	608,000	0.308

From this table one observes that any boundary layer development length between 0.5 and 2.0 ft. should be satisfactory

in that it gives the required shear velocity for a convenient free stream velocity range in laminar flow.

TABLE 1

AVERAGE FREE STREAM ACCELERATIONS MEASURED BETWEEN THE LEADING EDGE OF THE FLAT PLATE AT x = 0 INCHES AND THE TEST SECTION AT x = 12 INCHES

U_{∞_o} (ft/sec)	dU_∞/dx (1/sec)	$1/U_{\infty_o}\ dU_\infty/dx$ (1/ft)
0.125	0.0086	0.069
0.25	0.0130	0.052
0.50	0.0230	0.046
0.75	0.0330	0.044

U_{∞_o} = Free stream velocity at x = 12 inches.

TABLE 2

SUMMARY OF

PRE-CAVITY AND POST-CAVITY VELOCITY PROFILE DATA

U_∞ (ft/sec)	ϵ (in.)	x_1 (in.)	u_τ (ft/sec)	δ^* (in.)
0.125		-0.25	0.0152	0.112
0.125	1/4	0.31	0.0162	0.113
0.125	1/2	0.625	0.0164	0.117
0.125	1	1.25	0.0169	0.098
0.25		-0.25	0.0232	0.089
0.25	1/4	0.31	0.0251	0.080
0.25	1/2	0.625	0.0246	0.075
0.25	1	1.25	0.0248	0.080
0.50		-0.25	0.0346	0.070
0.50	1/4	0.31	0.0363	0.072
0.50	1/2	0.625	0.0367	0.064
0.50	1	1.25	0.0406	0.058
0.75		-0.25	0.0483	0.051
0.75	1/4	0.31	0.0507	0.050
0.75	1/2	0.625	0.0511	0.051

U_∞ = average free stream velocity

ϵ = cavity depth = cavity length

x_1 = distance from upstream cavity wall (+ in flow direction)

u_τ = $\sqrt{\nu \, du/dy\big|_{y=0}}$ determined from wall slope of velocity profiles

δ^* = displacement thickness of boundary layer determined from measured velocity profiles

TABLE 3

CAVITY ϵ^* and ϵ_c^* VALUES

ϵ (in.)	U_∞ (ft/sec)	ϵ^*	ϵ_c^*
1/8	0.125	15.8	est. 8.0
1/8	0.25	24.0	est. 14.0
1/8	0.50	35.8	est. 20.0
1/8	0.75	50.1	est. 28.0
1/4	0.125	31.6	14.6
1/4	0.25	48.0	24.4
1/4	0.50	71.6	38.2
1/4	0.75	100.2	53.4
1/2	0.125	63.2	27.0
1/2	0.25	96.0	44.6
1/2	0.50	143.2	73.3
1/2	0.75	200.4	103.0
1	0.125	126.4	50.8
1	0.25	192.0	86.7
1	0.50	286.4	133.6
1	0.75	400.8	est. 200.0

ϵ = cavity depth

U_∞ = average free stream velocity

$\epsilon^* = \epsilon u_\tau / \nu$

$\epsilon_c^* = \epsilon u_{\tau_c} / \nu$

TABLE 4

SUMMARY OF CAVITY VELOCITY PROFILE DATA

ϵ	x_1	U_∞	$(u_\tau)_{y=0}$	$(u/U_\infty)_{y=0}$	y_m/ϵ	$(u/U_\infty)_{y_m}$	y_δ/ϵ
(in.)	(in.)	(ft/sec)					
1/4	1/8	0.125	0.0070	0.27	-	< 0.002	-0.24
1/4	1/8	0.25	0.0117	0.28	-	0.002	-0.32
1/4	1/8	0.50	0.0183	0.27	-0.64	0.008	-0.32
1/4	1/8	0.75	0.0256	0.33	-0.80	0.030	-0.44
1/2	1/4	0.125	0.0065	0.27	-	< 0.002	-0.20
1/2	1/4	0.25	0.0107	0.23	-	0.002	-0.18
1/2	1/4	0.50	0.0176	0.29	-0.84	0.027	-0.22
1/2	1/4	0.75	0.0248	0.34	-0.86	0.078	-0.33
1	1/4	0.125	0.0068	0.26	-	< 0.002	-0.09
1	1/4	0.25	0.0107	0.34	-0.62	0.003	-0.11
1	1/4	0.50	0.0168	0.30	-0.55	0.028	-0.10
1	1/2	0.125	0.0061	0.27	-	< 0.002	-0.14
1	1/2	0.25	0.0104	0.33	-0.83	0.019	-0.22
1	1/2	0.50	0.0160	0.26	-0.85	0.030	-0.25
1	3/4	0.125	0.0060	0.33	-	< 0.002	-0.15
1	3/4	0.25	0.0103	0.37	-0.80	0.011	-0.19
1	3/4	0.50	0.0150	0.34	-0.93	0.026	-0.23

ϵ = cavity depth

TABLE 4 - Continued

x_1	=	distance from front wall of cavity
U_∞	=	average free stream velocity
$(u_\tau)_{y=0}$	=	shear velocity at y=0 plane of cavity interface
$(u/U_\infty)_{y=0}$	=	fraction of free stream velocity at y=0 plane of cavity interface
y_m/ϵ	=	relative cavity depth at which maximum cavity vortex velocity was observed
$(u/U_\infty)_{y_m}$	=	maximum relative cavity vortex velocity
y_δ/ϵ	=	relative cavity depth at which shear layer velocity becomes less than 1 percent of free stream velocity

TABLE 5

LAMINAR OSCILLATION FREQUENCIES

1 x 1 inch cavity

U_∞ (ft/sec)	f (cps)	S_ϵ	Re_ϵ
0.298	1.14	0.319	2480
0.305	1.21	0.330	2540
0.327	1.21	0.308	2720
0.341	1.32	0.322	2840
0.349	1.33	0.318	2910
0.377	1.46	0.322	3140
0.385	1.51	0.327	3200
0.386	1.48	0.319	3219
0.394	1.52	0.322	3280
0.403	1.60	0.331	3360
0.419	1.58	0.314	3490
0.422	1.65	0.326	3520
0.441	1.70	0.322	3670
0.453	1.77	0.326	3770
0.457	1.83	0.334	3800
0.474	1.90	0.334	3950
0.475	1.84	0.322	3960
0.484	1.98	0.340	4030
0.485	1.93	0.332	4050
0.499	2.00	0.334	4160
0.510	2.01	0.328	4250
0.535	2.24	0.349	4460
0.562	2.29	0.339	4680
0.587	2.32	0.329	4860
0.589	2.39	0.339	4900
0.641	2.57	0.334	5340
0.650	2.70	0.346	5410
0.676	2.84	0.350	5640
0.725	2.73	0.314	6050
0.730	2.94	0.336	6080
0.740	3.18	0.358	6170
0.764	3.09	0.337	6360
0.770	3.32	0.359	6410
0.825	3.39	0.343	6870
0.893	3.48	0.325	7440

TABLE 5 (continued)

1 inch deep x 1/2 inch long cavity

U_∞ (ft/sec)	f (cps)	S_ϵ	Re_ϵ
0.275	1.11	0.336	2290
0.322	1.29	0.334	2680
0.354	1.42	0.334	2950
0.380	1.49	0.327	3160
0.392	1.61	0.342	3260
0.445	1.89	0.354	3700
0.455	1.92	0.352	3790
0.484	2.08	0.358	4030
0.505	2.16	0.356	4200
0.524	2.24	0.356	4370
0.562	2.52	0.374	4680
0.625	2.81	0.374	5200
0.775	4.65	0.500	6450
0.796	4.61	0.483	6630
0.925	7.40	0.667	7700
0.970	7.33	0.630	8080
1.043	7.87	0.628	8670
1.110	8.78	0.657	9220

1/2 inch x 1/2 inch cavity

U_∞ (ft/sec)	f (cps)	S_ϵ	Re_ϵ
0.562	3.70	0.244	2340
0.606	4.00	0.275	2530
0.614	4.05	0.274	2560
0.687	4.78	0.290	2860
0.750	5.32	0.298	3120
0.816	5.95	0.304	3400
0.836	6.02	0.300	3480
0.920	6.91	0.313	3830
1.00	7.57	0.315	4170
1.23	9.52	0.322	5130
1.50	12.0	0.334	6250

TABLE 5 (continued)

1/2 inch deep x 1-1/4 inch long cavity

U_∞ (ft/sec)	f (cps)	S_ϵ	Re_ϵ
0.595	4.06	0.284	2480
0.642	4.33	0.281	2680
0.705	4.74	0.280	2940
0.784	5.41	0.288	3260
0.840	5.88	0.292	3500
1.00	7.30	0.304	4170

U_∞ = average free stream velocity

f = oscillation frequency

$S_\epsilon = f\epsilon / U_\infty$ = Strouhal number based on cavity depth and free stream velocity

$Re_\epsilon = U_\infty \epsilon / \nu$ = Reynolds number based on cavity depth and free stream velocity

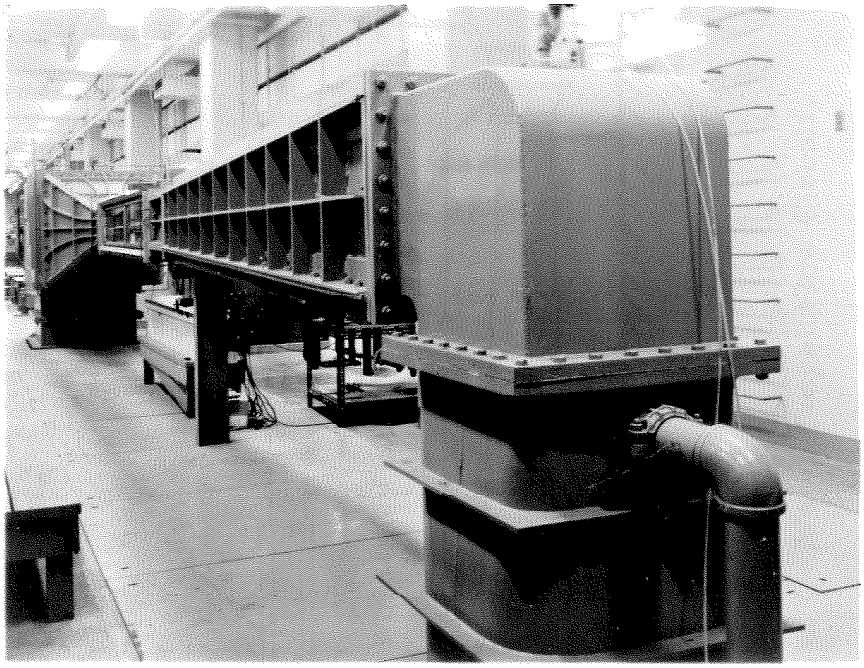

Fig. 1. Photograph of the Water Tunnel.

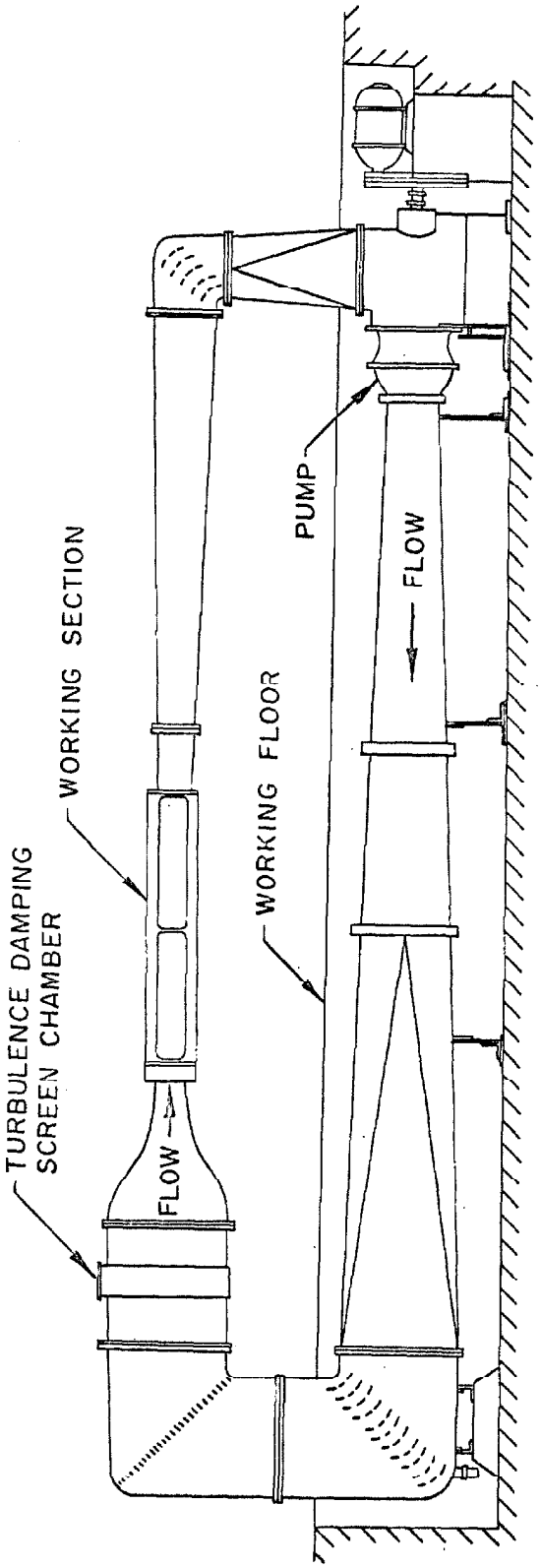

Fig. 2. Diagram of the Water Tunnel Flow Circuit.

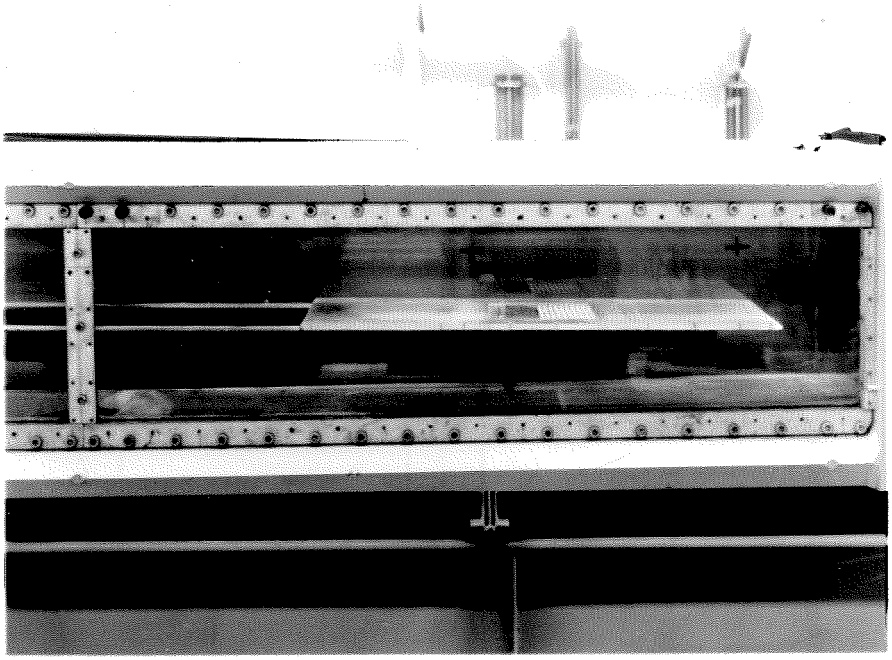

Fig. 3. Photograph of Water Tunnel Working Section with Flat Plate. Cavity section installed.

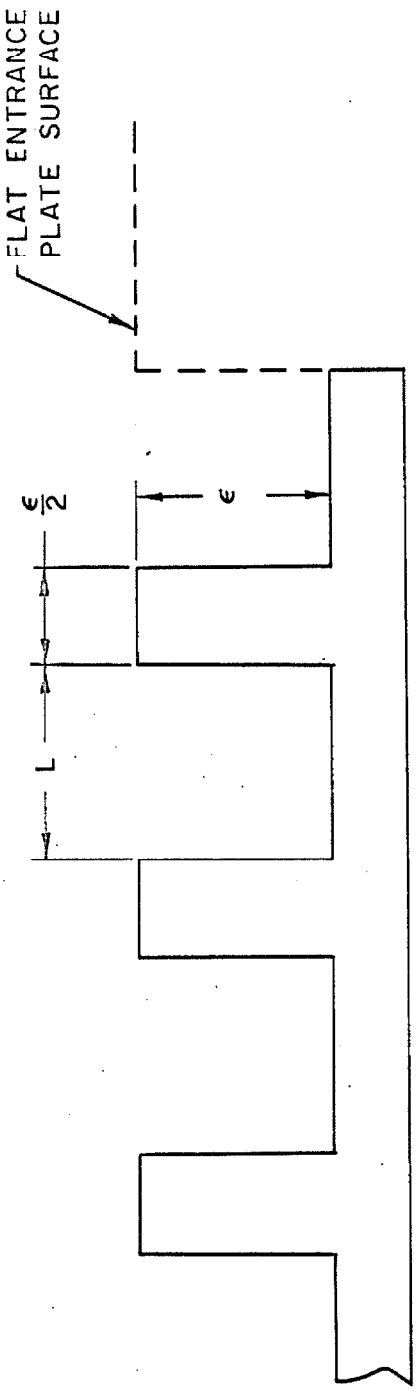

ε = CAVITY DEPTH
L = CAVITY LENGTH
7 IN. = CAVITY SPAN

Fig. 4. Cross Section of Cavity Plate.

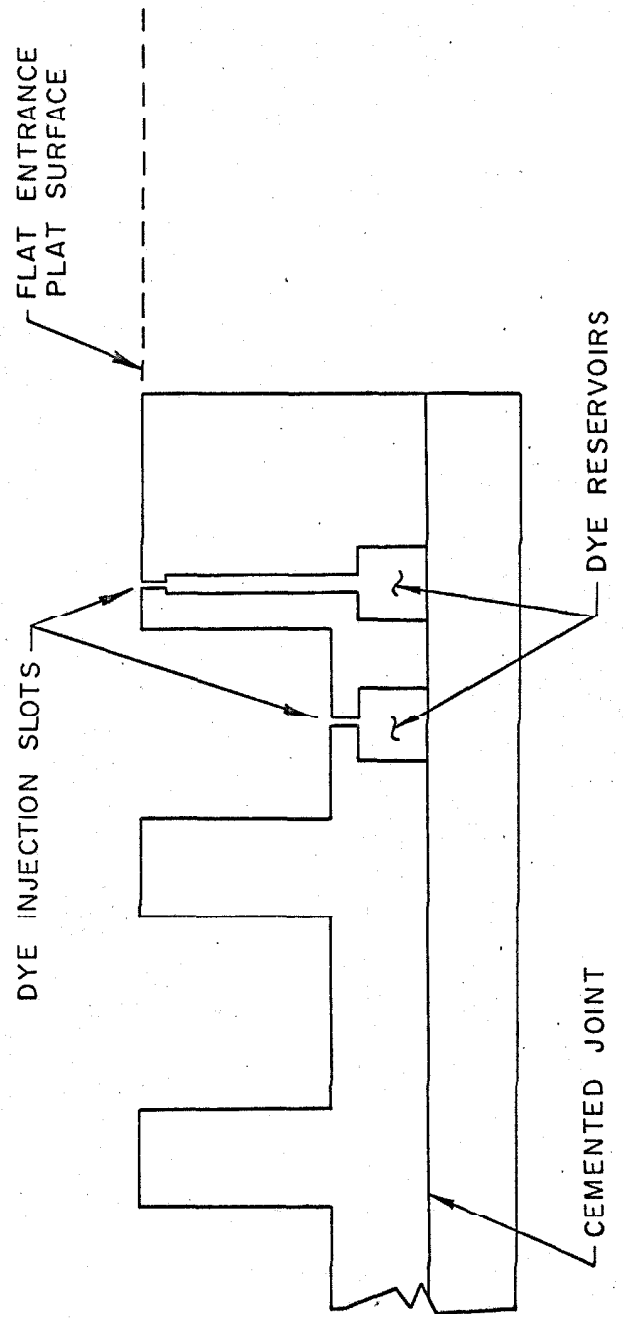

Fig. 5. Cross Section of Plate with Dye Slots. The span equals 7 inches and $\epsilon = L = \frac{1}{8}$ inch.

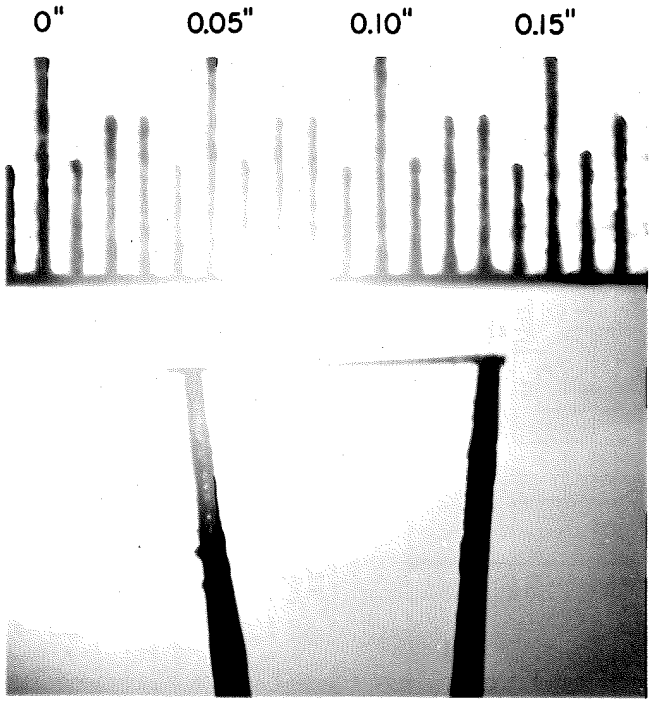

Fig. 6. Photograph of 0.001 in. dia. Hot-Film Sensor.

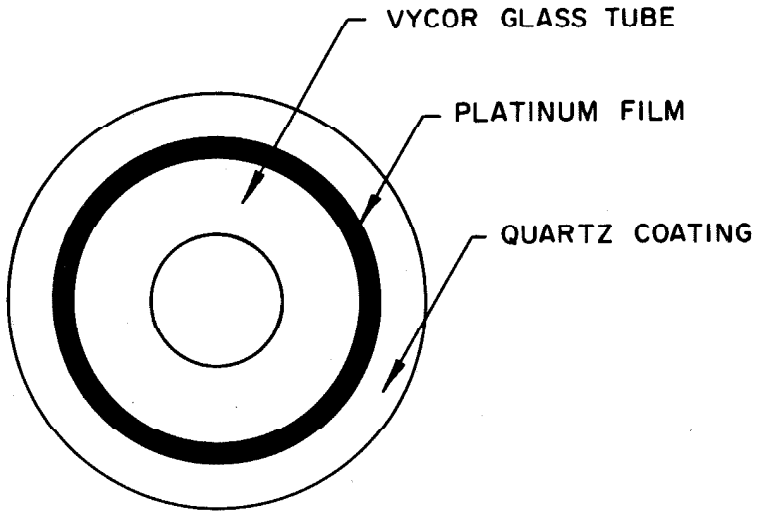

Fig. 7. Cross Section of Active Portion of the Hot-Film Sensor. The thicknesses of the platinum film and the quartz coating are greatly exaggerated.

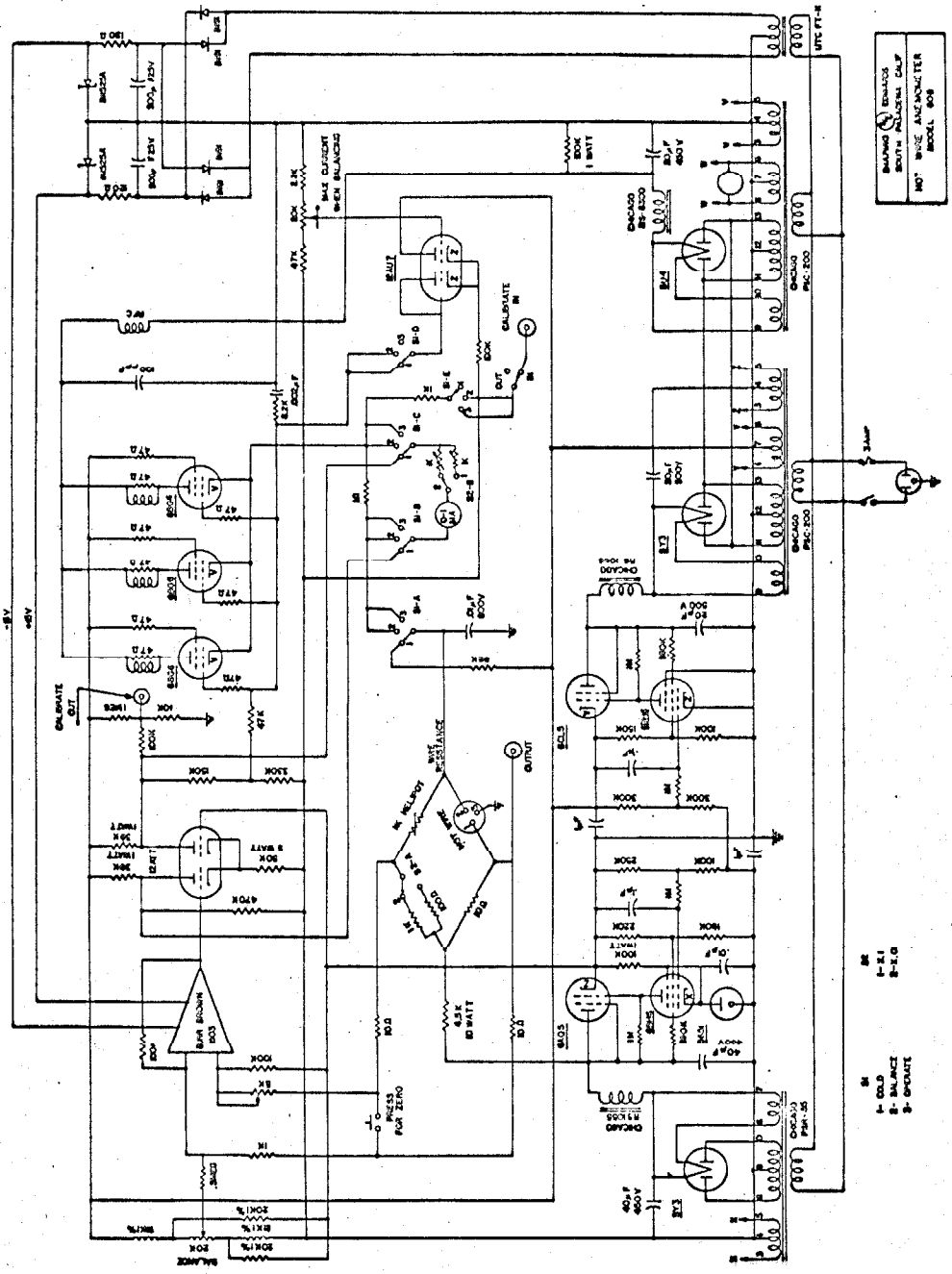

Fig. 8. Circuit Diagram of Shapiro & Edwards Model 60B, hot wire anemometer.

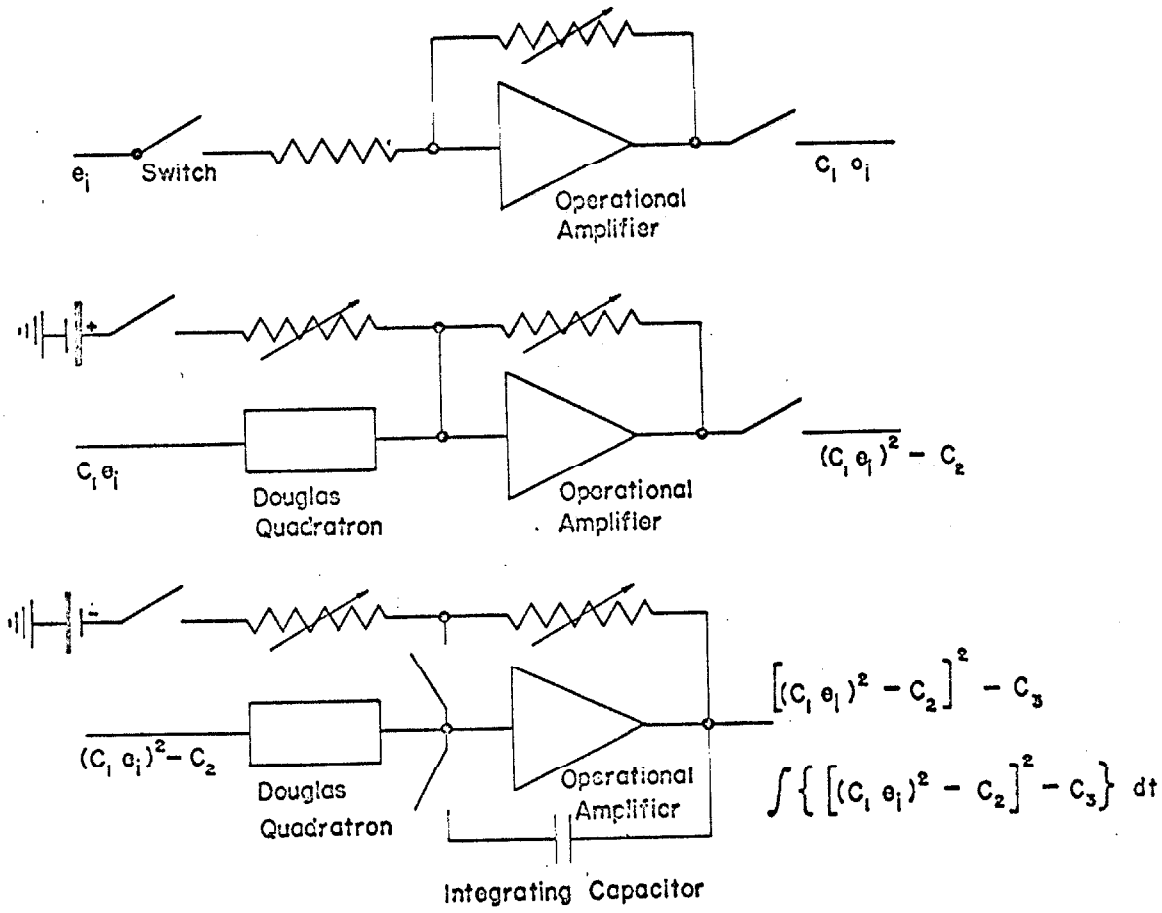

Fig. 9. Linearizing circuit diagram.

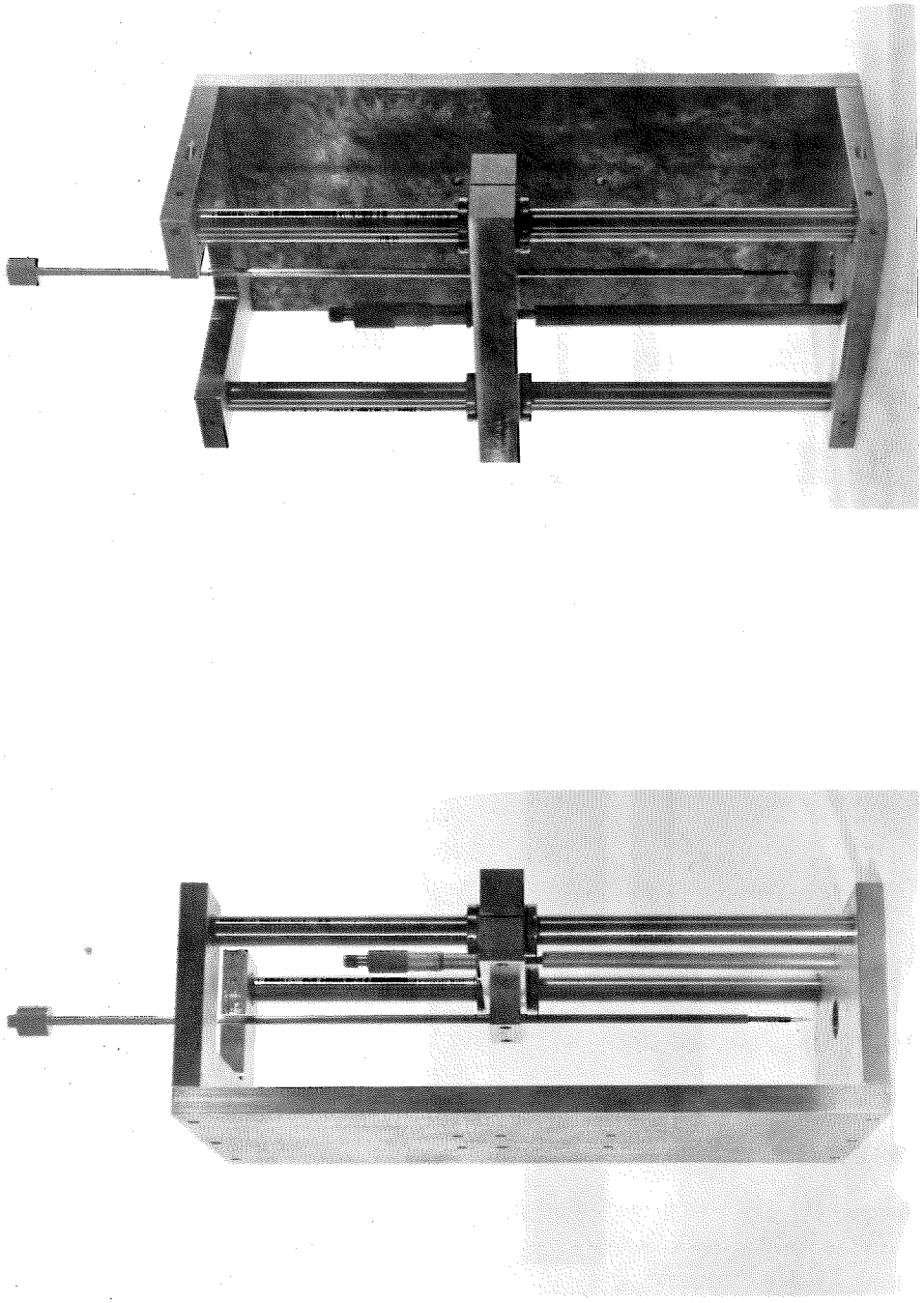

Fig. 10. Photographs of the traversing mechanism with the hot-film probe.

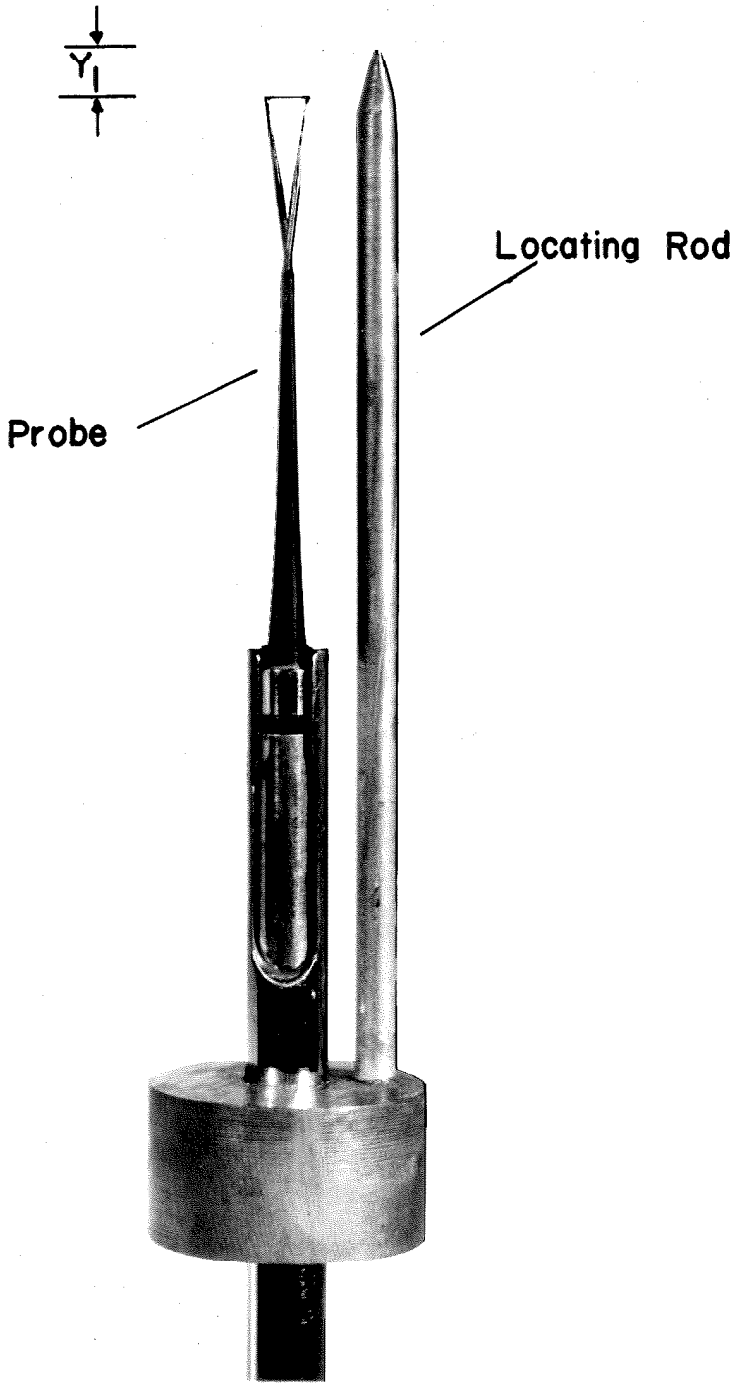

Fig. 11. The hot-film probe and locating rod.

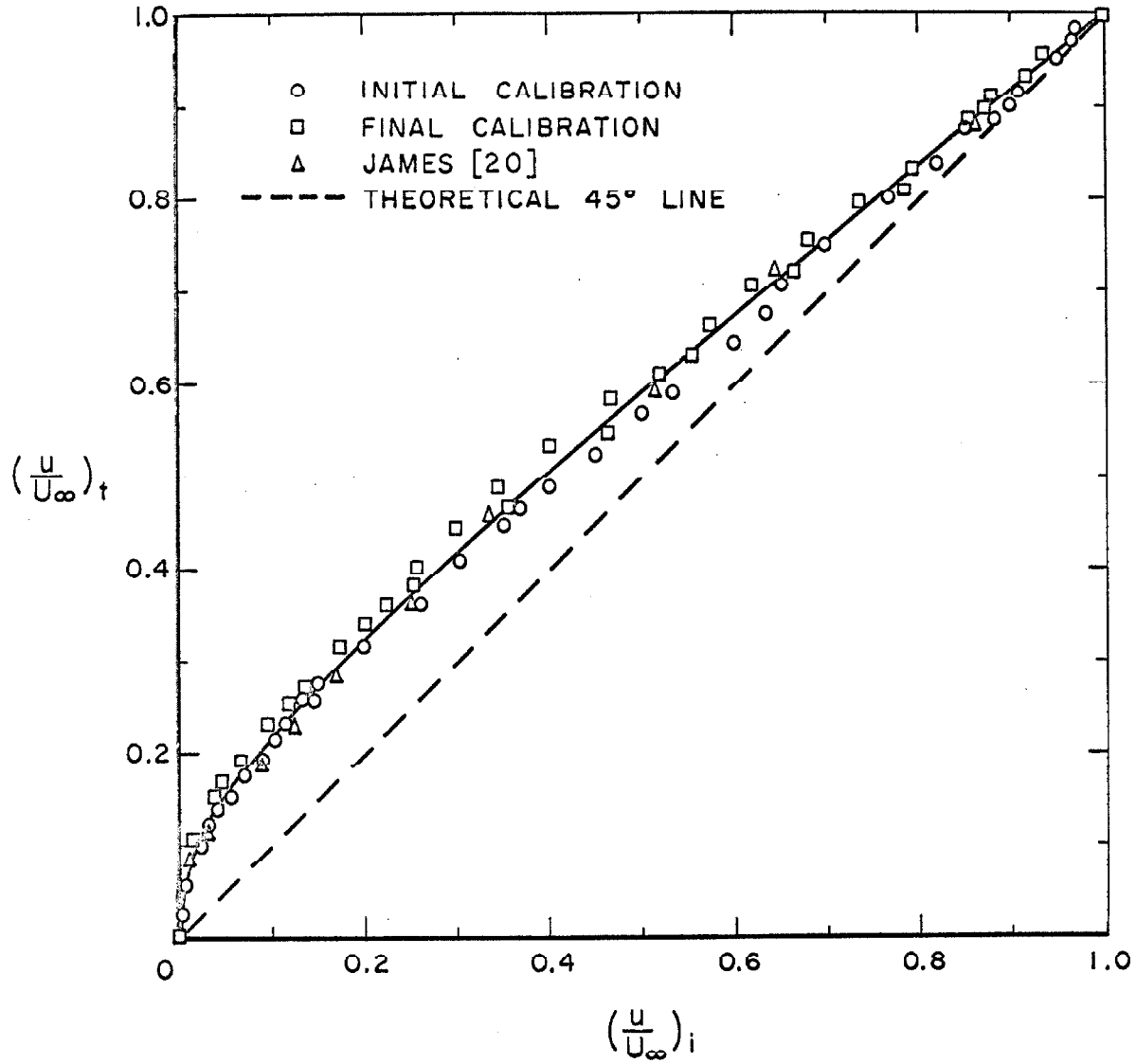

Fig. 12. Tow tank calibration curve for hot-film anemometer system. U_∞ = 0.125 ft/sec. The subscript i denotes velocities indicated by the anemometer system. The subscript t denotes velocities determined by tow tank time and distance measurements.

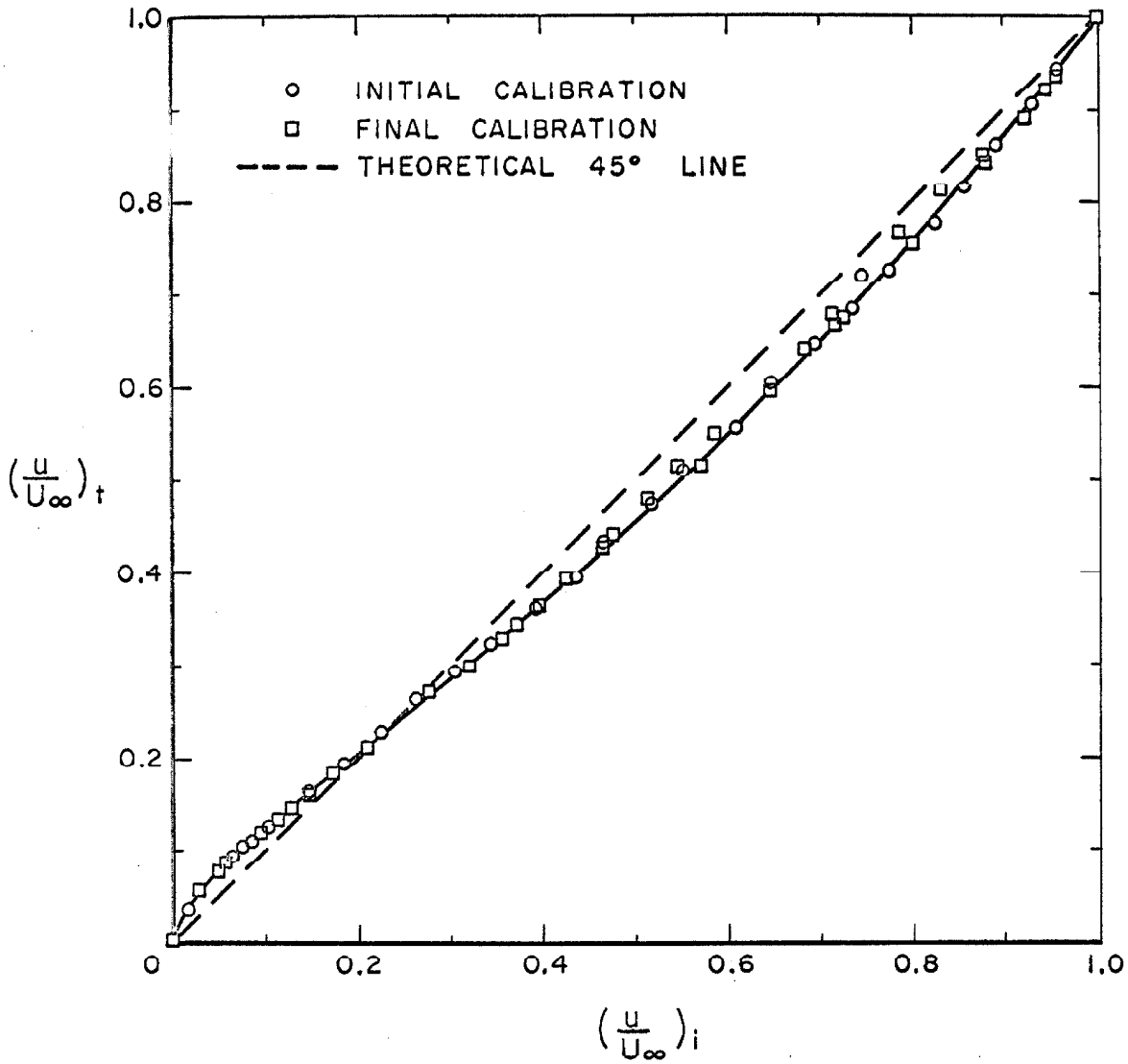

Fig. 13. Tow tank calibration curve for hot-film anemometer system. $U_\infty = 0.50$ ft/sec. The subscript i denotes velocities indicated by the anemometer system. The subscript t denotes velocities determined by tow tank time and distance measurements.

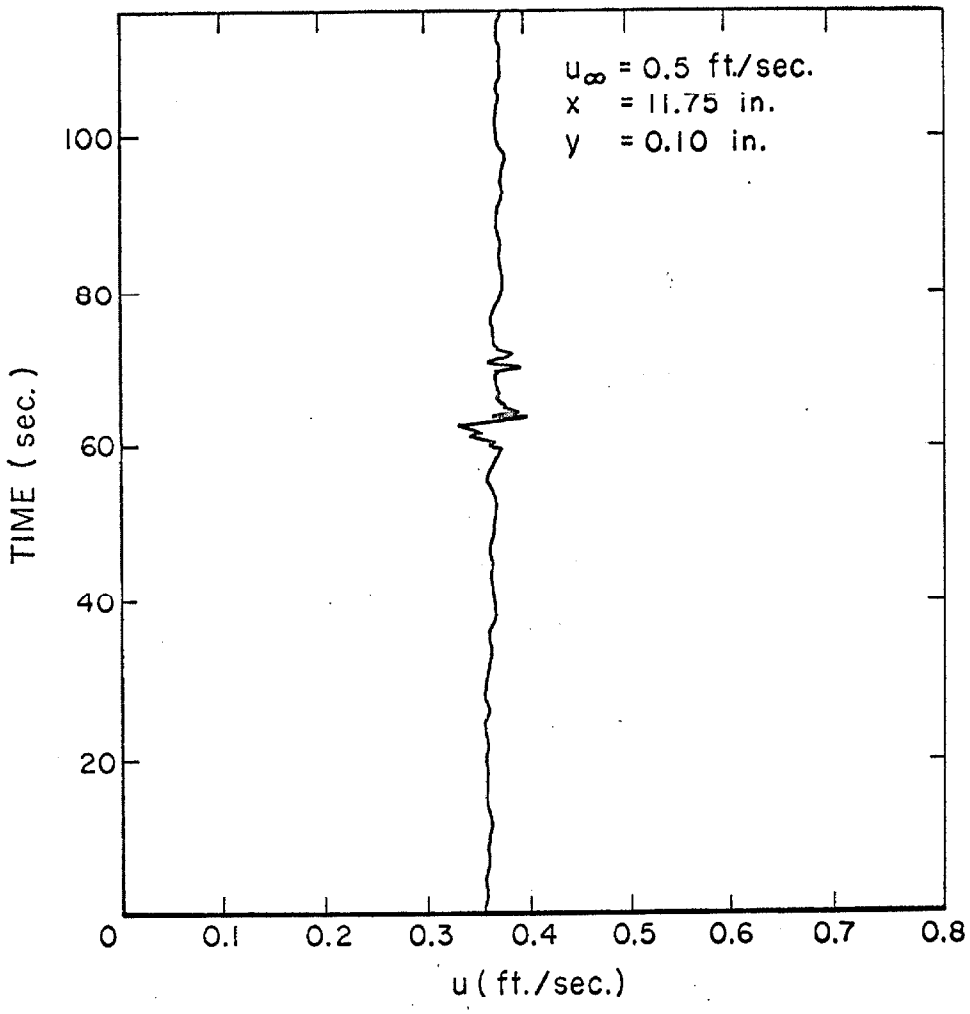

Fig. 14. Tracing of Sanborn velocity record showing typical turbulence-like disturbances.

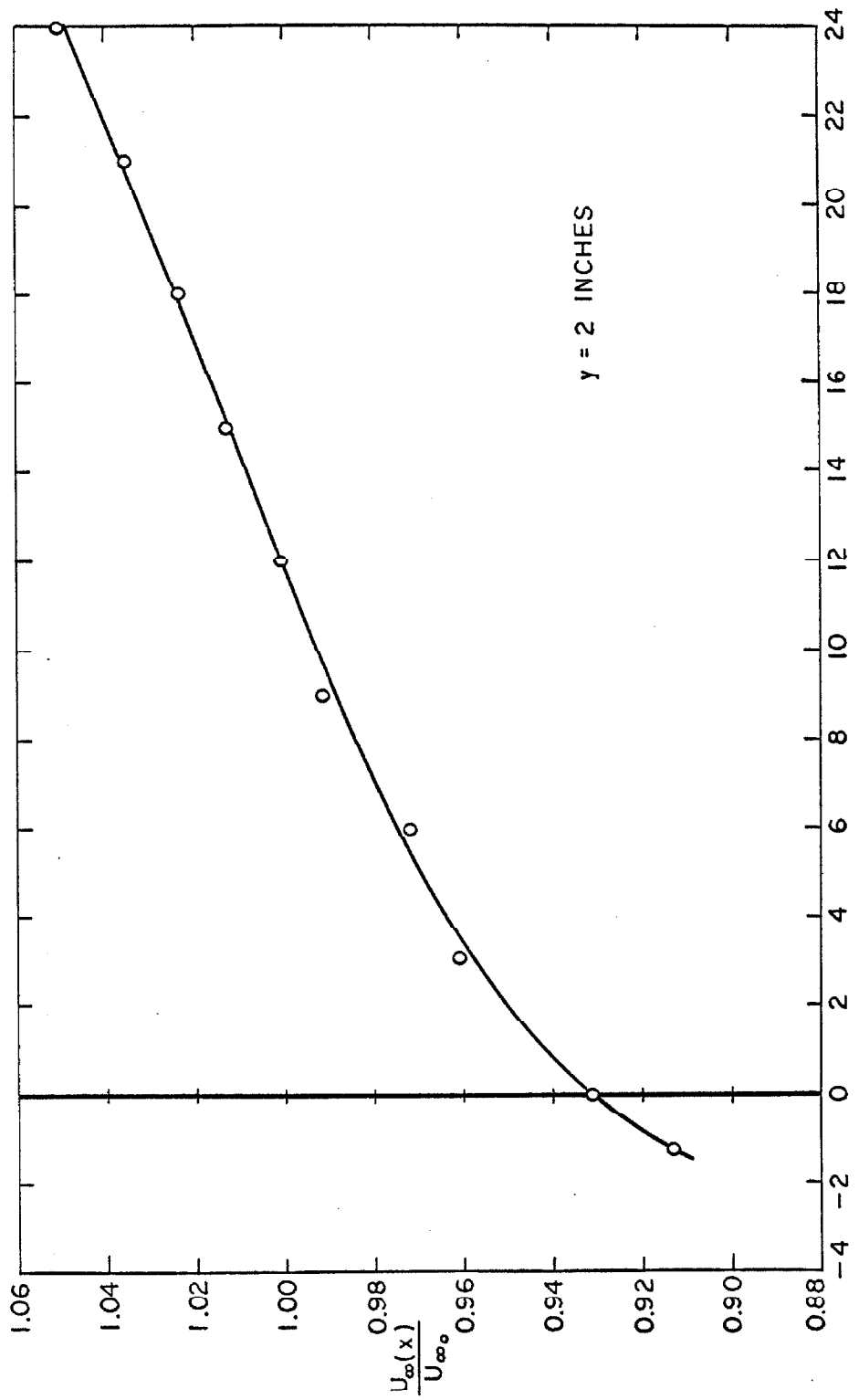

Fig. 15. Free stream accelcration for $U_{\infty_o} = 0.125$ ft/sec. U_{∞_o} denotes the free stream velocity at x = 12 inches.

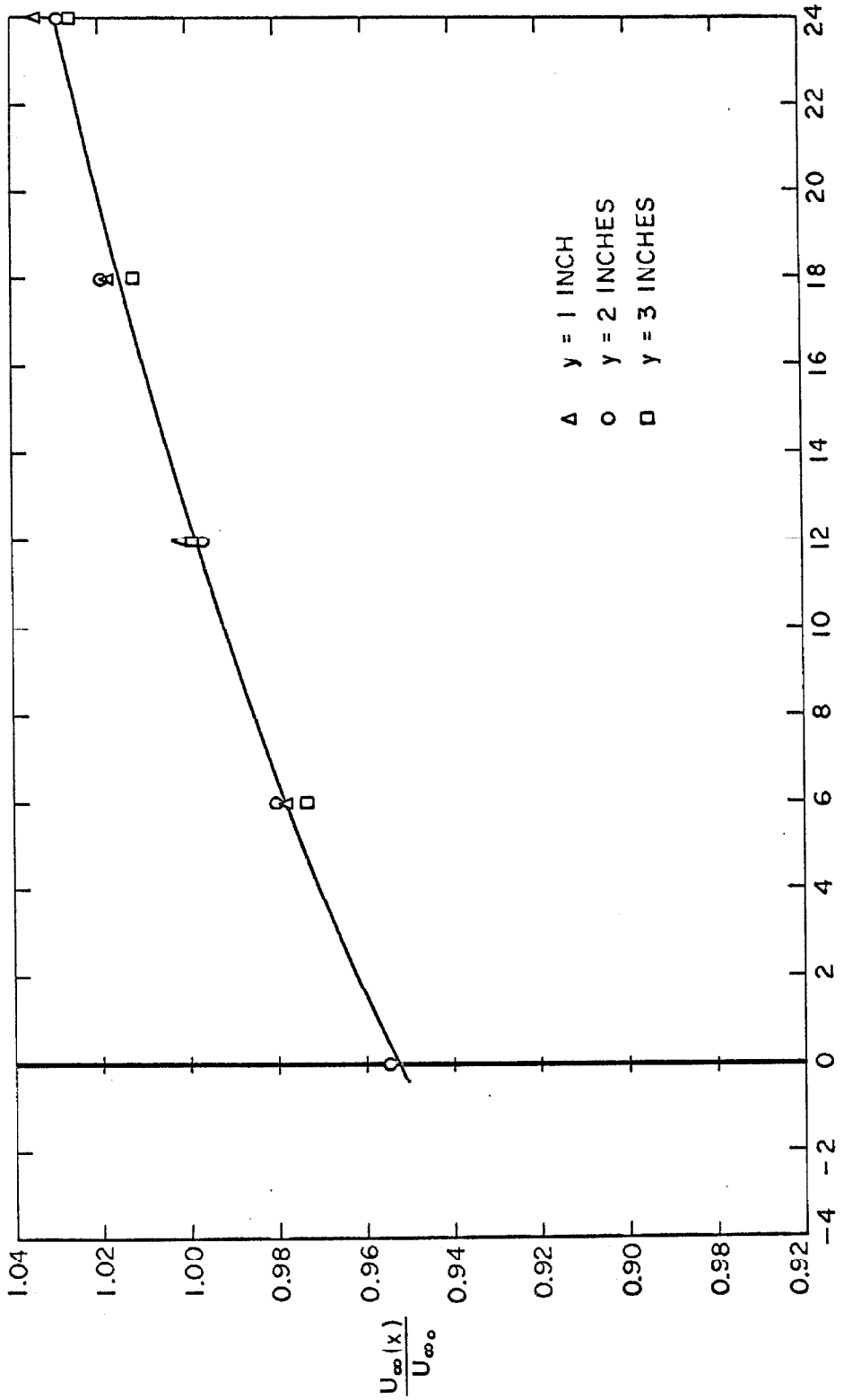

Fig. 16. Free stream acceleration for $U_{\infty o} = 0.75$ ft/sec. $U_{\infty o}$ denotes the free stream velocity at x = 12 inches.

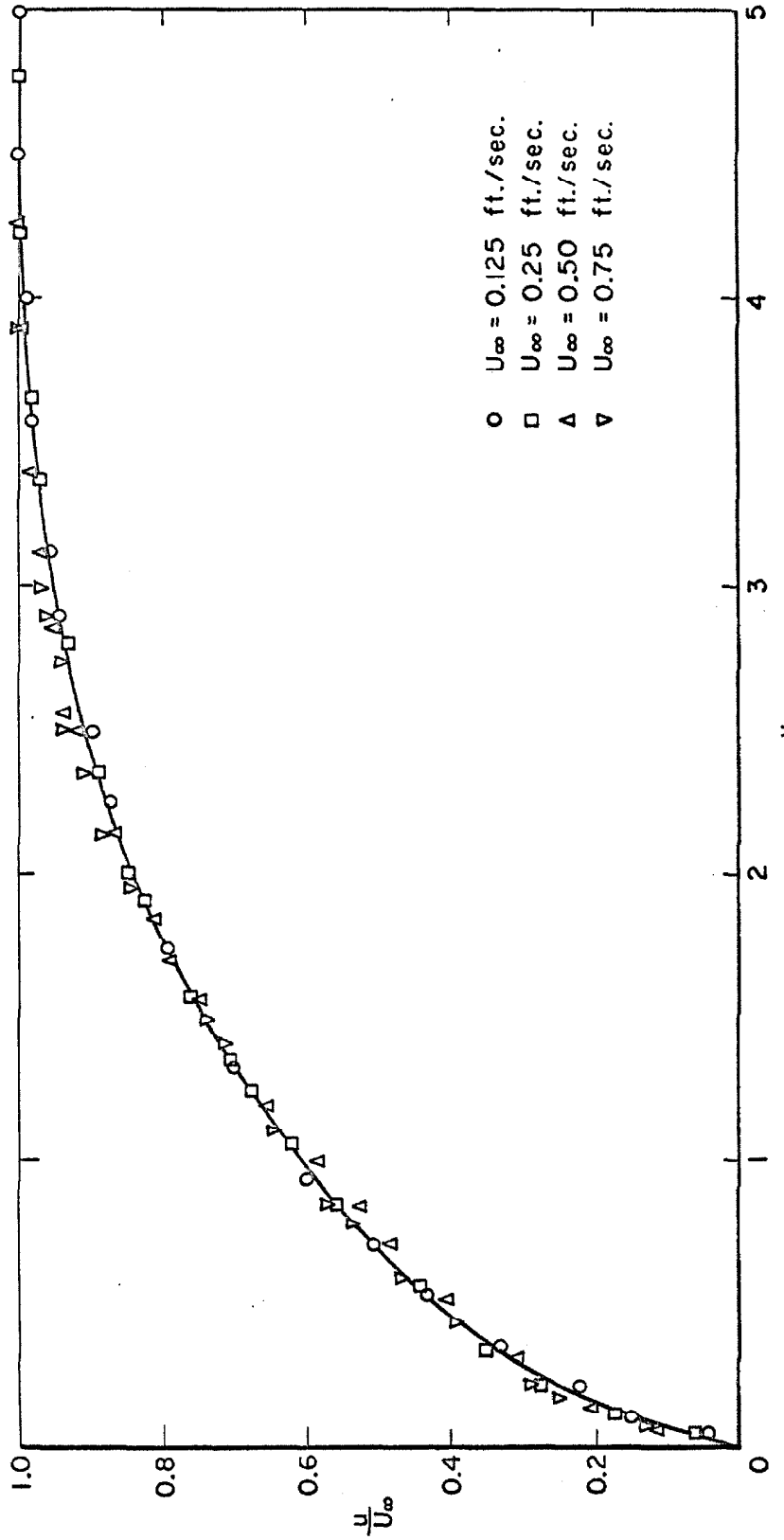

Fig. 17. Velocity profiles ahead of the cavity. x = 11.75 inches.

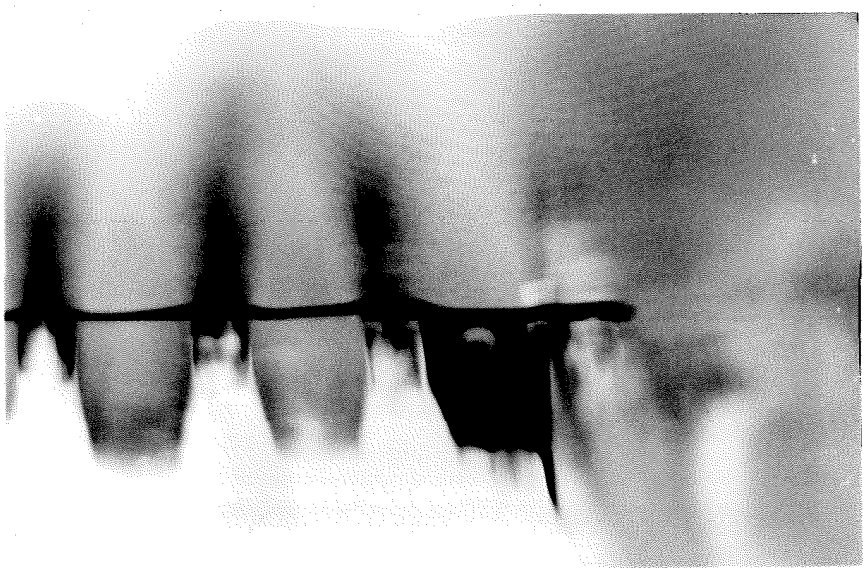

Fig. 18. Photograph of cavity flow. Flow is from right to left. 1/8 x 1/8 in. cavities, $U_\infty = 0.75$ ft/sec., $\epsilon^* = 15.8$.

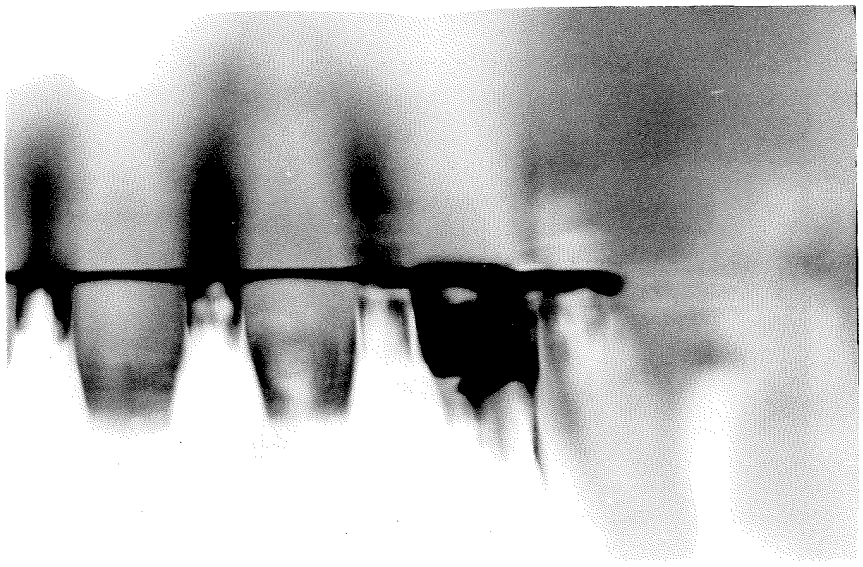

Fig. 19. Photograph of cavity flow. Flow is from right to left. 1/8 x 1/8 in. cavities, $U_\infty = 0.75$ ft/sec., $\epsilon^* = 50.1$.

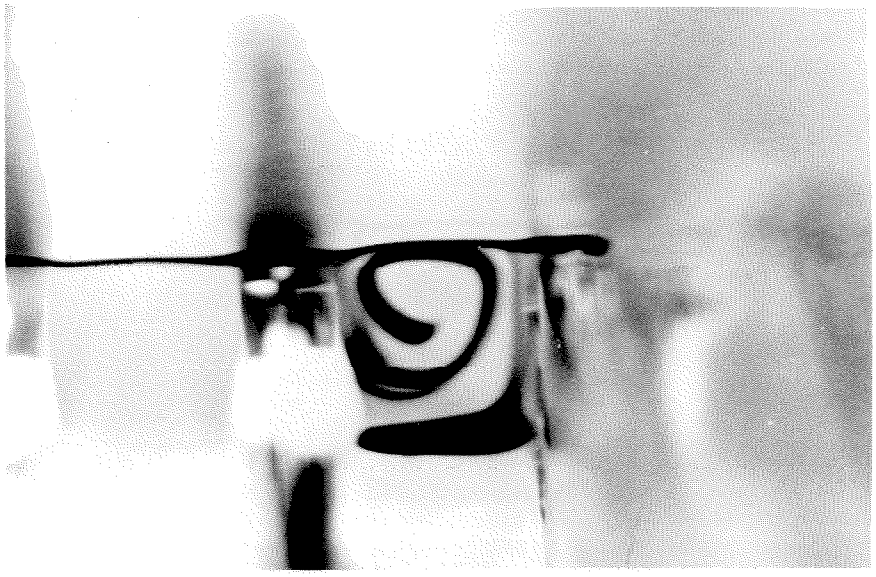

Fig. 20. Photograph of cavity flow. Flow is from right to left. 1/4 x 1/4 in. cavities, U_∞ = 0.125 ft/sec., ϵ^* = 31.6.

Fig. 21. Photograph of cavity flow. Flow is from right to left. 1/4 x 1/4 in. cavities, U_∞ = 0.50 ft/sec., ϵ^* = 71.6.

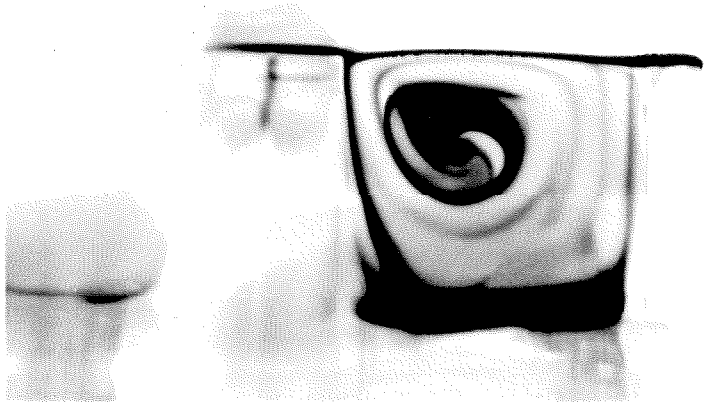

Fig. 22. Photograph of cavity flow. Flow is from right to left. 1/2 x 1/2 in. cavity, U_∞ = 0.125 ft/sec., ϵ^* = 63.2.

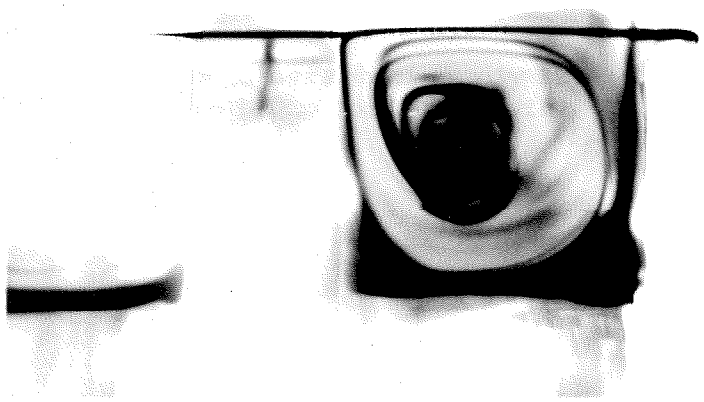

Fig. 23. Photograph of cavity flow. Flow is from right to left. 1/2 x 1/2 in. cavity, U_∞ = 0.50 ft/sec., ϵ^* = 143.2.

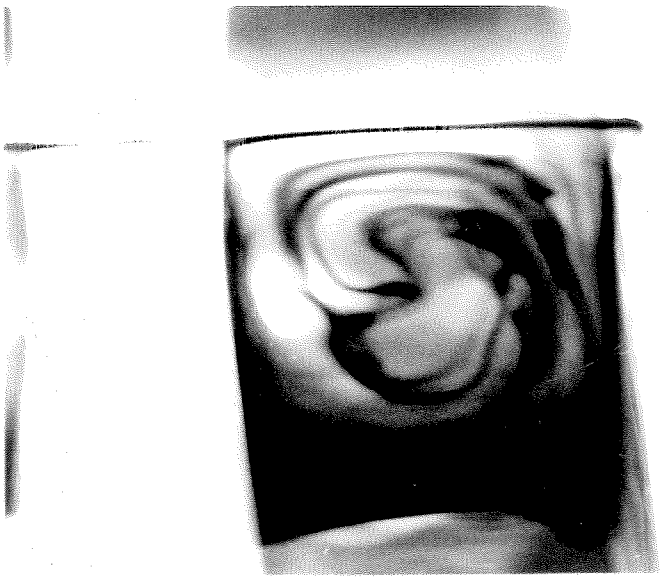

Fig. 24. Photograph of cavity flow. Flow is from right to left. 1 x 1 in. cavity, $U_\infty = 0.25$ ft/sec., $\epsilon^* = 192.0$.

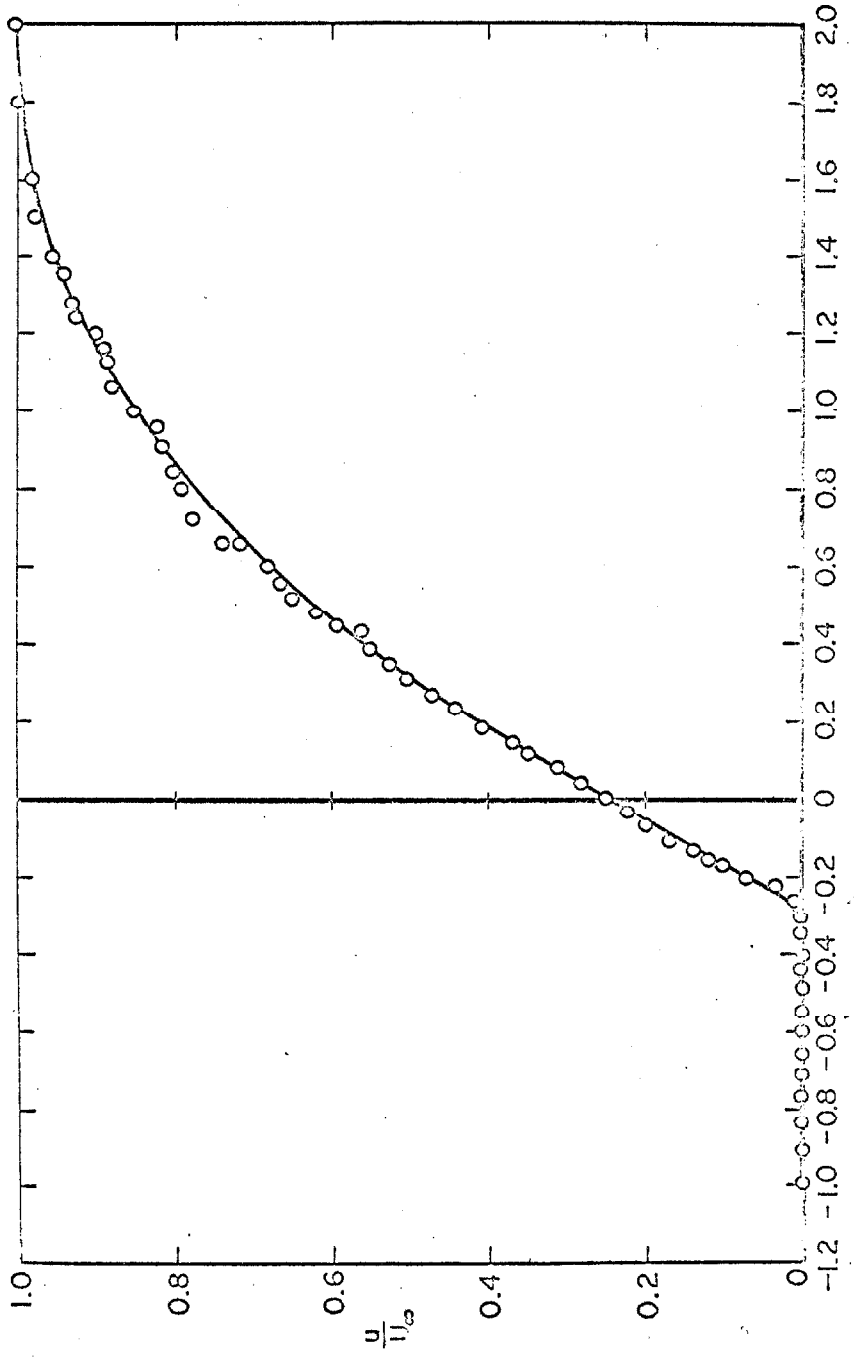

Fig. 25. Cavity center velocity profile. 1/4 x 1/4 in. cavity, $x_1 = 0.125$ in., $U_\infty = 0.125$ ft/sec., $\mathcal{R}^* = 31.6$. (Velocity ratios indicate absolute values—points at $u/U_\infty = 0$ represent readings smaller than margin of error)

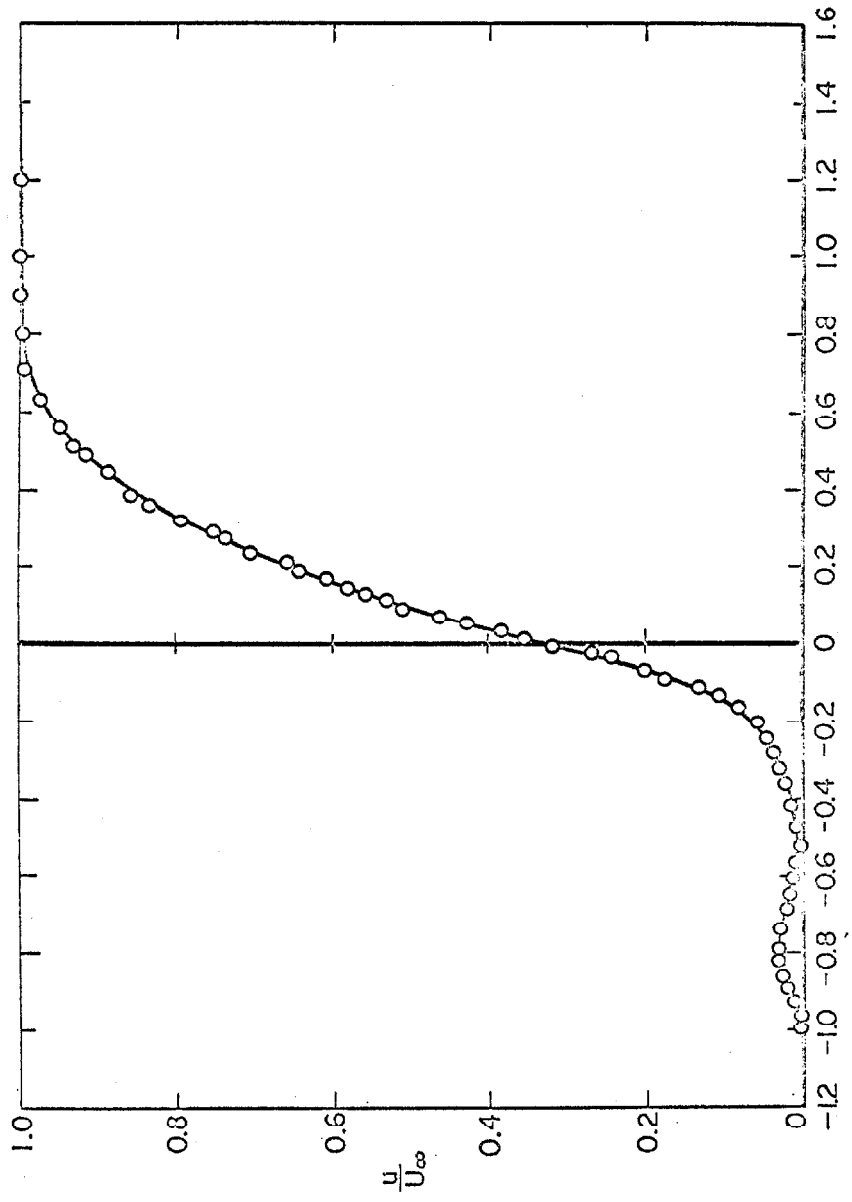

Fig. 26. Cavity center velocity profile, 1/4 x 1/4 in. cavity, $x_1 = 0.125$ in., $U_\infty = 0.75$ ft/sec., $\epsilon^* = 50.1$. (Velocity ratios indicate absolute values--points at $u/U_\infty = 0$ represent readings smaller than margin of error)

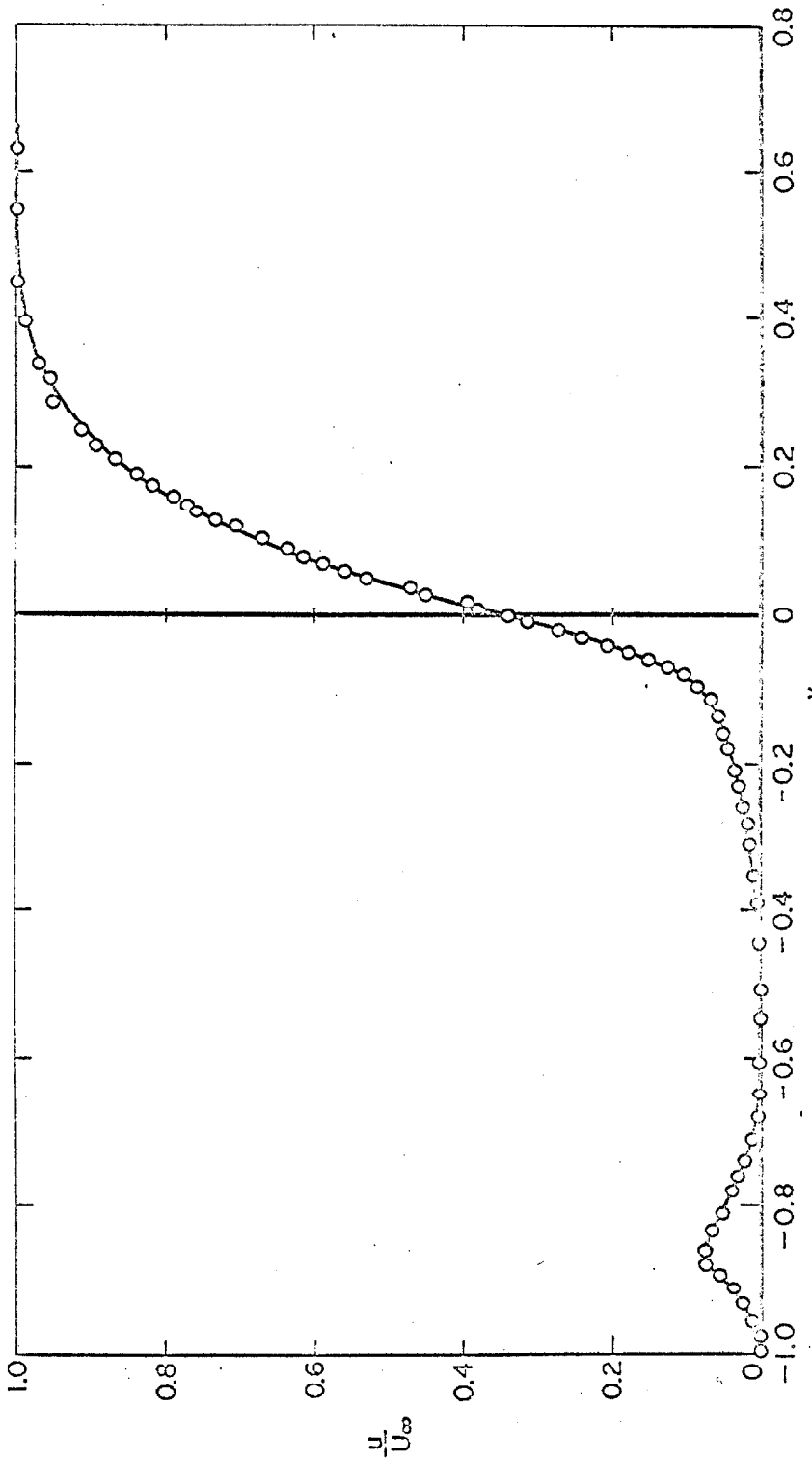

Fig. 27. Cavity center velocity profile. 1/2 x 1/2 in. cavity. x_1 = 0.25 in., U_∞ = 0.75 ft/sec., ϵ^* = 100.2. (Velocity ratios indicate absolute values--points at u/U_∞=0 represent readings smaller than margin of error)

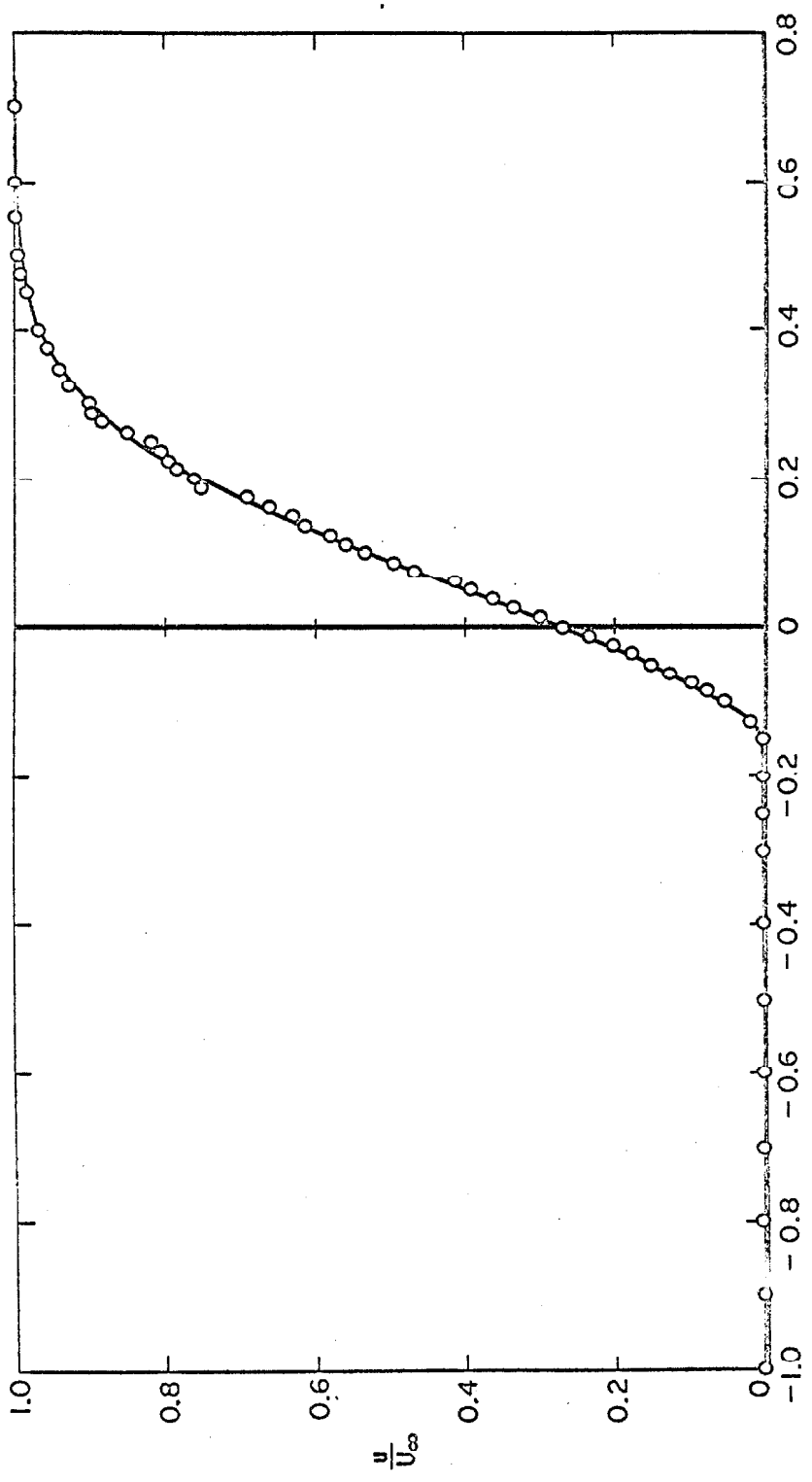

Fig. 28. Cavity center velocity profile. 1 x 1 in. cavity, $x_1 = 0.6$ in., $U_\infty = 0.125$ ft/sec., $\varepsilon^* = 126.4$. (Velocity ratios indicate absolute values--points at $u/U_\infty = 0$ represent readings smaller than margin of error)

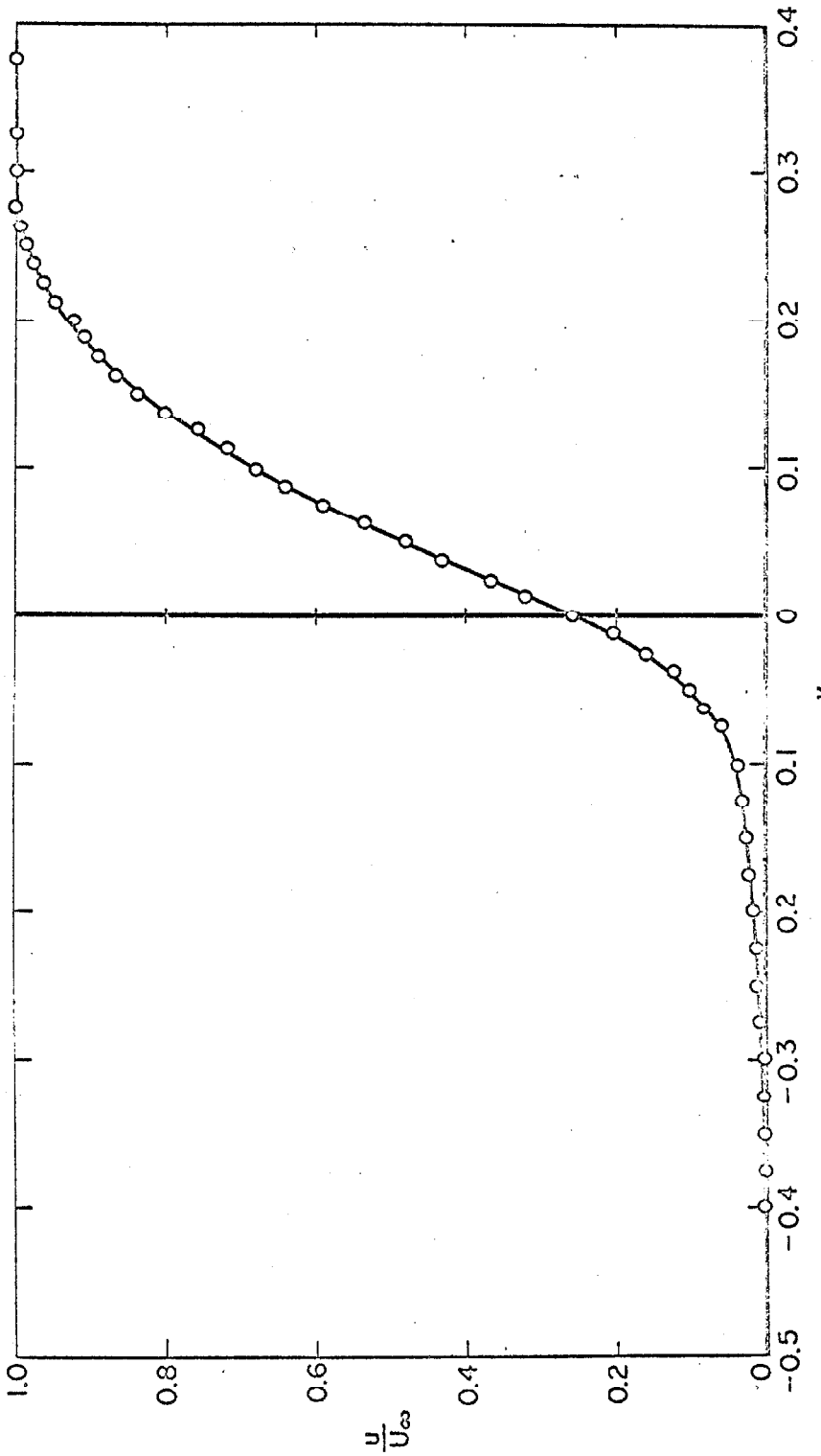

Fig. 29. Cavity center velocity profile, upper portion. 1 x 1 in. cavity, $x_1 = 0.5$ in., $U_\infty = 0.50$ ft/sec., $\varepsilon^* = 286.4$. (Velocity ratios indicate absolute values–points at $u/U_\infty = 0$ represent readings smaller than margin of error)

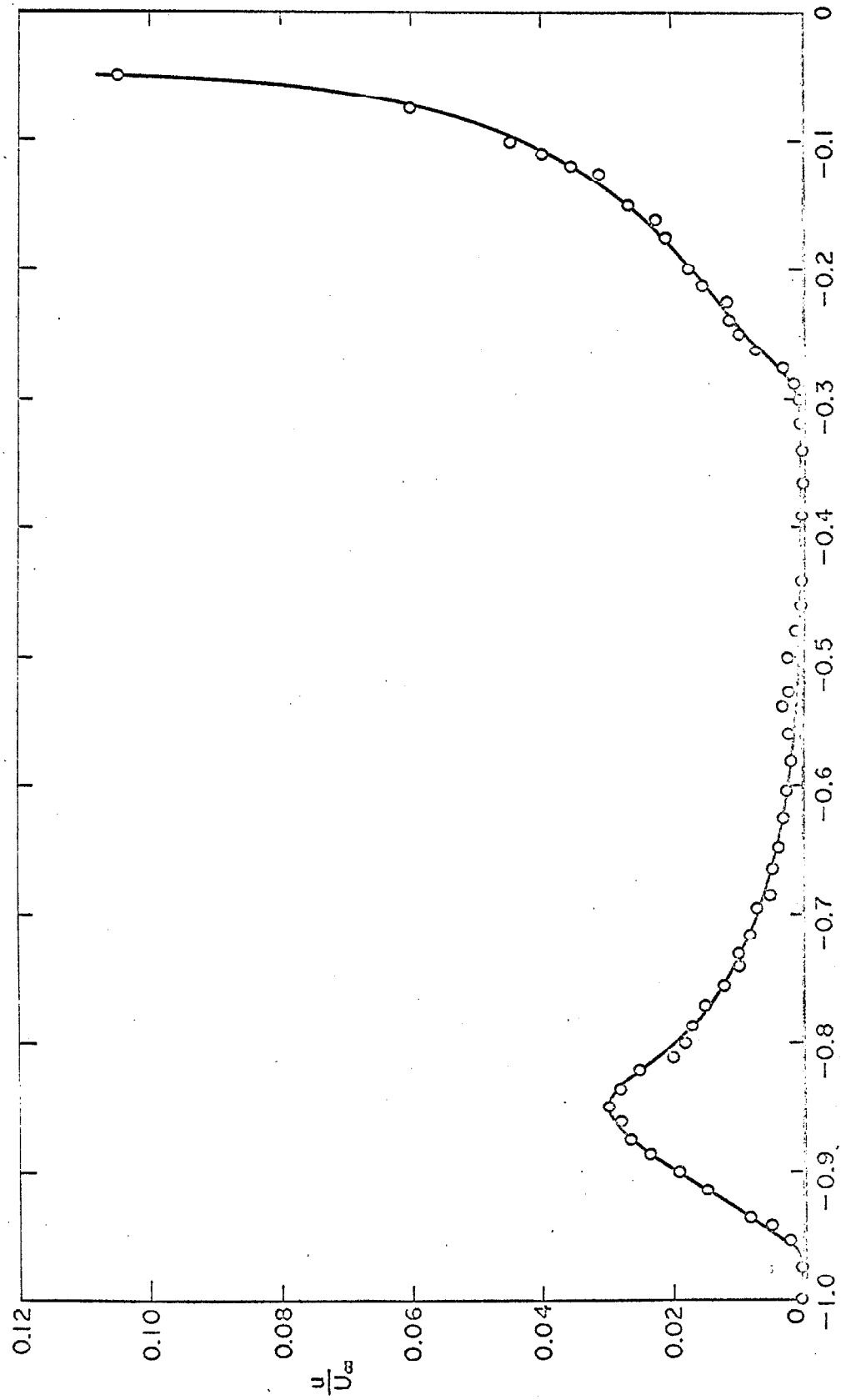

Fig. 30. Cavity center velocity profile, lower portion. 1 x 1 in. cavity, $x_1 = 0.5$ in., $U_\infty = 0.50$ ft/sec., $\epsilon^* = 286.4$. (Velocity ratios indicate absolute values—points at $u/U_\infty = 0$ represent readings smaller than margin of error)

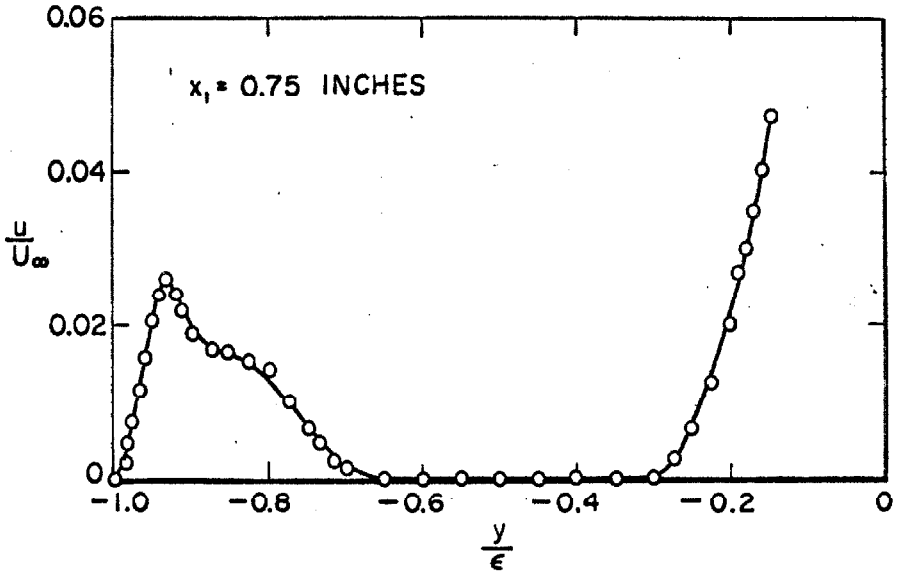

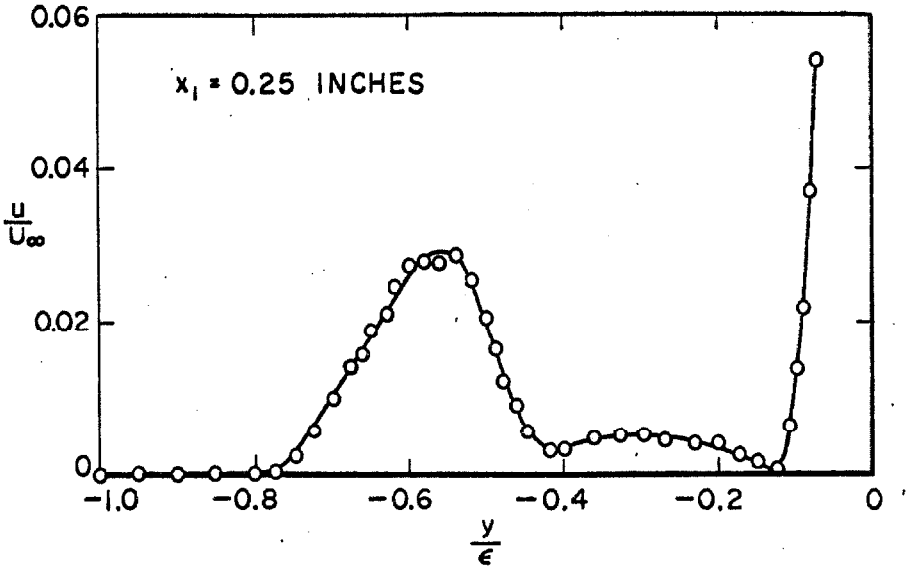

Fig. 31. Off-center cavity velocity profiles, 1 x 1 in. cavity, U_∞ = 0.50 ft/sec., ϵ^* = 286.4. (Velocity ratios indicate absolute values—points at u/U_∞=0 represent readings smaller than margin of error)

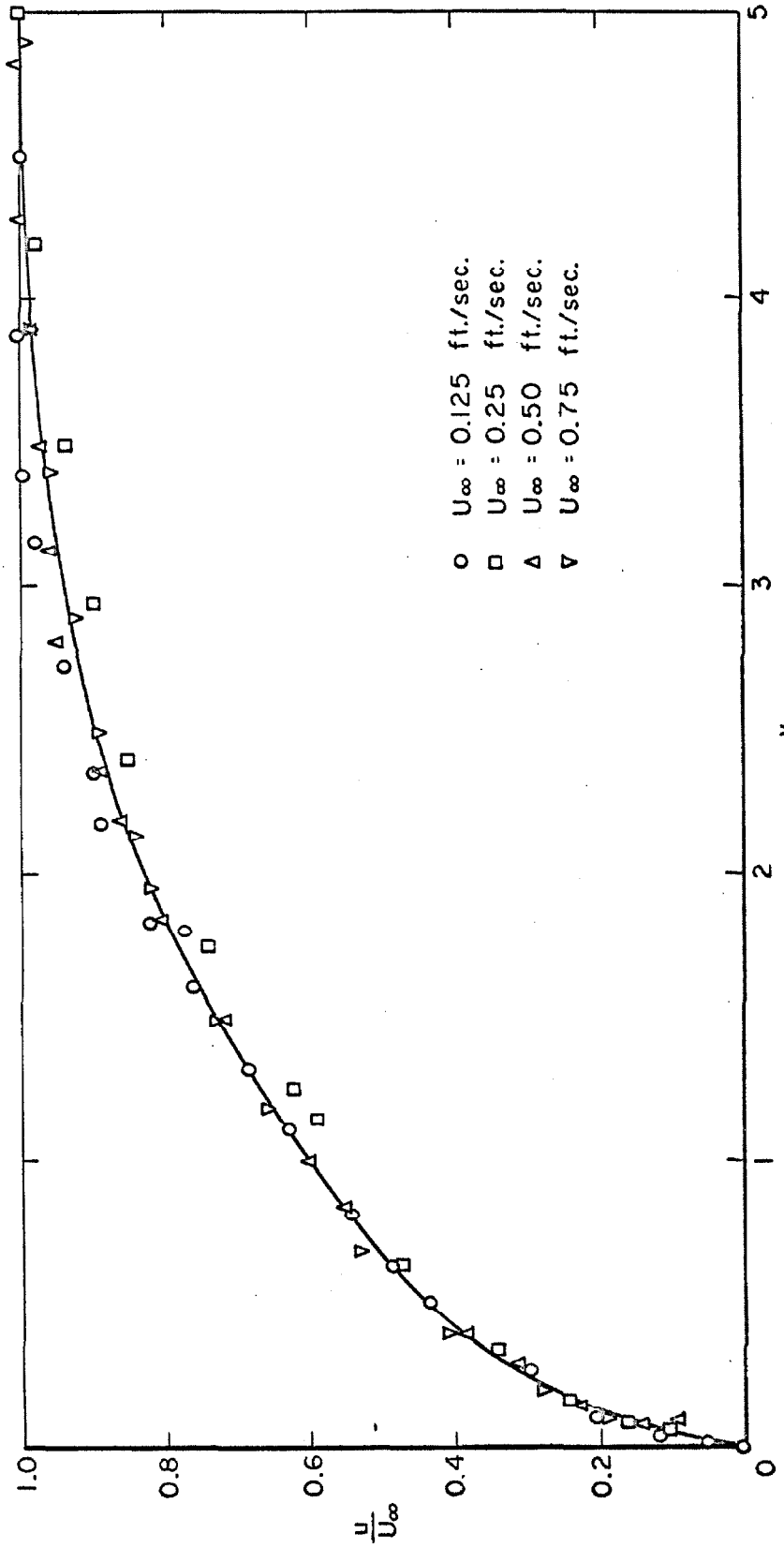

Fig. 32. Velocity profiles downstream of cavity. 1/4 x 1/4 in. cavity, $x_1 = 0.311$ in.

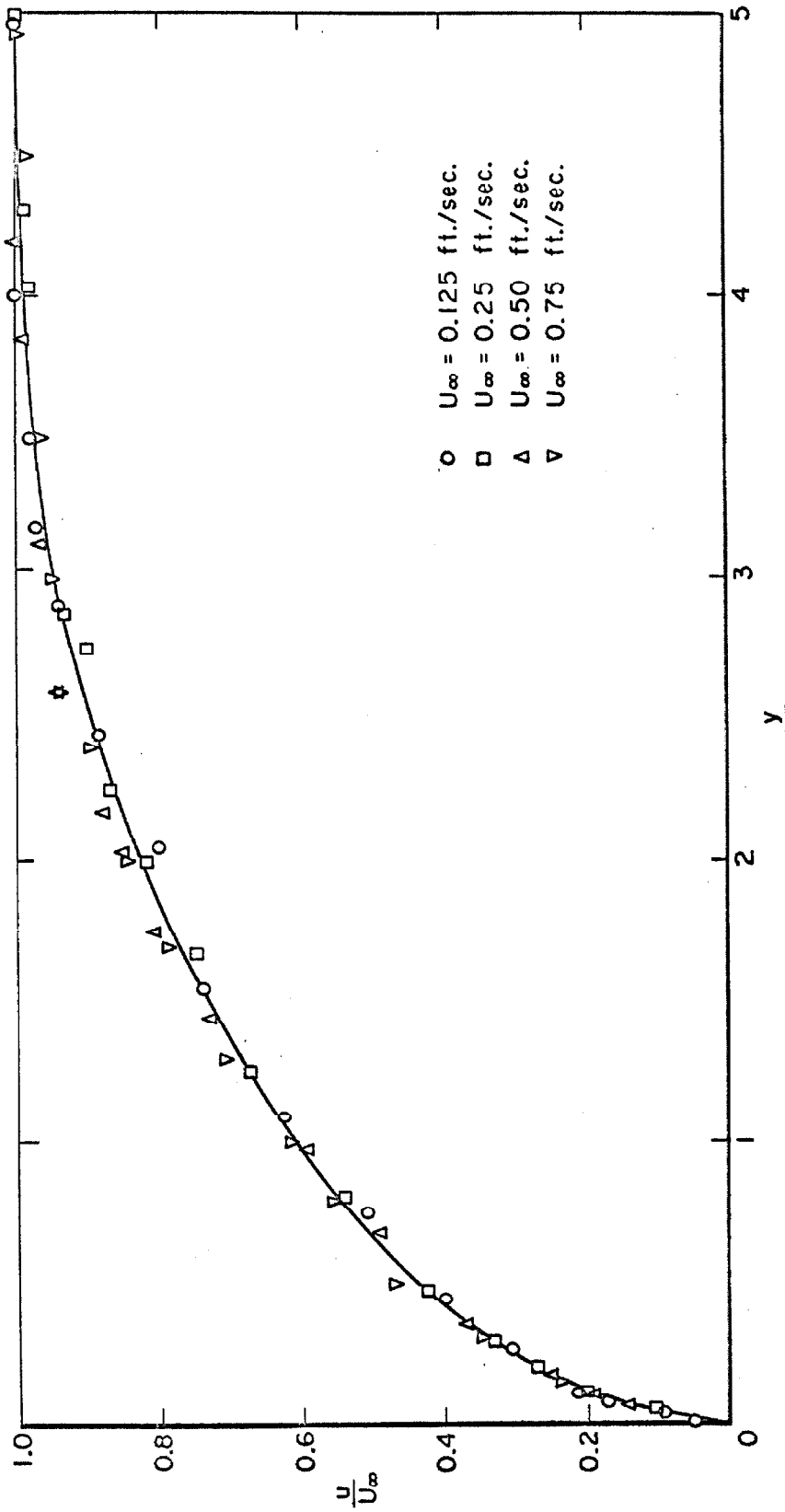

Fig. 33. Velocity profiles downstream of cavity. 1/2 x 1/2 in. cavity, x_1 = 0.625 in.

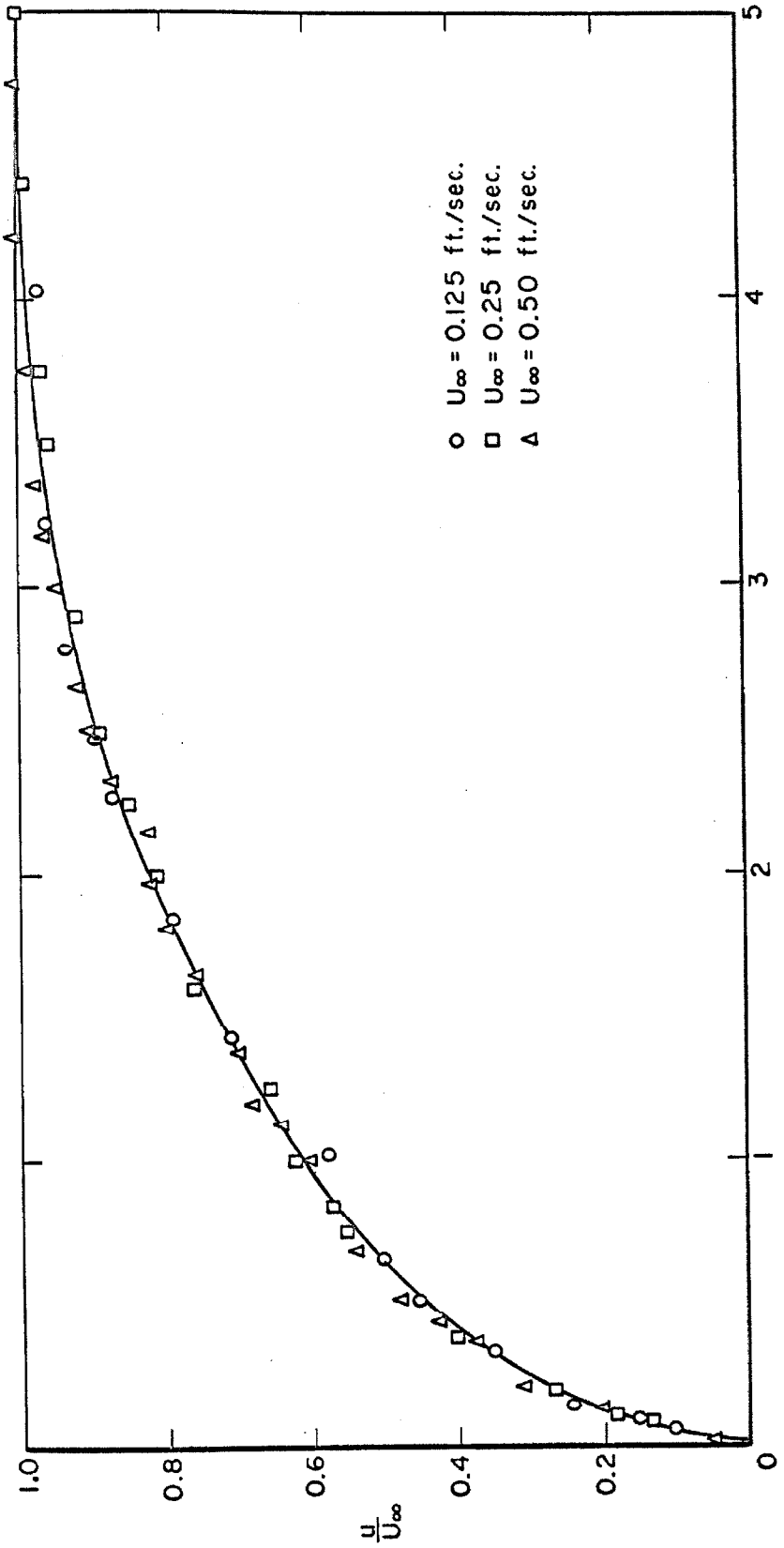

Fig. 34. Velocity profiles downstream of cavity. 1 x 1 in. cavity, x_1 = 1.24 in.

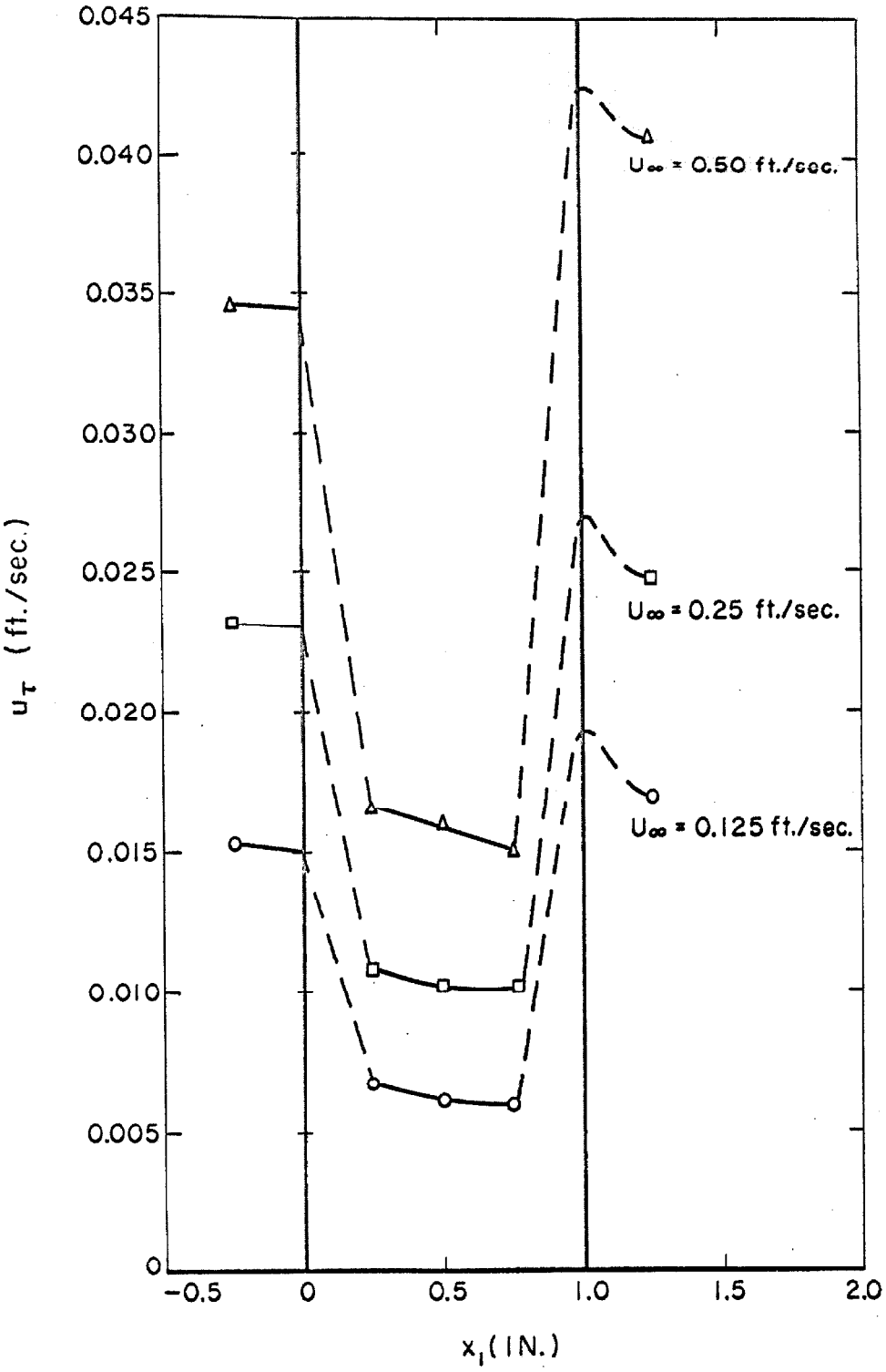

Fig. 35. Shear velocity development across top of cavity 1 x 1 in. cavity. Dashed lines represent estimates.

Fig. 36. Photograph of cavity flow. Flow is from right to left. 1/2 inch deep x 1-1/4 inch long cavity, U_∞ = 0.125 ft/sec., ϵ^* = 63.2.

Fig. 37. Photograph of cavity flow. Flow is from right to left. 1/2 inch deep x 1-1/4 inch long cavity, U_∞ = 0.25 ft/sec., ϵ^* = 96.0.

Fig. 38. Photograph of cavity flow. From is from right to left. 1/2 inch deep x 1-1/4 inch long cavity, U_∞ = 0.50 ft/sec., ϵ^* = 143.2.

Fig. 39. Photograph of cavity flow. Flow is from right to left. 1/2 inch deep x 1-1/4 inch long cavity, U_∞ = 0.75 ft/sec., ϵ^* = 200.4.

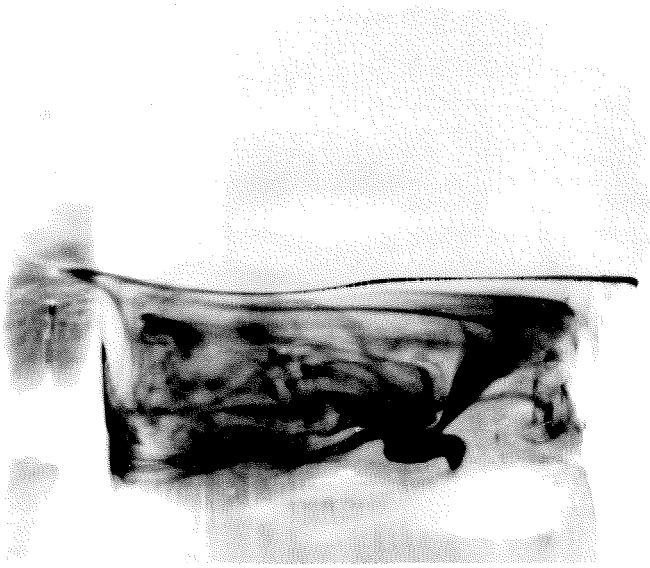

Fig. 40. Photograph of cavity flow. Flow is from right to left. 1/2 inch deep x 1-1/4 inch long cavity, U_∞ = 1.0 ft/sec., $\mathcal{R}^*$ = approx. 250.

Fig. 41. Photograph of cavity flow. Flow is from right to left. 1 in. deep x 1/2 in. long cavity, U_∞ = 0.25 ft/sec., 12 frames/sec.

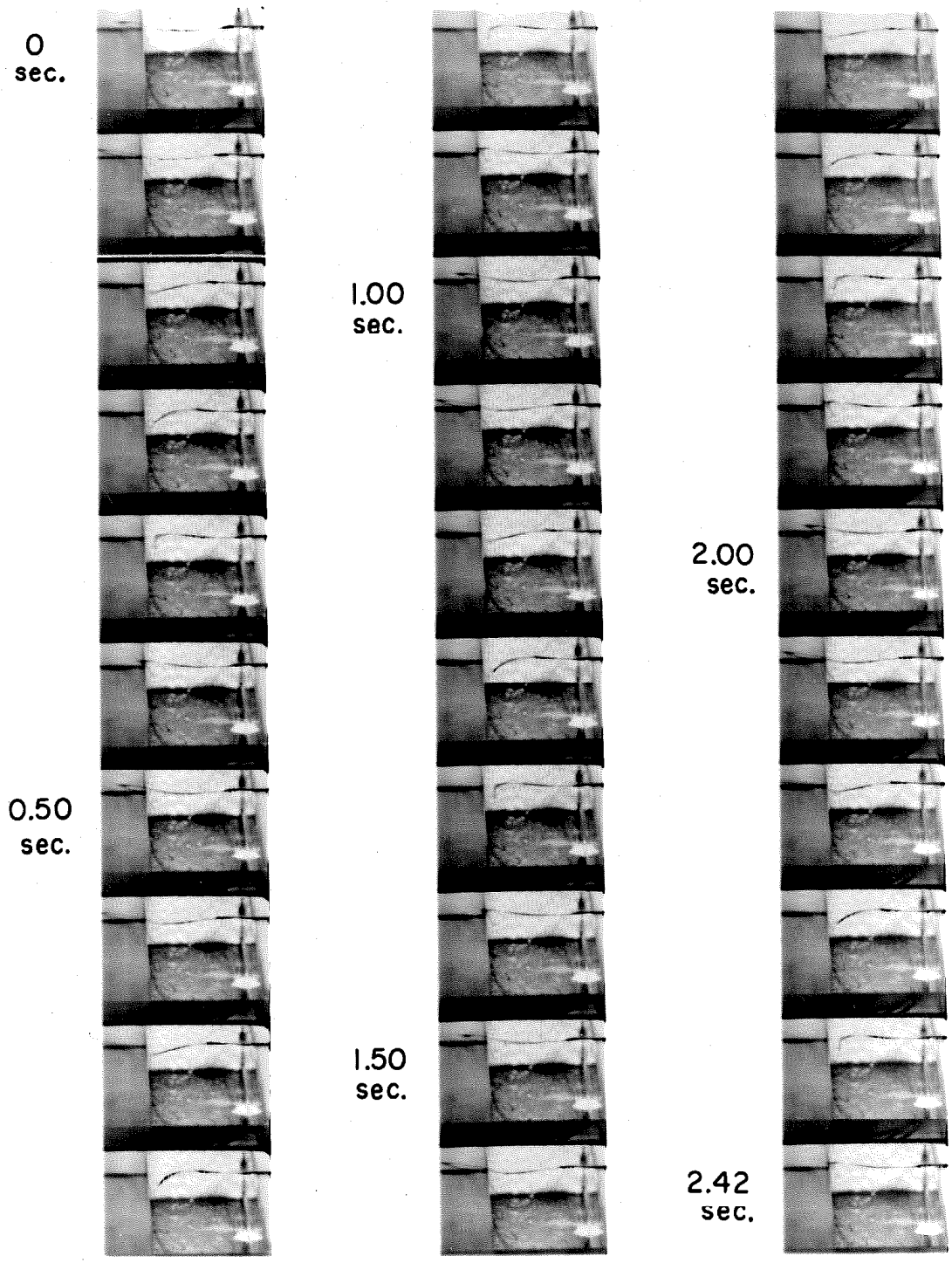

Fig. 42. 16mm Motion Picture Frames of Laminar Oscillation. 1 x 1 in. cavity, U_∞ = 0.50 ft/sec, 12 frames/sec.

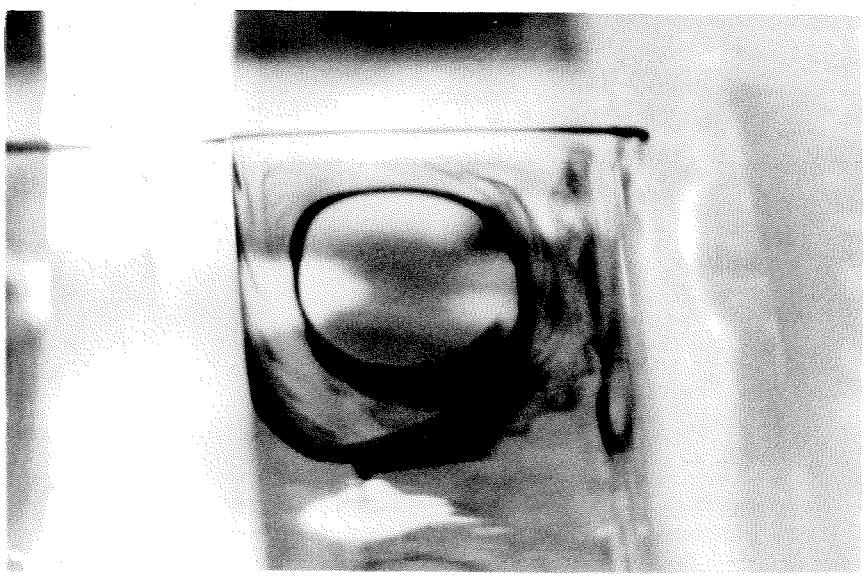

Fig. 43. Photograph of cavity flow showing the laminar oscillation. 1 x 1 in. cavity, U_∞ = 0.50 ft/sec., ϵ^* = 286.4.

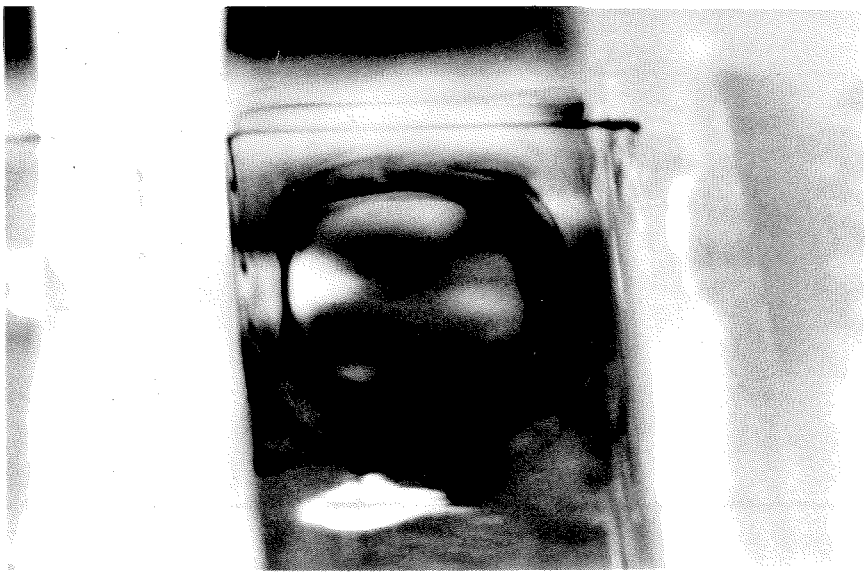

Fig. 44. Photograph of cavity flow showing the laminar oscillation. 1 x 1 in. cavity, U_∞ = 0.75 ft/sec., ϵ^* = 400.8.

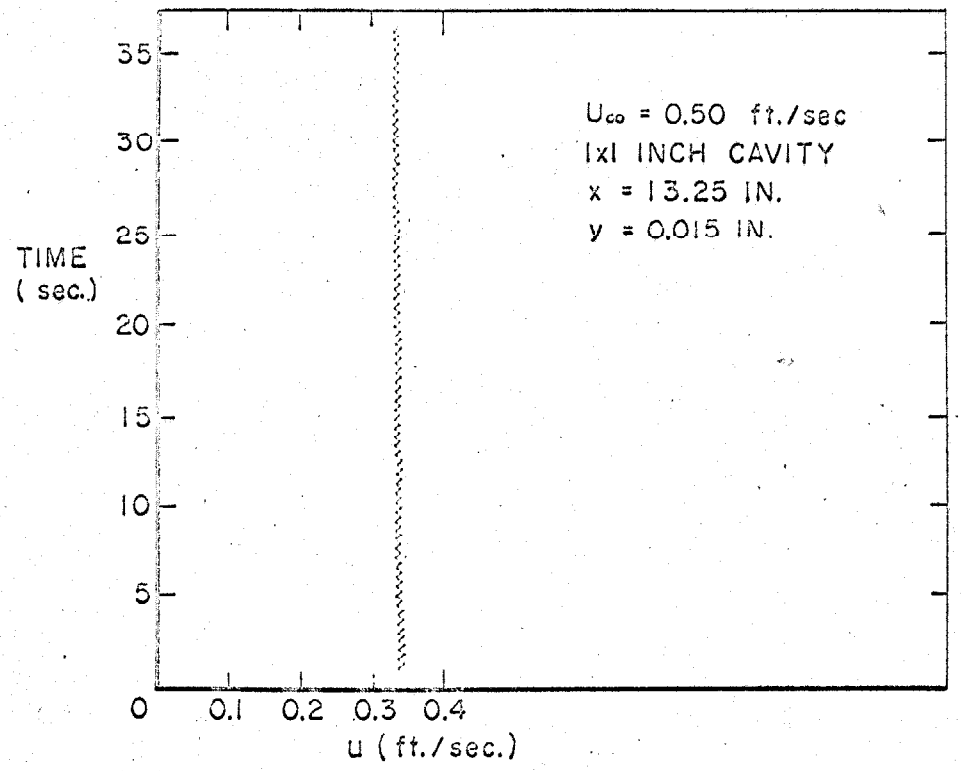

Fig. 45. Sanborn velocity record showing the laminar oscillations. 1 x 1 in. cavity, U_∞ = 0.50 ft/sec., x_1 = 1.25 in., y = 0.015 in.

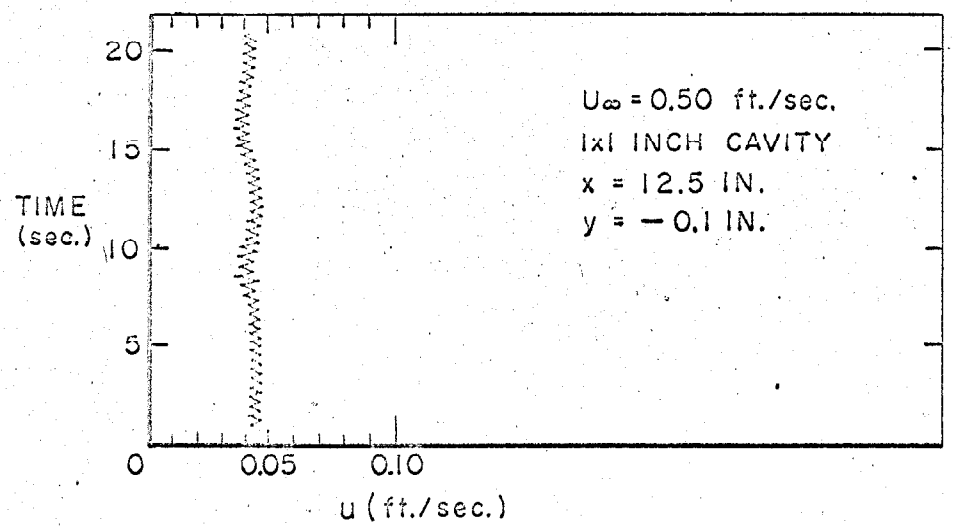

Fig. 46. Sanborn velocity record showing the laminar oscillation. 1 x 1 in. cavity, U_∞ = 0.50 ft/sec., x_1 = 0.50 in., y = -0.10 in.

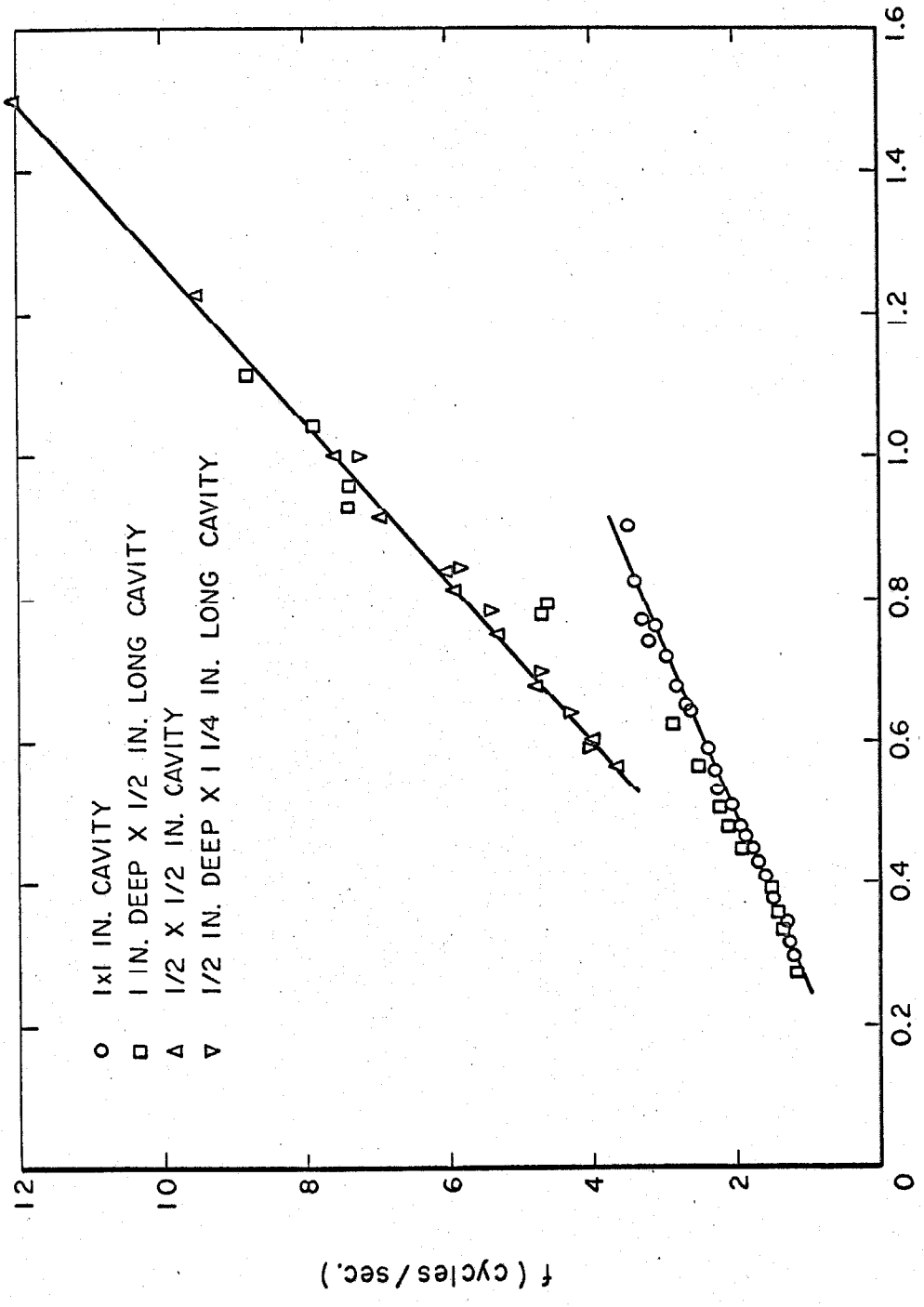

Fig. 47. Frequencies of laminar oscillations versus free stream velocity.

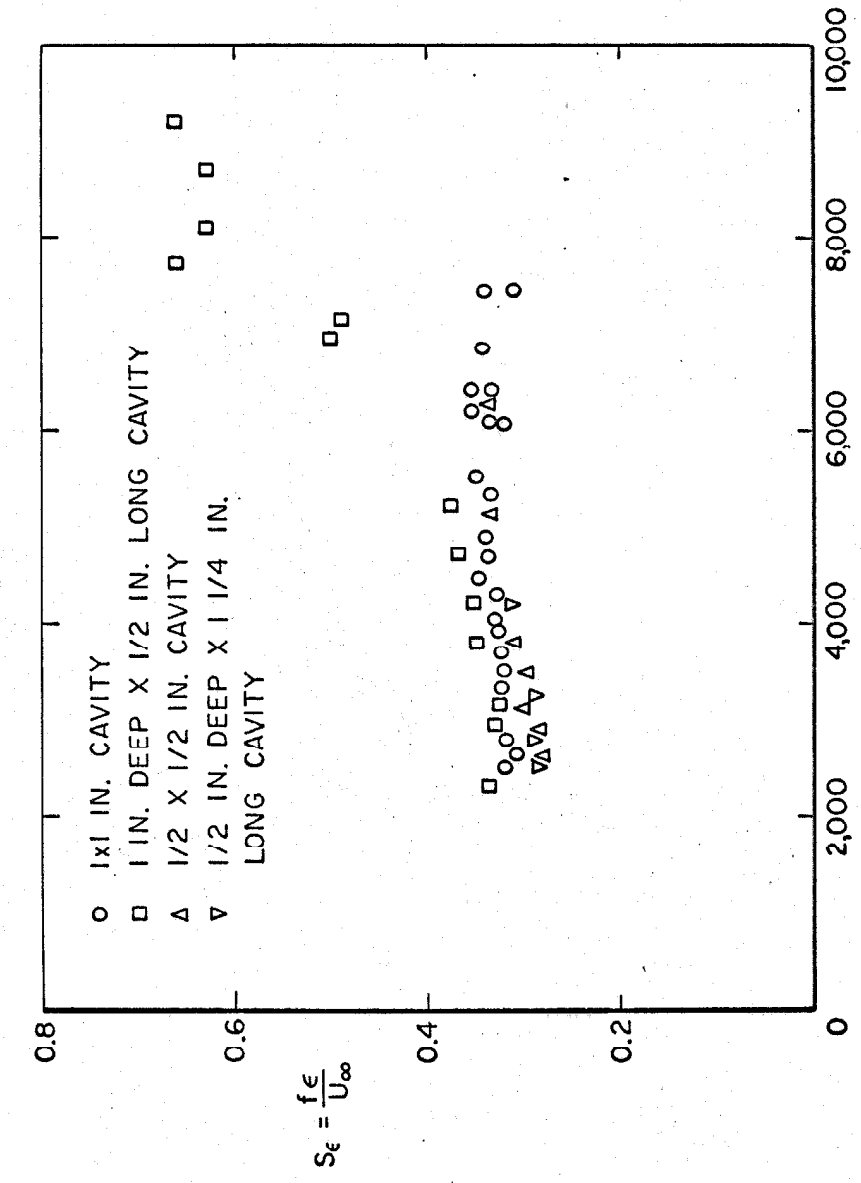

Fig. 48. Cavity Strouhal number for the laminar oscillations versus cavity Reynolds number.

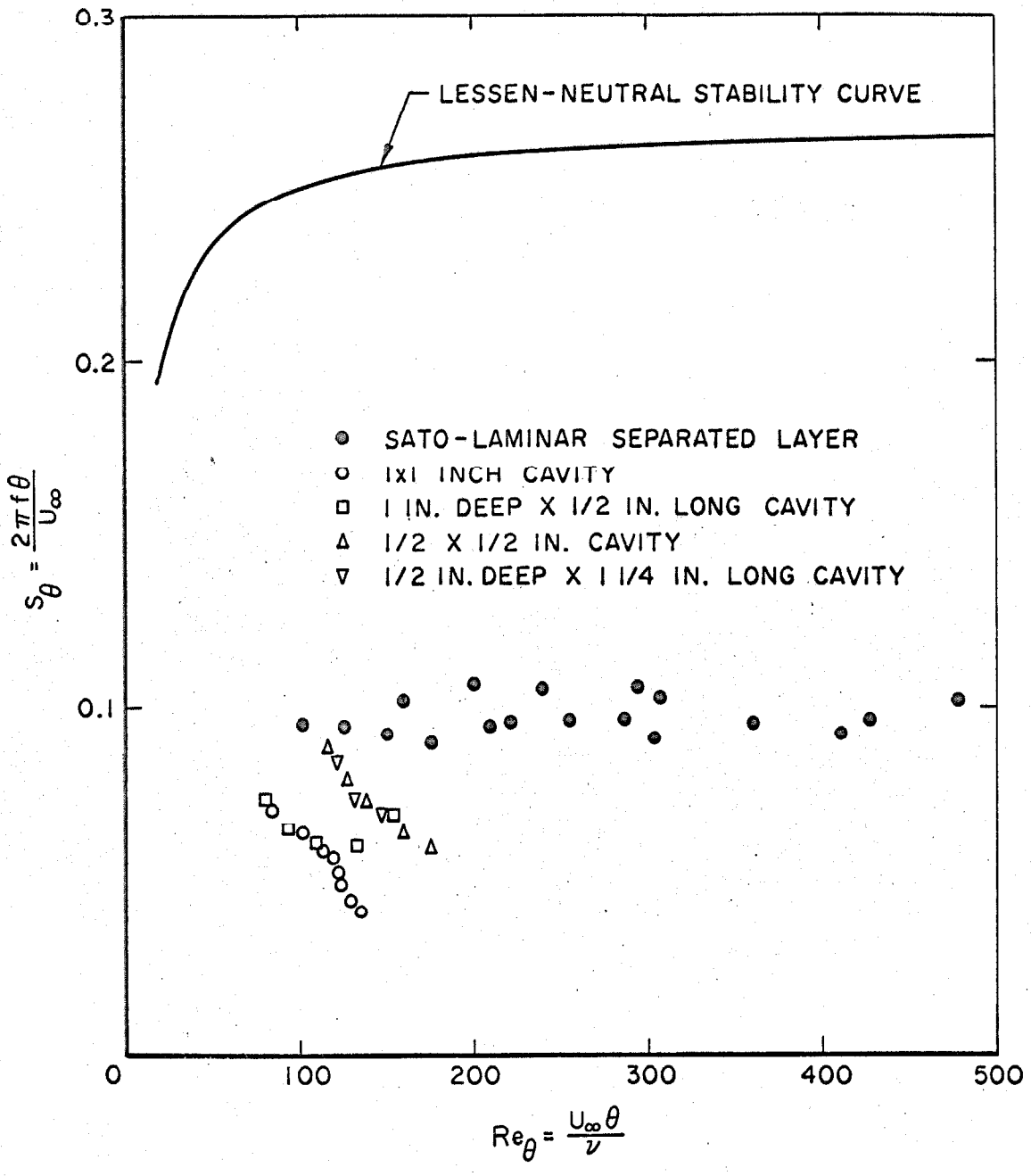

Fig 49. Strouhal number based on momentum thickness versus Reynolds number based on momentum thickness.